

FLUORESCENCE SENSORS FROM PYRENO[4,5-d]IMIDAZOLE DERIVATIVES



A Dissertation Submitted in Partial Fulfillment of the Requirements  
for the Degree of Doctor of Philosophy in Chemistry

Department of Chemistry

FACULTY OF SCIENCE

Chulalongkorn University

Academic Year 2020

Copyright of Chulalongkorn University

ฟลูออเรสเซนซ์เซนเซอร์จากอนุพันธ์ของไพรีโน[4,5-d]อิมิดาโซล



วิทยานิพนธ์นี้เป็นส่วนหนึ่งของการศึกษาตามหลักสูตรปริญญาวิทยาศาสตรดุษฎีบัณฑิต

สาขาวิชาเคมี ภาควิชาเคมี

คณะวิทยาศาสตร์ จุฬาลงกรณ์มหาวิทยาลัย

ปีการศึกษา 2563

ลิขสิทธิ์ของจุฬาลงกรณ์มหาวิทยาลัย



นิยามา ชนะวังเมือง : ฟลูออเรสเซนซ์เซนเซอร์จากอนุพันธ์ของไพรีโน[4,5-d]อิมิดาโซล. ( FLUORESCENCE SENSORS FROM PYRENO[4,5-d]IMIDAZOLE DERIVATIVES) อ.ที่ปรึกษาหลัก : ศ. ดร.ไพฑูริย์ รัชตะสาคร, อ.ที่ปรึกษาร่วม : ศ. ดร.มงคล สุขวัฒนาสินธุ์

งานวิจัยนี้มีการออกแบบและพัฒนาอนุพันธ์ของไพรีโนอิมิดาโซล (P1, P2, P3, P4 และ P5) ซึ่งสามารถสังเคราะห์ได้จากสารตั้งต้นไพรีโนใน 2 ขั้นตอน ได้ผลิตภัณฑ์ร้อยละ 26 – 40% หลังจากนั้นทำการศึกษาคุณสมบัติทางแสงและการตรวจจับไอออนโลหะของโมเลกุลทั้งห้า ผลการทดลองพบว่าโมเลกุล P5 ไม่มีการการเลือกจับกับไอออนของโลหะใดๆ ในขณะที่โมเลกุล P1, P2, P3 และ P4 มีการเลือกจับกับไอออนของโลหะที่มีเวเลนซ์อิเล็กตรอน 3+ (บิสมัทไอออน, อะลูมิเนียมไอออน, โครเมียมไอออน, ไอออนเหล็ก) ในสารละลายอะซิโตไนไตรล์ ( $\text{CH}_3\text{CN}$ ) แต่อย่างไรก็ตามมีเพียงอนุพันธ์ของไพรีโนอิมิดาโซลที่แทนที่บนวงอิมิดาโซลด้วยอนุพันธ์ของ 2-ไฮดรอกซิลฟีนิล (P2) ที่แสดงให้เห็นว่ามีความจำเพาะเจาะจงในการตรวจจับไอออนของบิสมัทในสารละลายผสม 20% ของไดเมทิลซัลฟอกไซด์ในอะซิโตไนไตรล์ แบบเพิ่มสัญญาณของฟลูออเรสเซนซ์ เนื่องมาจากกระบวนการเคลื่อนย้ายโปรตอน-อิเล็กตรอน ภายในโมเลกุลในสถานะกระตุ้น (excited state intramolecular proton transfer,ESIPT) โดยการเกิดสารประกอบระหว่างโมเลกุลและไอออนยับยั้งการเกิดพันธะไฮโดรเจนภายในโมเลกุล และโมเลกุล P2 มีการขยายสัญญาณฟลูออเรสเซนซ์ที่ความยาวคลื่น 447 นาโนเมตร สำหรับกลไกการเกิดสารประกอบระหว่างโมเลกุลและไอออนบิสมัทสามารถตรวจสอบได้โดยวิธีทางสเปกโทรสโกปี ได้แก่  $^1\text{H-NMR}$  และ เทคนิคการวัดไทเทรชันด้วยยูวีและฟลูออเรสเซนซ์ ซึ่งบ่งชี้ให้เห็นว่าอัตราส่วนที่จับกันเป็น 1:1 ระหว่างสารประกอบ P2 และบิสมัทไอออน และให้ค่าต่ำสุดที่สามารถตรวจวัดได้ (LOD) ประมาณ 1.20 ไมโครโมลาร์ในสารละลายผสม 20% ของไดเมทิลซัลฟอกไซด์ในอะซิโตไนไตรล์ และ 3.40 ไมโครโมลาร์ใน สารละลาย 10% น้ำในไดเมทิลซัลฟอกไซด์ในอะซิโตไนไตรล์ที่สภาวะพีเอช 5 นอกจากนี้ได้ทำการประยุกต์ใช้เซนเซอร์นี้ทดลองหาปริมาณบิสมัทในน้ำตัวอย่างสองชนิด พบว่ามีค่าร้อยละการกลับคืน 91-97%.

สาขาวิชา เคมี  
ปีการศึกษา 2563

ลายมือชื่อนิสิต .....  
ลายมือชื่อ อ.ที่ปรึกษาหลัก .....  
ลายมือชื่อ อ.ที่ปรึกษาร่วม .....

# # 5772816723 : MAJOR CHEMISTRY

KEYWORD: pyrene, Fluorescent sensor, Bismuth ions

Nichapa Chanawungmuang : FLUORESCENCE SENSORS FROM PYRENO[4,5-*d*]IMIDAZOLE DERIVATIVES. Advisor: Prof. PAITON RASHATASAKHON, Ph.D.

Co-advisor: Prof. MONGKOL SUKWATTANASINITT, Ph.D.

Herein, The five fluorescent probes (P1, P2, P3, P4 and P5) based on pyreno[4,5-*d*]imidazole were successfully prepared in two steps from pyrene in 26 – 40% overall yields. After that, all of the compounds were studied the photophysical properties and selectivity for sensing metal ions. The results showed compound P5 was not selective to metal ions while the others (P1, P2, P3 and P4) were selective to detection of trivalent metal ions such as  $\text{Bi}^{3+}$ ,  $\text{Al}^{3+}$ ,  $\text{Cr}^{3+}$  and  $\text{Fe}^{3+}$  in  $\text{CH}_3\text{CN}$ . However, only compound P2 with 2-hydroxyl phenyl substituent on imidazole ring formed complexation reaction selectively towards bismuth (III) ions and provided fluorescence enhancement signal attributing to the excited state intramolecular proton transfer (ESIPT) process. Compound P2 exhibited selective fluorescence turn-on at 447 nm. The sensing mechanism was determined by  $^1\text{H-NMR}$ , and UV-VIS and fluorescence titrations, and the Job's plot indicated a 1:1 binding between P2 and bismuth (III) ions. The detection limit was 1.20  $\mu\text{M}$  in  $\text{CH}_3\text{CN-DMSO}$  (8:2, v/v) mixture and 3.40  $\mu\text{M}$  in 10% aqueous in the mixed 80%  $\text{CH}_3\text{CN-DMSO}$  (pH =5). Moreover, the sensor was applied to quantitative analysis of spiked  $\text{Bi}^{3+}$  in real water samples from different sources. The recovery of  $\text{Bi}^{3+}$  was completed at 91-97%.

Field of Study: Chemistry

Academic Year: 2020

Student's Signature .....

Advisor's Signature .....

Co-advisor's Signature .....

## ACKNOWLEDGEMENTS

First of all, I would like to express my sincere gratitude to my advisor, Professor Dr. Paitoon Rashatasakhon, and my Co-Advisor Professor Dr. Mongkol Sukwattanasinitt, for giving me opportunities, invaluable advices, the best guidance and encouragement throughout the course of this research. Sincere thanks are also extended to Assistant Professor Dr. Anawat Ajavakom, Professor Dr. Sumrit Wacharasindhu and Assistant Professor Dr. Sakulsuk Unarunotai for their generous advice, precious guidance, and encouragement.

I also would like to gratefully acknowledge the committee, Associate Professor Dr. Vidhichai Parasuk, Professor Dr. Thawatchai Tuntulani, Assistant Professor Dr. Panuwat Padungros and Associate Professor Dr. Pitak Chuawong for their kindness, valuable suggestion, and recommendations.

My appreciation is giving to many people; Dr Kanokthorn Boonkitpataraku, Dr. Kannikar Vongnam, Dr. Pornpat Samang, and Dr. Komthep Silpharu, for their helpful, suggestions and guidance. I would like to thank Dr. Tianchai Chooppawa, Ms. Rungthiwa Arunchai, Ms. Chittranuch Pongsawad, Mrs. Chomchanok Kanjanatanyarat, Mr. Jakkrit Srisa, Ms. Chantipa Lerswipapat, and Ms. Pawittra Chaibuth who are my best colleagues, best friend, and best encouragement. Moreover, I gratefully thank to everyone in MAPS group for a great friendship, spirit, smile, good wish, and their helps in everything.

I would like to thank my financial support Development and Promotion of Science and Technology Talents Project (DPST).

Finally, A deep affectionate gratitude is acknowledged to my beloved father who always stand by my side for my pleasant and hard time and my beloved family for their understanding, encouragement, and support.

Nichapa Chanawungmuang

## TABLE OF CONTENTS

	Page
ABSTRACT (THAI).....	iii
ABSTRACT (ENGLISH).....	iv
ACKNOWLEDGEMENTS.....	v
TABLE OF CONTENTS.....	vi
LIST OF FIGURES.....	ix
LIST OF TABLES.....	xiv
LIST OF SCHEMES.....	1
LIST OF ABBREVIATIONS.....	2
CHAPTER I INTRODUCTION.....	4
1.1 Fluorescence.....	4
1.2 Fluorescent sensor.....	5
1.3 Sensing Mechanisms.....	6
1.4 Fluorescent sensors based on Pyreno[4,5- <i>d</i> ]imidazole.....	8
1.5 Objective of this research.....	18
CHAPTER II EXPERIMENTAL.....	19
2.1 Materials and Chemicals.....	19
2.2 Analytical instruments.....	19
2.3 Synthesis and characterization.....	19
2.3.1 Pyrene-4,5-diones (1).....	19
2.3.2 Pyreno[4,5- <i>d</i> ]imidazole derivatives (P1-P5).....	20
2.3.2.1 10-phenyl-9 <i>H</i> -pyreno[4,5- <i>d</i> ]imidazole (P1).....	20

2.3.2.2 2-(9H-pyreno[4,5-d]imidazol-10-yl)phenol (P2) .....	21
2.3.2.3 10-(2-methoxyphenyl)-9H-pyreno[4,5-d]imidazole (P3).....	21
2.3.2.4 2-methoxy-6-(9H-pyreno[4,5-d]imidazol-10-yl)phenol (P4).....	22
2.3.3.5 10-(pyridin-2-yl)-9H-pyreno[4,5-d]imidazole (P5).....	23
2.4 Studies of photophysical properties .....	24
2.4.1 UV-visible spectroscopy .....	24
2.4.2 Molar extinction coefficient ( $\epsilon$ ).....	24
2.4.3 Fluorescence spectroscopy.....	24
2.4.4 Relative quantum yield .....	24
2.5 Studies of metal ions sensing properties .....	25
2.5.1 Effect of solvents.....	25
2.5.2 Metal ion selectivity.....	26
2.5.3 Metal ions interference.....	26
2.5.4 Fluorescence titration and Detection limit .....	26
2.6 Studies of sensing mechanism .....	27
2.6.1 Time dependent.....	27
2.6.2 UV-visible and Fluorescence studies.....	27
2.6.3 $^1\text{H}$ NMR experiment.....	27
2.6.4 Job's plot .....	27
2.7 Quantitative analysis for $\text{Bi}^{3+}$ .....	27
2.7.1 Effect of water content .....	27
2.7.2 Effect of pH.....	28
2.7.3 $\text{Bi}^{3+}$ in real water samples.....	28
CHAPTER III RESULTS AND DISCUSSION.....	29



3.1 Synthesis and characterization of fluorophores (P1-P5) .....	29
3.2 Photophysical properties.....	35
3.3 Metal ions sensing properties.....	36
3.1.1 Solvent effect .....	36
3.3.2 Preliminary screening on metal ion selectivity.....	39
3.3.3 Interference studies.....	46
3.3.4 Fluorescence titration and detection limit.....	47
3.4 Sensing mechanism studies .....	48
3.4.1 Time dependence .....	48
3.4.2 UV-visible studies and decomplexation.....	49
3.4.3 $^1\text{H}$ NMR experiment.....	50
3.4.4 Job's plot .....	51
3.5 Quantitative analysis for $\text{Bi}^{3+}$ .....	52
3.5.1 Effect of water content .....	52
3.5.2 Effect of pH .....	52
3.5.3 $\text{Bi}^{3+}$ in real water samples.....	54
CHAPTER IV CONCLUSION.....	57
REFERENCES .....	58
APPENDIX.....	64
VITA.....	73

## LIST OF FIGURES

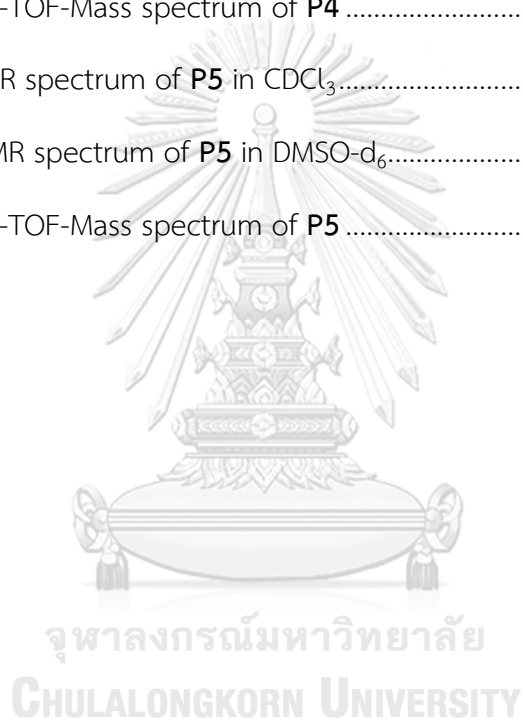
<b>Figure 1.1</b> Jablonski diagram.....	4
<b>Figure 1.2</b> Modes of fluorescent sensors.....	5
<b>Figure 1.3</b> Principle of photo-induced electron transfer (PET) effect.....	7
<b>Figure 1.4</b> Principle of Excited state intramolecular proton transfer (ESIPT) process ...	8
<b>Figure 1.5</b> The reactions on positions of pyrene .....	9
<b>Figure 1.6</b> (a) Structure of HBIZ; (b) The fluorescence ratio of HBIZ (50 $\mu$ M) in the presence of various metal ions (10 $\mu$ M) in <i>N,N</i> -Dimethylformamide, $\lambda_{\text{ex}} = 330$ nm.....	9
<b>Figure 1.7</b> (a) Synthesis of DPIN-A.; (b) Fluorescent spectra of DPIN-A (10 mM) in pure water (PBS buffer, pH =7.2) towards biothiols (10 eq of GSH, Cys, Hcy.) were obtained after 30 min and other amino acids (100 eq.) were recorded after 1 hour.), $\lambda_{\text{ex}} = 371$ nm.....	10
<b>Figure 1.8</b> (a) Possible sensing mechanism of sensor <b>L</b> and $\text{Hg}^{2+}$ ; (b) Fluorescence spectra of <b>L</b> (20 $\mu$ M) towards various metal ions (10 equiv.) in $\text{H}_2\text{O}$ -DMSO (1:9, v/v) ( $\lambda_{\text{ex}} = 325$ nm).....	11
<b>Figure 1.9</b> (a) Possible binding mechanism between <b>1H</b> and $\text{Al}^{3+}$ ; (b) Fluorescence spectra of <b>1H</b> (2.5 $\mu$ M) towards various metal ions (10 equiv.) in $\text{CH}_3\text{CN}/\text{H}_2\text{O}$ (1:9, v/v), $\lambda_{\text{ex}} = 375$ nm.....	12
<b>Figure 1.10</b> (a) Binding mechanism of Probe <b>1</b> with $\text{Cu}^{2+}$ undergo CT process.; (b) Fluorescence intensity of Probe <b>1</b> (10 $\mu$ M) without metal ions ( <b>Green</b> ), in the presence of various metal ions (1 equiv.) ( <b>Blue</b> ), and with 10 $\mu$ M of $\text{Cu}^{2+}$ in the presence of other metal ions ( <b>Red</b> ), $\lambda_{\text{em}} = 387$ nm.....	13
<b>Figure 1.11</b> (a) Sensing mechanism of PAN-Bn-PB with $\text{H}_2\text{O}_2$ ; (b) Fluorescence intensity of PAN-Bn-PB (10 $\mu$ M) in various molecules that could exist in biological system (200 $\mu$ M).....	13
<b>Figure 1.12</b> Proposed sensing mechanism of PIF in acid-base conditions.....	14
<b>Figure 1.13</b> The one-step to synthesis of pyrene–imidazole skeletons.....	14

<b>Figure 1.14</b> Structure of Py-BiimzH <sub>2</sub> and luminescence spectra of Py-BiimzH <sub>2</sub> upon addition of various anions as their tetrabutylammonium (TBA) salts (300 equiv.) in H <sub>2</sub> O–DMSO (9:1, v/v), $\lambda_{ec}$ = 350 nm [47].	15
<b>Figure 1.15</b> UV-Vis spectra and luminescence spectra of complex <b>A</b> and <b>B</b> upon addition of various anions as their tetrabutylammonium (TBA) or sodium salts (300 equiv.) in pure water (HEPES buffer, pH = 7) [48].	16
<b>Figure 1.16</b> Luminescence spectra of complex <b>C</b> and <b>D</b> upon addition of various anions as their tetrabutylammonium (TBA) in CH <sub>3</sub> CN.	17
<b>Figure 1.17</b> Proposed mechanism and fluorescence titration of (9H-pyreno[4,5- <i>d</i> ]imidazol10-yl)-benzaldehyde in DMSO.	17
<b>Figure 1.18</b> Target molecules <b>P1-P5</b> .	18
<b>Figure 3.1</b> <sup>1</sup> H NMR spectrum of dione <b>1</b> in CDCl <sub>3</sub> .	30
<b>Figure 3.2</b> <sup>1</sup> H NMR spectra of <b>P1</b> , <b>P2</b> and <b>P3</b> in DMSO-d <sub>6</sub> .	31
<b>Figure 3.3</b> The <sup>1</sup> H- <sup>1</sup> H COSY spectrum of <b>P2</b> in DMSO-d <sub>6</sub> .	32
<b>Figure 3.4</b> FT-IR spectra of <b>P1</b> and <b>P2</b> .	32
<b>Figure 3.5</b> Comparison of <sup>1</sup> H NMR spectra of <b>P2</b> and <b>P4</b> CD <sub>3</sub> OD.	33
<b>Figure 3.6</b> Comparison of <sup>1</sup> H NMR spectra of each fractions of <b>P5</b> and picolinaldehyde in CDCl <sub>3</sub> .	34
<b>Figure 3.7</b> MALDI-TOF-Mass spectrum of <b>P5</b> .	34
<b>Figure 3.8</b> Normalized absorption and emission spectra of <b>P1-P3</b> in EtOH.	35
<b>Figure 3.9</b> Absorption spectra of <b>P1-P5</b> in various solvents.	37
<b>Figure 3.10</b> Fluorescence spectra of <b>P1-P5</b> in CH <sub>3</sub> CN, THF and EtOH.	38
<b>Figure 3.11</b> Fluorescence spectra and fluorescence enhancement ratio of <b>P1-P5</b> (10 $\mu$ M) in CH <sub>3</sub> CN upon addition of 10 equiv. of various metal ions.	40
<b>Figure 3.12</b> Comparison of fluorescence enhancement ratio of <b>P1-P5</b> (10 $\mu$ M) in CH <sub>3</sub> CN upon addition of 10 equiv. of various metal ions.	41

<b>Figure 3.13</b> Fluorescence spectra of <b>P2</b> (10 $\mu\text{M}$ ) in $\text{CH}_3\text{CN}$ upon addition of 10 equiv. of various anions.....	41
<b>Figure 3.14</b> Fluorescence spectra of <b>P2</b> (10 $\mu\text{M}$ ) upon addition 1 to 5 equiv. of $\text{PO}_4^{3-}$ in $\text{CH}_3\text{CN}$ . .....	42
<b>Figure 3.15</b> Fluorescence spectra of <b>P2</b> (10 $\mu\text{M}$ ) in presence of $\text{PO}_4^{3-}$ (10 equiv.) upon addition 10 equiv. of various metal ions in $\text{CH}_3\text{CN}$ . .....	42
<b>Figure 3.16</b> UV-Vis titration spectra of <b>P2</b> (10 $\mu\text{M}$ ) in the presence of 10 equiv. of $\text{PO}_4^{3-}$ upon addition of various concentrations of $\text{Fe}^{3+}$ in $\text{CH}_3\text{CN}$ .....	43
<b>Figure 3.17</b> Fluorescence titration spectra of <b>P2</b> (10 $\mu\text{M}$ ) in the presence of 10 equiv. of $\text{PO}_4^{3-}$ upon addition of various concentrations of $\text{Fe}^{3+}$ in $\text{CH}_3\text{CN}$ .....	44
<b>Figure 3.18</b> Fluorescence spectra of <b>P2</b> (10 $\mu\text{M}$ ) (a) in various ratio of $\text{CH}_3\text{CN}$ -EtOH (b). in various ratio of $\text{CH}_3\text{CN}$ -DMSO.....	44
<b>Figure 3.19</b> Fluorescence spectra and of fluorescence enhancement ratio of <b>P2</b> (10 $\mu\text{M}$ ) in $\text{CH}_3\text{CN}$ -DMSO 1:1 and 8:2, v/v upon addition of 10 equiv. of trivalent metal ions ( $\text{Fe}^{3+}$ , $\text{Al}^{3+}$ , $\text{Bi}^{3+}$ and $\text{Cr}^{3+}$ ).....	45
<b>Figure 3.20</b> Fluorescence spectra and fluorescence enhancement ratio of <b>P1-P3</b> (10 $\mu\text{M}$ ) in $\text{CH}_3\text{CN}$ -DMSO (8:2, v/v) before and after addition 10 equiv. of metal ions.....	46
<b>Figure 3.21</b> Interference of other metal ions (10 eq) on <b>P2</b> (10 $\mu\text{M}$ ) in the presence of $\text{Bi}^{3+}$ (10 eq). .....	47
<b>Figure 3.22</b> Fluorescence spectra of <b>P2</b> (10 $\mu\text{M}$ ) in the different concentration of $\text{Bi}^{3+}$ . and relationship between concentration of $\text{Bi}^{3+}$ and fluorescence enhancement ratio of complex.....	47
<b>Figure 3.23</b> Linear Plot between concentration of $\text{Bi}^{3+}$ and fluorescence enhancement ratio of complex with <b>P2</b> (10 $\mu\text{M}$ ). .....	48
<b>Figure 3.24</b> Fluorescence intensity of <b>P2</b> (10 $\mu\text{M}$ ) upon addition 10 equiv. of $\text{Bi}^{3+}$ in $\text{CH}_3\text{CN}$ -DMSO (8:2, v/v) for 30 min. ....	48

<b>Figure 3.25</b> UV-Vis titration of <b>P2</b> (10 $\mu$ M) upon addition of various concentrations of $\text{Bi}^{3+}$ .....	49
<b>Figure 3.26</b> UV-Vis and Fluorescence spectra of the restoration <b>P2</b> in the presence of $\text{Bi}^{3+}$ by $\text{Na}_2\text{S}$ .....	50
<b>Figure 3.27</b> $^1\text{H}$ NMR spectra of <b>P2</b> in $\text{CD}_3\text{OD}$ in the absence and the presence of $\text{Bi}^{3+}$ . .....	51
<b>Figure 3.28</b> Job's plot for determination of binding stoichiometry between <b>P2</b> and $\text{Bi}^{3+}$ .....	51
<b>Figure 3.29</b> UV-Vis spectra and Fluorescence spectra of <b>P2</b> in the presence of water fraction in $\text{CH}_3\text{CN}$ . .....	52
<b>Figure 3.30</b> The variation of fluorescent intensity of <b>P2</b> (10 $\mu$ M) in the absence and presence of 10 equiv. of $\text{Bi}^{3+}$ with difference pH levels (3-9) and fluorescence enhancement ratio in 10% pH-buffers (20 $\mu$ M) in mixed organic solvent $\text{CH}_3\text{CN}$ -DMSO (8:2, v/v).....	53
<b>Figure 3.31</b> The variation of fluorescent intensity of <b>P2</b> (10 $\mu$ M) in the absence and presence of 10 equiv. of $\text{Bi}^{3+}$ and fluorescence enhancement ratio in 10% aqueous solution at various pH (HCl-NaOH) in mixed organic solvent $\text{CH}_3\text{CN}$ -DMSO (8:2, v/v) .	53
<b>Figure 3.32</b> Linear Plot between the concentration of $\text{Bi}^{3+}$ and fluorescence enhancement ratio of <b>P2</b> in 10% (v/v) of pH 5 aqueous solution in mixed organic solvents ( $\text{CH}_3\text{CN}$ -DMSO (8:2, v/v)).....	54
<b>Figure A.1</b> $^1\text{H}$ NMR spectrum of dione in $\text{DMSO-d}_6$ .....	64
<b>Figure A.2</b> $^1\text{H}$ NMR spectrum of <b>P1</b> in $\text{DMSO-d}_6$ .....	64
<b>Figure A.3</b> $^{13}\text{C}$ NMR spectrum of <b>P1</b> in $\text{DMSO-d}_6$ .....	65
<b>Figure A.4</b> MALDI-TOF-Mass spectrum of <b>P1</b> .....	65
<b>Figure A.5</b> $^1\text{H}$ NMR spectrum of <b>P2</b> in $\text{DMSO-d}_6$ .....	66
<b>Figure A.6</b> $^1\text{H}$ - $^1\text{H}$ COSY NMR spectrum of <b>P2</b> in $\text{DMSO-d}_6$ .....	66
<b>Figure A.7</b> $^{13}\text{C}$ NMR spectrum of <b>P2</b> in $\text{DMSO-d}_6$ .....	67

Figure A.8 ESI Mass spectrum of <b>P2</b> .....	67
Figure A.9 $^1\text{H}$ NMR spectrum of <b>P3</b> in $\text{DMSO-d}_6$ .....	68
Figure A.10 $^{13}\text{C}$ NMR spectrum of <b>P3</b> in $\text{DMSO-d}_6$ .....	68
Figure A.11 MALDI-TOF-Mass spectrum of <b>P3</b> .....	69
Figure A.12 $^1\text{H}$ NMR spectrum of <b>P4</b> in $\text{CDCl}_3$ .....	69
Figure A.13 $^{13}\text{C}$ NMR spectrum of <b>P4</b> in $\text{DMSO-d}_6$ .....	70
Figure A.14 MALDI-TOF-Mass spectrum of <b>P4</b> .....	70
Figure A.15 $^1\text{H}$ NMR spectrum of <b>P5</b> in $\text{CDCl}_3$ .....	71
Figure A.16 $^{13}\text{C}$ NMR spectrum of <b>P5</b> in $\text{DMSO-d}_6$ .....	71
Figure A.17 MALDI-TOF-Mass spectrum of <b>P5</b> .....	72



**LIST OF TABLES**

<b>Table 3.1</b> Photophysical properties of molecules .....	36
<b>Table 3.2</b> Solubility product constants ( $K_{sp}$ ) [53].....	43
<b>Table 3.3</b> Quantitative analysis for Bi(III) in real water samples (n=3).....	55
<b>Table 3.4</b> Comparison of the Bi(III) fluorescent sensors .....	56



## LIST OF SCHEMES

Scheme 3.2 Synthesis of pyreno[4,5- <i>d</i> ]imidazole derivatives (P1-P5) .....	29
---	----





## LIST OF ABBREVIATIONS

Ar	aromatic
calcd	calculated
$^{13}\text{C}$ NMR	carbon-13 nuclear magnetic resonance
$\text{CH}_3\text{CN}$	acetonitrile
DMSO	dimethyl sulfoxide
d	doublet (NMR)
dd	doublet of doublet (NMR)
equiv	equivalent (s)
ESI-MS	electrospray ionization mass spectrometry
EtOH	ethanol
FT-IR	fourier transform infrared spectroscopy
g	gram (s)
$^1\text{H}$ NMR	proton nuclear magnetic resonance
Hz	Hertz
h	hour (s)
J	coupling constant
$K_{\text{SP}}$	solubility product constant
MALDI-TOF	matrix assisted laser desorption/ionization-time of flight
mg	milligram (s)
mL	milliliter (s)
mmol	millimole (s)
m/z	mass per charge
m	multiplet (NMR)
M.W.	molecular weight
M	molar

MHz	megahertz
rt	room temperature
s	singlet (NMR)
THF	tetrahydrofuran
TLC	thin layer chromatography
UV	ultraviolet
$\delta$	chemical shift
$^{\circ}\text{C}$	degree Celsius
$\mu\text{L}$	microliter (s)
$\mu\text{M}$	micromolar (s)
$\Phi$	quantum yield
% yield	percentage yield

# CHAPTER I

## INTRODUCTION

### 1.1 Fluorescence

The phenomenon of fluorescence is one of radiative processes. Fluorescence is the emission of light that results from deactivation of excited molecules to lower energy level occurring in highly conjugated molecules or aromatic compounds. The absorption and emission of light in fluorescence process can be classically presented by the Jablonski diagram as shown in Figure 1.1 [1]. This diagram showed electronic and vibrational energy levels. When a molecule absorbed light energy, electron in the molecule were excited to the excitation state ( $S_1$ ) to form excited molecule. The molecule is not stable and will rapidly relax to the lowest vibrational level of the first excited state ( $S_1$ ) via releasing some energy as kinetic energy (rotation or vibration) or thermal energy (heat). This process is non-radiative transition known as geometric relaxation. Then, the molecule will deexcited and return to the ground state ( $S_0$ ) via emission of a longer wavelength photon. The lifetime of fluorescence process takes in nano-second.

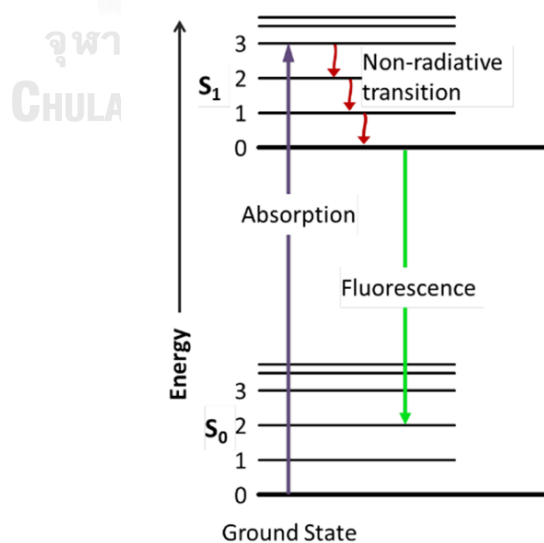


Figure 1.1 Jablonski diagram

## 1.2 Fluorescent sensor

Nowadays, fluorescent sensors play an important role as detection methods in chemical, biological, and environmental fields such as detection of metal ions, anions, and biological molecules in water samples or living cells. Fluorescence technique is a simple method that has several advantages such as high selectivity, high sensitivity, short response time, cost-effectiveness in instrumentation, and non-destructive technique of sample. In general, a fluorescent sensor consists of two components: one is a unit for selective binding with analyte of interest that is called “receptor” and the other is “reporter” that translates the signal changing. The reporter of fluorescent sensor is called “fluorophore”. The response of fluorophore can be read-out from changing of fluorescence intensities or emission wavelengths as turn-on fluorescence, turn-off fluorescence or wavelength shift (ratiometric sensor) [2] as shown in Figure 1.2.

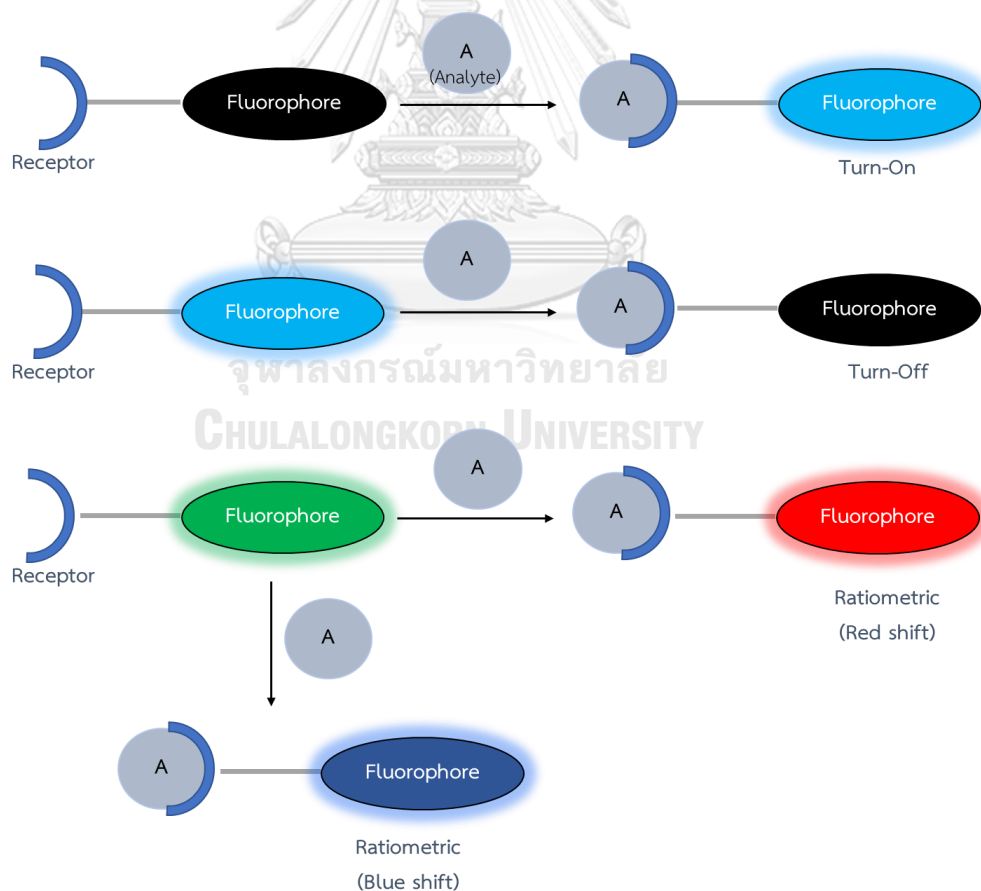


Figure 1.2 Modes of fluorescent sensors

### 1.3 Sensing Mechanisms

The photophysical signaling mechanisms between interaction or reaction of analyte and receptor which could be explained by the photoinduced electron transfer (PET) [3-7], fluorescence resonance energy transfer (FRET) [5,7-11], Intermolecular charge transfer (ICT) [5,12-15], excited-state intramolecular proton transfer (ESIPT) [12,13,16-20], structure isomerization, aggregation-induced enhancement fluorescence (AIE) [21-24], aggregation-caused quenching (ACQ) [22,23,25,26] and excimer formation [27]. Therefore, fluorescent sensors could be designed on one or more than one sensing mechanism which related to the responding of fluorophore. In this work, the sensing compounds will be designed based on ESIPT and PET process.

#### Photo-induced electron transfer (PET)

Photo-induced electron transfer (PET) is fluorescence quenching process that can occur when either the highest occupied molecular orbital (HOMO) or the lowest unoccupied molecular orbital (LUMO) level of receptor or analyte is located between the HOMO-LUMO gap of fluorophore. The first case, a fluorescent compound can act as an electron acceptor since the HOMO level of fluorophore is lower than the HOMO level of binding site (Figure 1.3A). After an electron of the fluorophore was excited, one of the electrons at the HOMO level of the donor (receptor or analyte) will be transferred to the singly occupied HOMO of the fluorophore. As the results of the proton transfer process, it precludes the releasing of energy from LUMO to HOMO for fluorophore, so the fluorescence process is inhibited. The other case, a fluorescent compound acts as an electron donor for the LUMO level of receptor or analyte and the HOMO-LUMO gap of fluorophore are shown in Figure 1.3B. In this case, an excited electron at the LUMO level of the fluorophore will be transferred to the empty LUMO of the receptor or analyte resulting in the return to the ground state but it is non-radiative process.

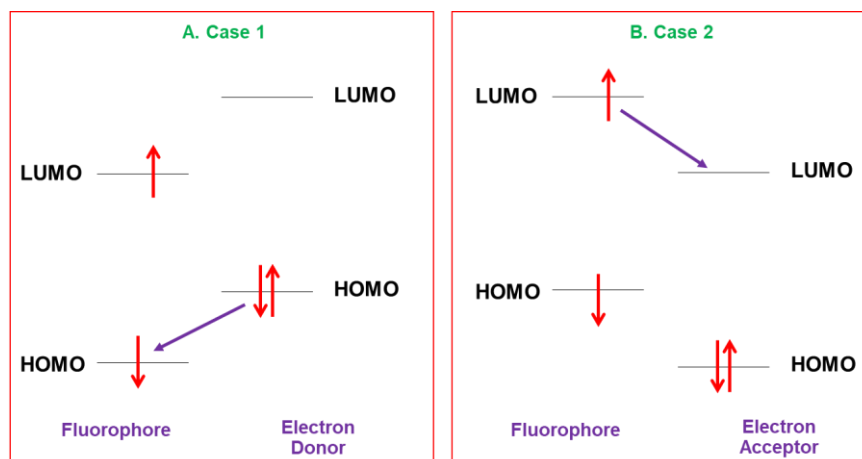


**Figure 1.3** Principle of photo-induced electron transfer (PET) effect.

#### Excited state intramolecular proton transfer (ESIPT)

Excited state intramolecular proton transfer (ESIPT) is generally occurred for suitable organic compounds containing both a basic site or hydrogen bond acceptor such as carbonyl group, ( $-C=O$ ) or imine nitrogen ( $=N-$ ) and a protic group or hydrogen bond donor such as hydroxyl ( $-OH$ ), amino ( $-NH_2$ ) or thiol group ( $-SH$ ) that forms a fast process of an intramolecular hydrogen bond. The classical model of ESIPT photophysical process was demonstrated by 2-(2'-hydroxyphenyl) benzoxazole (HBO), -benzothiazole (HBT) and -benzimidazole (HBI) as illustrated in Figure 1.4 [16,28]. After photoexcitation, the excited state enol form ( $E_c^*$ ) is converted to its excited state keto form ( $K^*$ ) in the picosecond time scale. The significantly red shift emission and unusually large Stoke shift can be observed for ESIPT molecule. A large Stoke shift is useful in fluorescence sensing to keep away from the inner filter or the self-absorption effect.

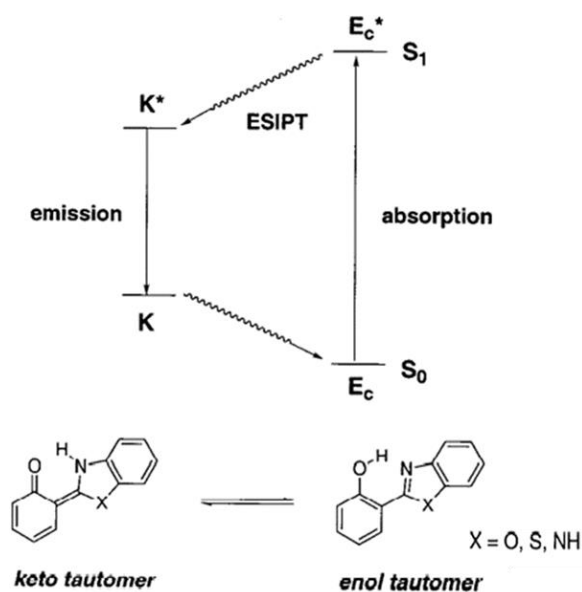


**Figure 1.4** Principle of Excited state intramolecular proton transfer (ES IPT) process

#### 1.4 Fluorescent sensors based on Pyreno[4,5-*d*]imidazole

To design and synthesize new molecules based on pyrene as the reactant because of its photophysical properties. Pyrene is a polycyclic aromatic which has been widely used for organic electronics, for examples, to make field-effect transistors and organic light-emitting diodes (OLEDs) [29-31]. It is also capable as fluorophores due to its emission wavelength in the visible region, long fluorescence lifetime and high fluorescence quantum yield [32-35]. Moreover, it could be connected and modified to different binding unit. The position of pyrene molecule could be easy to modify by electrophilic aromatic substitution reaction at position 1, 3, 6, and 8 and addition of steric hindrance to molecule could be substituted at position 2 and 7 [36,37]. Moreover, position 4, 5, 9, and 10 could be oxidized to diones or tetrone depending on the reagents, equivalents of oxidizing reagent and time of reaction (Figure 1.5) [38-40].

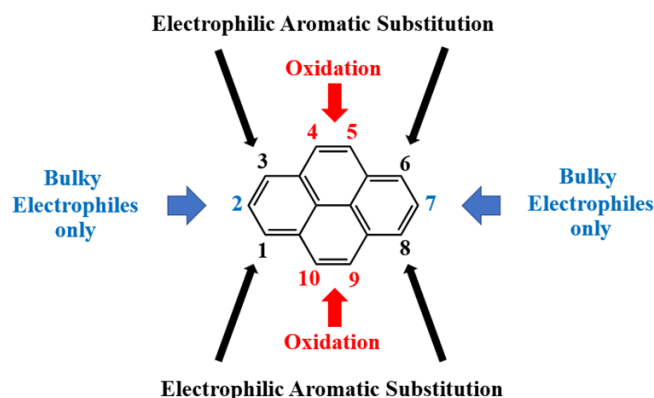


**Figure 1.5** The reactions on positions of pyrene

For the connecting unit is an imidazole fragment that contains N and H atom which play an essential role in an intramolecular and intermolecular interactions such as hydrogen bond, metal-organic coordination, excited state intramolecular proton transfer (ESIPT), or concerted proton-electron transfer (CPET) [41]. Thus, many researchers are interested to use imidazole part for design the fluorescent sensor.

In 2011, Ju and co-worker [42] synthesized 2-(1-phenyl-1*H*-benzo[d]imidazol-2-yl)phenol (HBIZ) for sensing zinc ( $Zn^{2+}$ ). The results found that the fluorescence intensity of molecule was increased by addition of  $Zn^{2+}$  and  $Mg^{2+}$  in 120 and 15 folds, respectively (Figure 1.6a). The complexation of  $Zn^{2+}$  and HBIZ was 1:1 stoichiometry that was investigated by Job's plot. However, the coexist of other metal ions such as  $Cu^{2+}$ ,  $Fe^{2+}$ ,  $Ni^{2+}$  could be quenched the fluorescence intensities (Figure 1.6b).

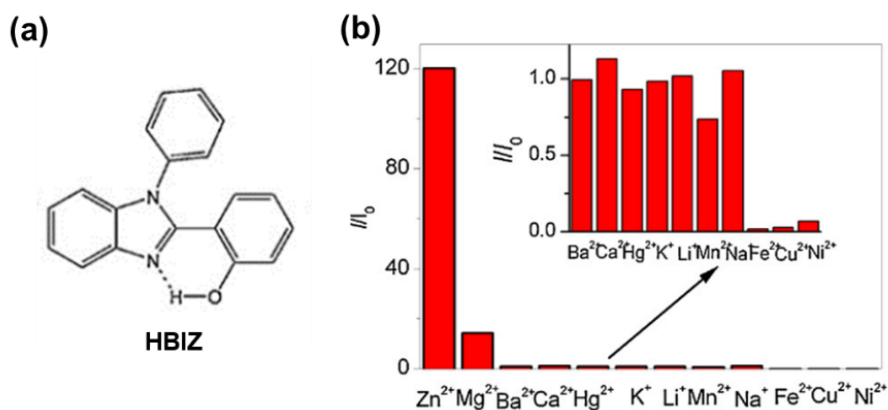


**Figure 1.6** (a) Structure of HBIZ; (b) The fluorescence ratio of HBIZ (50  $\mu$ M) in the presence of various metal ions (10  $\mu$ M) in *N,N*-Dimethylformamide,  $\lambda_{ex} = 330$  nm.



In 2014, Zhang et al. developed derivative of 3-(4,5-diphenyl-1*H*-imidazol-2-yl)naphthalen-2-ol (DPIN) as fluorescent sensor displaying the ESIPT process [19]. The hydroxyl group of DPIN was conjugated with acryloyl group to DPIN-A (Figure 1.7a) that can react with biothiols (glutathione (GSH), cysteine (Cys), homocysteine (Hcy)). The result showed high selectivity and sensitivity to detection of cys in water (Figure 1.7b).

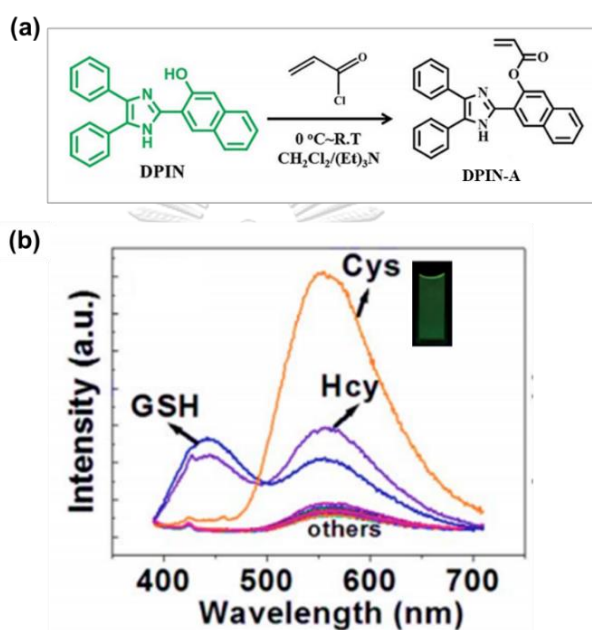


**Figure 1.7** (a) Synthesis of DPIN-A.; (b) Fluorescent spectra of DPIN-A (10 mM) in pure water (PBS buffer, pH =7.2) towards biothiols (10 eq of GSH, Cys, Hcy.) were obtained after 30 min and other amino acids (100 eq.) were recorded after 1 hour.),  $\lambda_{\text{ex}} = 371$  nm.

In 2015, Hu and co-worker designed and developed fluorescent sensor without sulfur atom (S) in the molecule to sensing mercury ions ( $\text{Hg}^{2+}$ ) [43]. The sensor (L) was designed based on the benzimidazole group as recognition group and the quinoline group as a fluorophore group. The sensor was selectively quenched by  $\text{Hg}^{2+}$  in water- dimethyl sulfoxide (DMSO) (1:9, v/v) through concerted proton-electron transfer (CPEF) process (Figure 1.8b). The binding between sensor L and  $\text{Hg}^{2+}$  was presented to form a stable complex  $[\text{L} + \text{Hg}^{2+} + 2\text{H}_2\text{O}]$  in Figure 1.8a that was investigated by  $^1\text{H}$  NMR titration, IR spectra and mass spectrum.

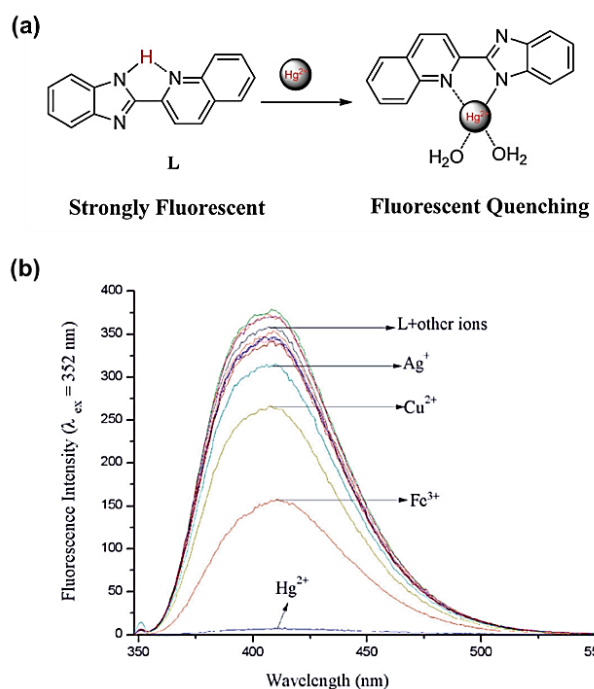


**Figure 1.8** (a) Possible sensing mechanism of sensor **L** and  $\text{Hg}^{2+}$ ; (b) Fluorescence spectra of **L** ( $20 \mu\text{M}$ ) towards various metal ions (10 equiv.) in  $\text{H}_2\text{O}$ -DMSO (1:9, v/v) ( $\lambda_{\text{ex}} = 325 \text{ nm}$ ).

Based on previous research, small aromatic rings such as benzene or naphthalene compounds were acted to fluorophore. In 2016, phenanthrene, a large aromatic compound, were used as fluorophore connecting with imidazole moiety. For instance, a ratiometric fluorescent sensor based on ESIPT mechanism between phenolic (-OH) and imidazole nitrogen (C=N) was developed by Shinha and co-worker [44]. The sensor **1H** was selective with aluminum ions ( $\text{Al}^{3+}$ ) in  $\text{CH}_3\text{CN}$ - $\text{H}_2\text{O}$  (1:9, v/v) about sixfold enhancement in fluorescence intensity and a blue-shift from 445 to 412 and 430 nm. The possible binding mechanism was shown in Figure 1.9a. However, the large concentration of chromium ions ( $\text{Cr}^{3+}$ ) and indium ions ( $\text{In}^{3+}$ ) was very small increased fluorescence intensity and copper ions ( $\text{Cu}^{2+}$ ) could affect to quench the fluorescence intensity of **1H** due to its paramagnetic property as shown in Figure 1.9b.

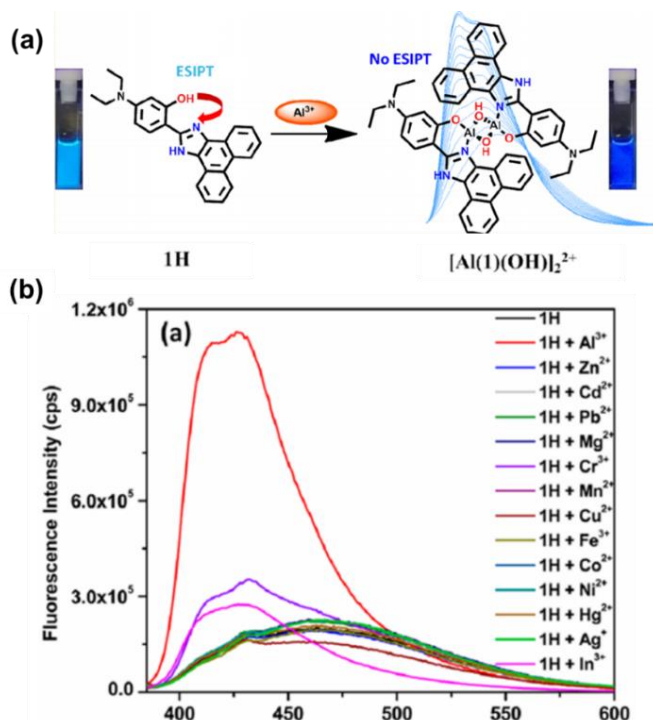


**Figure 1.9** (a) Possible binding mechanism between **1H** and  $\text{Al}^{3+}$ ; (b) Fluorescence spectra of **1H** (2.5  $\mu\text{M}$ ) towards various metal ions (10 equiv.) in  $\text{CH}_3\text{CN}/\text{H}_2\text{O}$  (1:9, v/v),  $\lambda_{\text{ex}} = 375 \text{ nm}$ .

Moreover, in 2017, Cheng et al. synthesized a novel fluorescent sensor (Probe **1**) based on phenanthro-imidazole connecting with a *N,N*-bis(pyridin-2-ylmethyl) benzeneamine unit that was a binding site for detection of copper ions ( $\text{Cu}^{2+}$ ) (Figure 1.10a). Upon addition of  $\text{Cu}^{2+}$ , the fluorescence sensing was quenched through the electron charge transfer (CT) process based on 1:1 stoichiometry binding. The sensing was also highly and quickly selective towards  $\text{Cu}^{2+}$  in ethanol (EtOH) without significant influence from other metal ions as presented in Figure 1.10b. The low detection limit was 1.77 ppb.

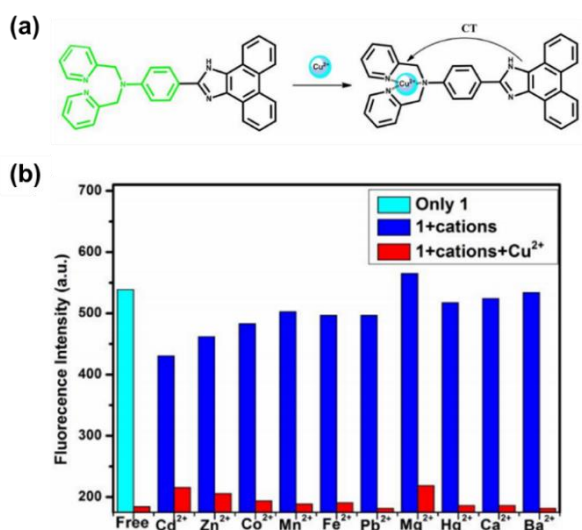


**Figure 1.10** (a) Binding mechanism of Probe 1 with  $\text{Cu}^{2+}$  undergo CT process.; (b) Fluorescence intensity of Probe 1 (10  $\mu\text{M}$ ) without metal ions (**Green**), in the presence of various metal ions (1 equiv.) (**Blue**), and with 10  $\mu\text{M}$  of  $\text{Cu}^{2+}$  in the presence of other metal ions (**Red**),  $\lambda_{\text{em}} = 387 \text{ nm}$ .

In the same year, Chen et al. [45] designed a three-components fluorescent probe (PAN-Bn-PB), phenanthroline-imidazole, benzonitrile, and phenyl boronate, based on an intramolecular charge transfer (ICT) process for sensing hydrogen peroxide ( $\text{H}_2\text{O}_2$ ) in vitro and in vivo. The turn-on fluorescence sensor was good selectivity and sensitivity to detecting  $\text{H}_2\text{O}_2$  in several minutes. However, it could not be perfect probe for  $\text{H}_2\text{O}_2$  in vivo because its emission wavelength was blue.

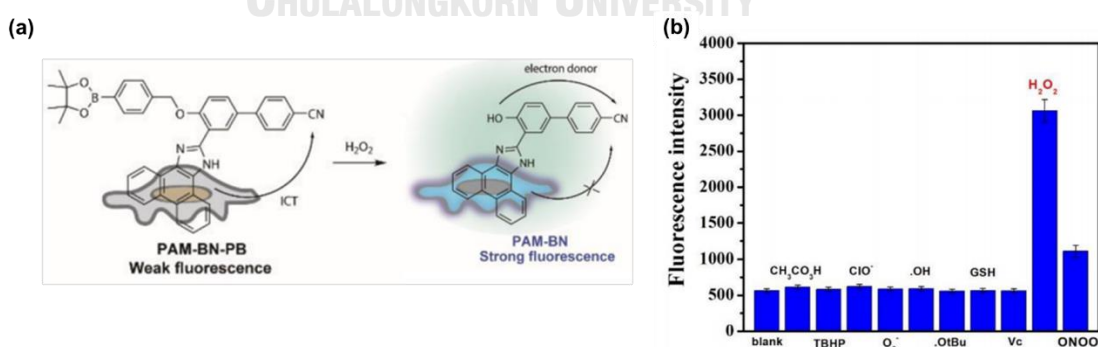


**Figure 1.11** (a) Sensing mechanism of PAN-Bn-PB with  $\text{H}_2\text{O}_2$ .; (b) Fluorescence intensity of PAN-Bn-PB (10  $\mu\text{M}$ ) in various molecules that could exist in biological system (200  $\mu\text{M}$ ).

Recently, Li and co-worker [12] synthesized and designed a pH fluorescence probe (PIF) from phenanthrol-imidazole connect with fluorescein by a hydroxyl phenyl imine group based on ES IPT and ICT process (Figure 1.12). The pH sensing of PIF is capable to respond pH from 6.5 to 9.5 without interference of cations and anions.

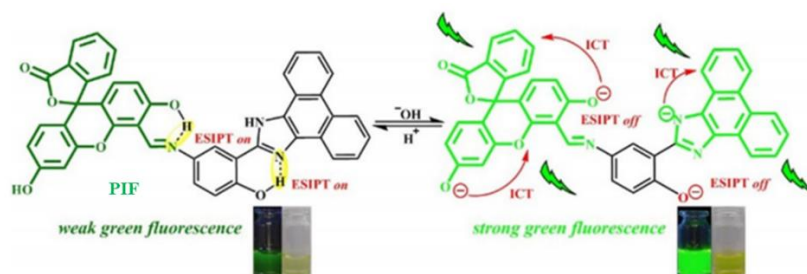


**Figure 1.12** Proposed sensing mechanism of PIF in acid-base conditions.

For pyreno[4,5-*d*]imidazole derivatives, in 2013, Liu et al [46] reported the properties of a novel skeleton containing pyrene and imidazole units that was synthesized in one step. The results found that both PyDPI and PyDCzl were stable in high thermal and showed deep-blue emission in solution. Furthermore, both molecules tended to aggregate into thin films and crystallize as powders. These properties could be applied to use in material field, for examples, organic light emitting diodes (OLEDs) or dye-sensitized solar cells (DSSCs).

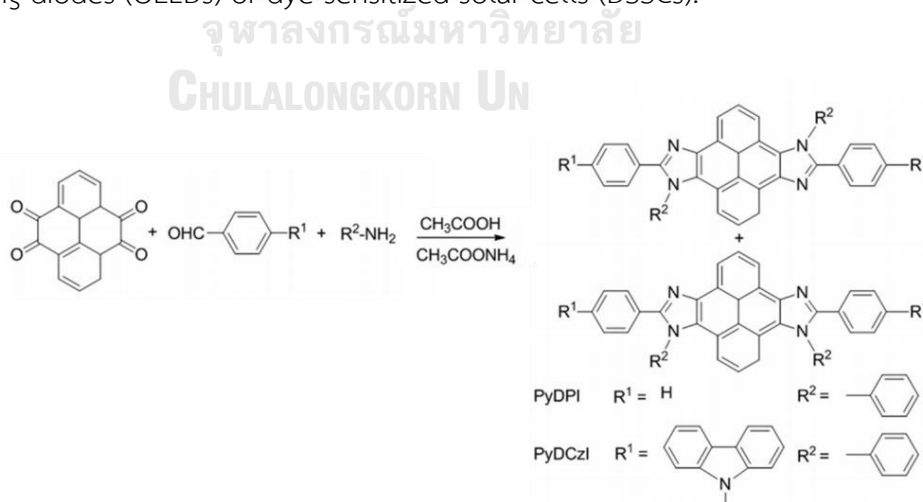


**Figure 1.13** The one-step to synthesis of pyrene–imidazole skeletons.

Nevertheless, a few researches developed pyreno[4,5-*d*]imidazole derivatives to fluorescent sensor for sensing anions such as cyanide sensor, fluoride sensors.

In 2015, 10-(1-*H*-imidazole-2-yl)-9*H*-pyreno[4,5-*d*]imidazole (Py-BiimzH<sub>2</sub>) was synthesized by Mardanya et al. [47,48] that was studied to sensing anions. Upon addition of various anions to Py-BiimzH<sub>2</sub>, it was selective to sensing cyanide ions (CN<sup>-</sup>) and fluoride ions (F<sup>-</sup>) in DMSO. The detection limits were calculated to  $1.70 \times 10^{-7}$  M. for CN<sup>-</sup> and  $1.54 \times 10^{-7}$  M. for F<sup>-</sup>. However, in aqueous medium, only CN<sup>-</sup> was enhanced fluorescence intensity at 475 nm. in H<sub>2</sub>O–DMSO (9:1, v/v) as shown in Figure 1.14. It might be CN<sup>-</sup> is a stronger base than F<sup>-</sup> in aqueous solution. The detection limit was  $1.04 \times 10^{-6}$  M in aqueous solution.

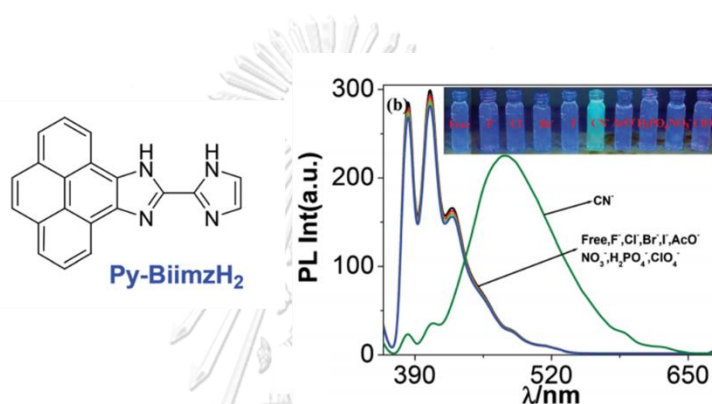


**Figure 1.14** Structure of Py-BiimzH<sub>2</sub> and luminescence spectra of Py-BiimzH<sub>2</sub> upon addition of various anions as their tetrabutylammonium (TBA) salts (300 equiv.) in H<sub>2</sub>O–DMSO (9:1, v/v),  $\lambda_{ec} = 350$  nm [47].

In the same year, Mardanya and co-worker also developed high selectivity of fluorogenic sensors for cyanide ions in aqueous solution, the two complexation between Ru(II) or Os(II) with Py-BiimzH<sub>2</sub> and 2,2'-bipyridine was synthesized to form [(bpy)<sub>2</sub>Ru(Py-BiimzH<sub>2</sub>)](ClO<sub>4</sub>)·H<sub>2</sub>O (**A**) and [(bpy)<sub>2</sub>Os(Py-BiimzH<sub>2</sub>)](ClO<sub>4</sub>)·H<sub>2</sub>O (**B**). Quenching luminescence intensity was observed upon addition of CN<sup>-</sup> for both sensors (Figure 1.15). Both complexes were high selectivity to detection of CN<sup>-</sup> in aqueous media in the presence of various anions. The detection limit of **1** and **2** to CN<sup>-</sup> in aqueous media was determined to be  $1.03 \times 10^{-8}$  M and  $1.24 \times 10^{-8}$  M, respectively.



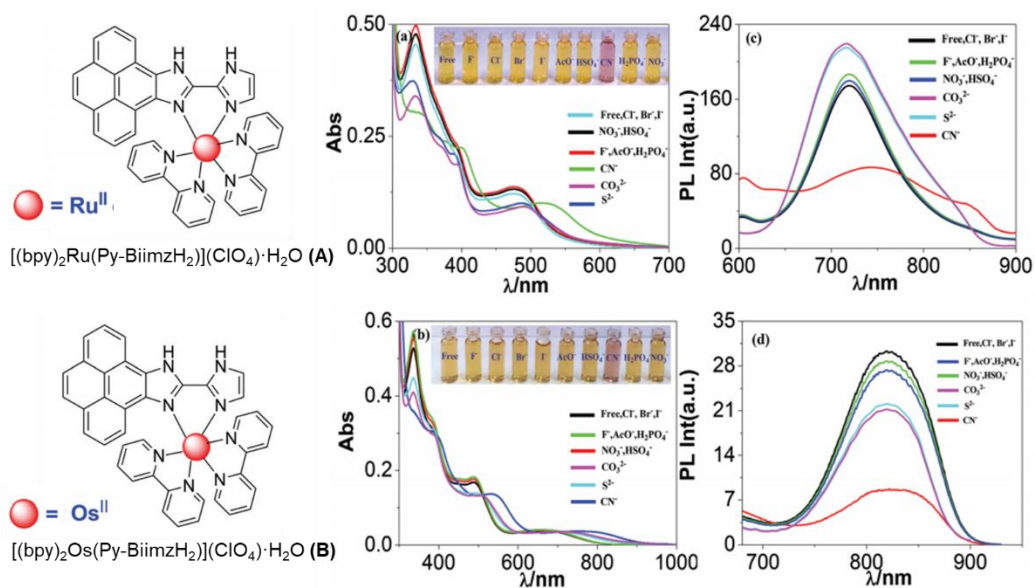


**Figure 1.15** UV-Vis spectra and luminescence spectra of complex A and B upon addition of various anions as their tetrabutylammonium (TBA) or sodium salts (300 equiv.) in pure water (HEPES buffer, pH = 7) [48].

In addition, Mardanya and co-worker [49] studied and synthesized the new complexation of  $Ru^{2+}$  (C) and  $Os^{2+}$  (D) with 10-pyridin-2-yl-9H-9,11-diazacyclopenta[e]pyrene (HlmzPPy) and 2,2'-bipyridine. The complexes could be enhanced intensity as turn-on luminescence for sensing dihydrogen phosphate ions ( $H_2PO_4^-$ ) resulting from the interaction of hydrogen-bonding between NH proton of imidazole and  $H_2PO_4^-$  and quenched intensity as turn-off luminescence for sensing fluoride ions ( $F^-$ ) and acetate ions ( $AcO^-$ ) resulting from the deprotonation of NH proton of imidazole. The range of detection limit of 1 and 2 to each anion was calculated about  $10^{-9}$  M as shown in (Figure 1.16).

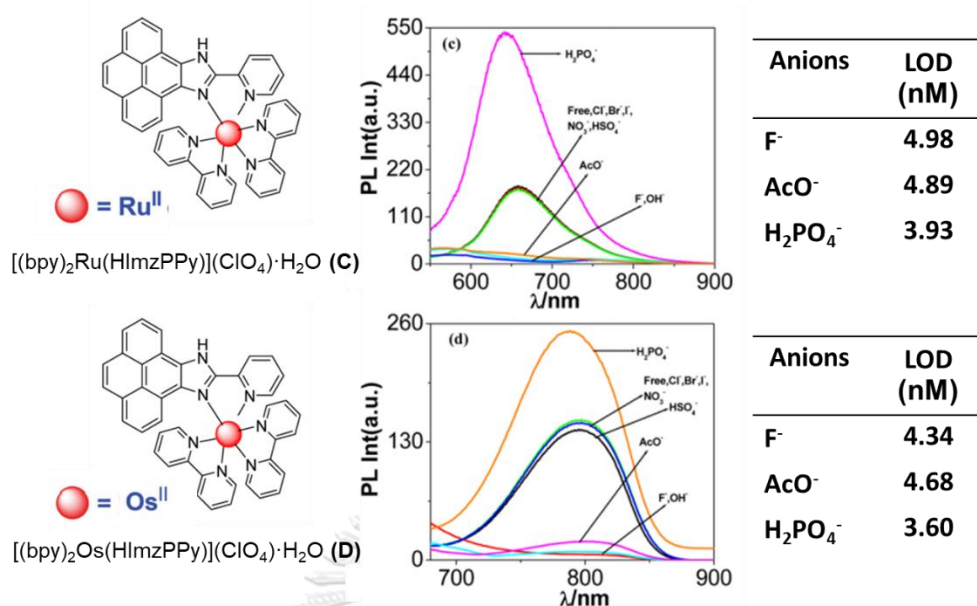


**Figure 1.16** Luminescence spectra of complex **C** and **D** upon addition of various anions as their tetrabutylammonium (TBA) in CH<sub>3</sub>CN.

In recently, Tabasi et al. [50] synthesized and studied the two isomers of (9*H*-pyreno[4,5-*d*]imidazol-10-yl)-benzaldehyde, para (**4**) and meta (**5**) isomers. The para isomer acts as ratiometric fluorescent sensor which could be reacted with fluoride ions (F<sup>-</sup>) in polar solvents (acetone and DMSO) undergo ICT process. (Figure 1.17)

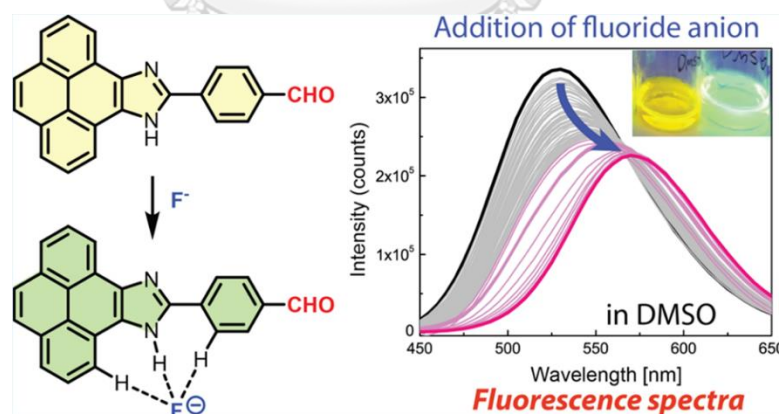


**Figure 1.17** Proposed mechanism and fluorescence titration of (9*H*-pyreno[4,5-*d*]imidazol10-yl)-benzaldehyde in DMSO.

From the literatures, it could be support to design and synthesize new derivative of pyreno[4,5-*d*]imidazole in order to fluorescent sensor to detection of



metal ions, anions or other analytes because of a few research using this derivatives as fluorescence sensor.

### 1.5 Objective of this research

To this end, we designed about five pyreno[4,5-*d*]imidazole derivatives (**P1-P5**), (Figure 1.18) and aim to use them as specific fluorescent sensors for metal ions . The five compounds contain different type of aromatic ring that can provide information on mechanism of sensing such as the Excited State Intramolecular Proton Transfer (ESIPT) or photo-induced electron transfer (PET).

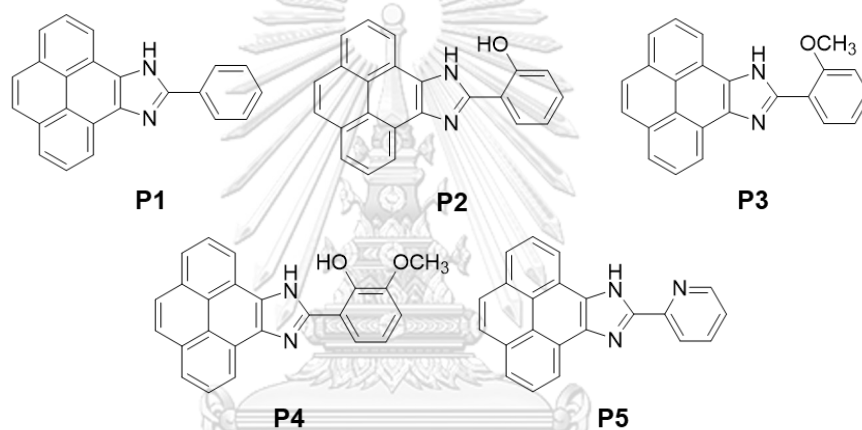


Figure 1.18 Target molecules P1-P5

## CHAPTER II

### EXPERIMENTAL

#### 2.1 Materials and Chemicals

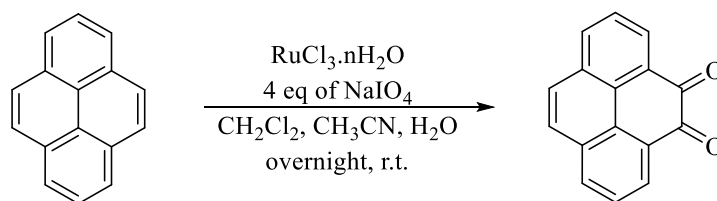
All reagents used in reactions were analytical grade purchased from Sigma-Aldrich (USA), Merck (Germany) or Fluka (Switzerland). Solvents for extraction and chromatography such as dichloromethane (CH<sub>2</sub>Cl<sub>2</sub>), hexanes, ethyl acetate (EtOAc) and methanol (CH<sub>3</sub>OH) were commercial grade and used without further purification. All column chromatography was operated using Merck silica gel 60 (70–230 mesh) and Thin layer chromatography (TLC) was performed on silica gel plates (Merck F245). The stock solutions of the 3 compounds, 10-phenyl-9H-pyreno[4,5-*d*]imidazole (**P1**), 2-(9H-pyreno[4,5-*d*]imidazol-10-yl)phenol (**P2**) and 10-(2-methoxyphenyl)-9H-pyreno[4,5-*d*]imidazole (**P3**), were prepared at 1 mM in acetonitrile (CH<sub>3</sub>CN) that were used as fluorescent sensors and at 1 mM in ethanol (EtOH) that were used for studies the photophysical properties.

#### 2.2 Analytical instruments

The target molecules were characterized by MALDI-TOF mass spectrometer (Bruker Daltonics) using  $\alpha$ -cyano-4-hydroxycinnamic acid (CCA) as a matrix. All <sup>1</sup>H-NMR spectra were acquired from sample solution in Deuterated NMR solvents such as CDCl<sub>3</sub>, DMSO-D<sub>6</sub>, D<sub>2</sub>O and CD<sub>3</sub>CN, on Varian Mercury 400 MHz and Jeol 500 MHz. <sup>13</sup>C-NMR spectra were acquired using Bruker at 100 MHz. The UV-Vis absorption spectra were obtained from a Varian Cary 50 UV-vis spectrophotometer (Varian, USA) and the fluorescence emission spectra were recorded on a Varian Cary Eclipse spectrofluorometer (Varian, USA).

#### 2.3 Synthesis and characterization

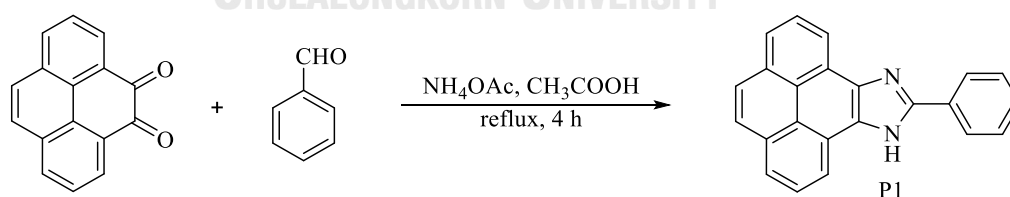
##### 2.3.1 Pyrene-4,5-diones (**1**)



To the solution of pyrene (2.02g, 10 mmol) was dissolved in a 1:1 mixture of  $\text{CH}_2\text{Cl}_2$  (40 mL) and  $\text{CH}_3\text{CN}$  (40 mL), then  $\text{RuCl}_3 \cdot n\text{H}_2\text{O}$  (0.20 g, 0.96 mmol) was mixed to the solution. After that,  $\text{NaIO}_4$  (10.00 g, 46.8 mmol) and  $\text{H}_2\text{O}$  (50 mL) were added. The reaction was stirred overnight at room temperature. The mixture was poured into  $\text{H}_2\text{O}$  (500 mL). The organic phase was separated and the aqueous phase was extracted with  $\text{CH}_2\text{Cl}_2$  (50 mL) 3 times. The combined organic phases were washed with  $\text{H}_2\text{O}$  (200 mL) 3 times and dried over anhydrous  $\text{Na}_2\text{SO}_4$  to give an orange solution. The solvent was removed under reduced pressure to give a dark orange solid which was purified by column chromatography using  $\text{CH}_2\text{Cl}_2$ . The product was obtained as bright orange crystal in 1.6302 g, 70% yield.  $^1\text{H-NMR}$  (400 MHz,  $\text{CDCl}_3$ )  $\delta$  8.47 (dd,  $J = 7.4, 1.1$  Hz, 2H), 8.16 (dd,  $J = 8.0, 1.2$  Hz, 2H), 7.82 (s, 2H), 7.76 (t,  $J = 7.7$  Hz, 2H).

### 2.3.2 Pyreno[4,5-*d*]imidazole derivatives (P1-P5)

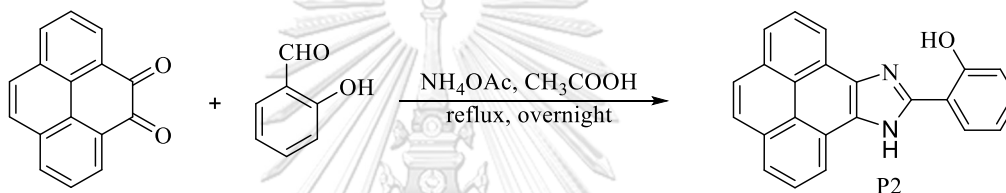
#### 2.3.2.1 10-phenyl-9*H*-pyreno[4,5-*d*]imidazole (P1)



To a mixture of dione **1** (0.23 g, 1 mmol) and benzaldehyde (0.13 g, 1.2 mmol) in  $\text{CH}_3\text{COOH}$  (10 mL) was added ammonium acetate (0.54 g, 7.5 mmol). The reaction was refluxed for 4 h to form a yellow precipitate. The mixture was cooled and poured into ice- $\text{H}_2\text{O}$  mixture (10 mL) to remove soluble salt and facilitate a complete precipitate. The solid crude product was filtrated, washed with water, and

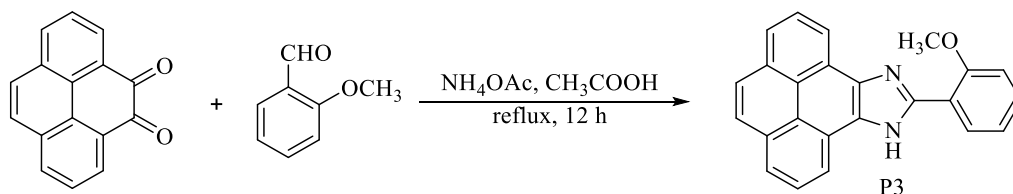
dried by suction. The yellow solid was purified by column chromatography using 20-25% ethyl acetate in hexanes. 10-Phenyl-9*H*-pyreno[4,5-*d*]imidazole (**P1**) was obtained as a yellow solid in 75% yield. <sup>1</sup>H-NMR (400 MHz, DMSO-*d*<sub>6</sub>)  $\delta$  ppm 13.84 (s, br, NH), 8.85 (d, *J* = 7.5 Hz, 2H), 8.40 (d, *J* = 7.5 Hz, 2H), 8.27 (d, *J* = 7.4 Hz, 2H), 8.21 (s, 2H), 8.17 (t, *J* = 7.6 Hz, 2H), 7.65 (t, *J* = 7.6 Hz, 2H), 7.54 (t, *J* = 7.3 Hz, 1H); <sup>13</sup>C-NMR (100 MHz, DMSO-*d*<sub>6</sub>)  $\delta$  149.41, 133.5, 130.35, 129.32, 128.96, 126.22, 124.13, 121.77, 118.97; MS (MALDI-TOF) Calcd for C<sub>23</sub>H<sub>14</sub>N [M<sup>+</sup>]: 318.116; found: 318.027.

### 2.3.2.2 2-(9*H*-pyreno[4,5-*d*]imidazol-10-yl)phenol (**P2**)



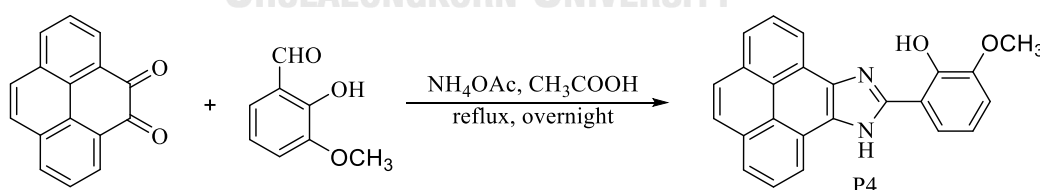
To a mixture of dione **1** (0.23 g, 1 mmol) and salicylaldehyde (0.15 g, 1.2 mmol) in CH<sub>3</sub>COOH (10 mL) was added ammonium acetate (0.54 g, 7.5 mmol). The reaction was refluxed overnight to form a yellow-orange precipitate. The mixture was cooled and poured into ice-H<sub>2</sub>O mixture (10 mL) to remove soluble salt and facilitate a complete precipitate. The solid crude product was filtrated, washed with water, and dried by suction. The orange solid was purified by column chromatography using dichloromethane. 2-(9*H*-Pyreno[4,5-*d*]imidazol-10-yl)phenol (**P2**) was obtained as bright orange solid in 55% yield. <sup>1</sup>H-NMR (400 MHz, DMSO-*d*<sub>6</sub>)  $\delta$  ppm 13.99(s, OH), 13.21 (s, NH), 8.87 (d, *J* = 7.6 Hz, 2H), 8.78 (d, *J* = 7.6 Hz, 2H), 8.32 (d, *J* = 7.6 Hz, 1H), 8.23 (s, 2H), 8.19 (t, *J* = 6.9 Hz, 2H), 7.44 (t, *J* = 7.7 Hz, 1H), 7.16– 7.11 (m, 2H); <sup>13</sup>C-NMR (100 MHz, DMSO-*d*<sub>6</sub>)  $\delta$  157.44, 149.56, 131.51, 131.18, 127.67, 126.46, 125.89, 124.62, 121.83, 119.13, 117.22, 112.98; MS (ESI) Calcd C<sub>23</sub>H<sub>14</sub>N<sub>2</sub>O [M+H]: 335.12; found: 335.02.

### 2.3.2.3 10-(2-methoxyphenyl)-9*H*-pyreno[4,5-*d*]imidazole (**P3**)



To a mixture of dione 1 (0.23 g, 1 mmol) and 2-methoxybenzaldehyde (0.20 g, 1.5 mmol) in  $\text{CH}_3\text{COOH}$  (10 mL) was added ammonium acetate (0.54 g, 7.5 mmol). The reaction was refluxed for 12 h to form an orange precipitate. The mixture was cooled and poured into ice- $\text{H}_2\text{O}$  mixture (10 mL) to remove soluble salt and facilitate a complete precipitate. The solid crude product was filtrated, washed with water, and dried by suction. The orange solid was purified by column chromatography using 20-25% ethyl acetate in hexanes. 10-(2-Methoxyphenyl)-9H-pyreno[4,5-*d*]imidazole (**P3**) was obtained as dark orange solid in 86 %yield.  $^1\text{H-NMR}$  (400 MHz,  $\text{DMSO-d}_6$ )  $\delta$  ppm 13.07 (s, br, NH), 8.91 (d,  $J = 7.5$  Hz, 2H), 8.31 (d,  $J = 6.8$  Hz, 1H), 8.25 (d,  $J = 7.6$  Hz, 2H), 8.21 (s, 2H), 8.13 (t,  $J = 7.6$  Hz, 2H), 7.54 (t,  $J = 7.2$  Hz, 1H), 7.31 (d,  $J = 8.3$  Hz, 1H), 7.20 (t,  $J = 7.4$  Hz, 1H), 4.08 (s, 3H);  $^{13}\text{C-NMR}$  (100 MHz,  $\text{DMSO-d}_6$ )  $\delta$  156.79, 147.39, 131.65, 131.13, 130.31, 127.80, 126.33, 124.26, 121.92, 121.02, 119.41, 112.12, 56.11; MS (MALDI-TOF) Calcd  $\text{C}_{24}\text{H}_{16}\text{N}_2\text{O}$  [ $\text{M}^+$ ]: 348.126; found: 348.716.

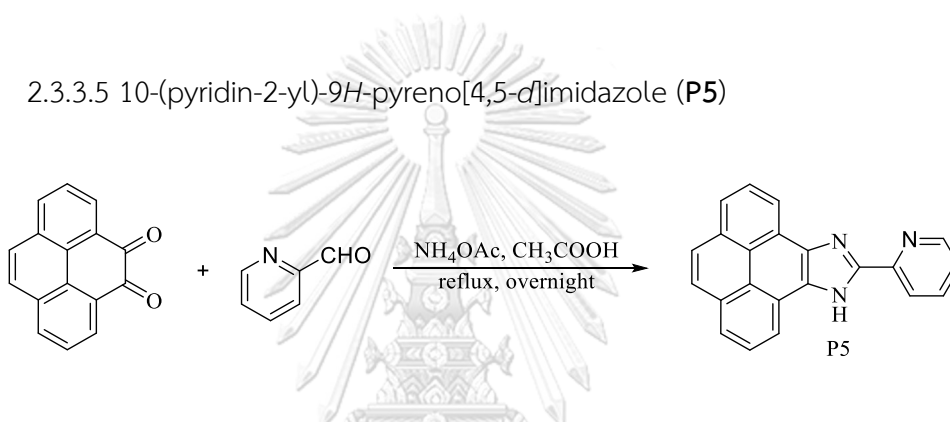
#### 2.3.2.4 2-methoxy-6-(9H-pyreno[4,5-*d*]imidazol-10-yl)phenol (**P4**)



To a mixture of dione 1 (0.23 g, 1 mmol) and *o*-vanillin or 2-hydroxy-3-methoxybenzaldehyde (0.23 g, 1 mmol) in  $\text{CH}_3\text{COOH}$  (10 mL) was added ammonium acetate (0.54 g, 7.5 mmol). The reaction was refluxed overnight to form a precipitate. The mixture was cooled and poured into ice- $\text{H}_2\text{O}$  mixture (10 mL) to remove soluble salt and facilitate a complete precipitate. The solid crude product was filtrated,

washed with water, and dried by suction. The yellow solid was purified by column chromatography using 20-25% ethyl acetate in hexanes. 2-methoxy-6-(9*H*-pyreno[4,5-*d*]imidazol-10-yl)phenol (**P4**) was obtained as light yellow solid in 0.0463 g, 13% yield.  $^1\text{H-NMR}$  (400 MHz,  $\text{CDCl}_3$ )  $\delta$  ppm 8.74 (d,  $J = 6.1$  Hz, 2H), 8.31 (d,  $J = 4.8$  Hz, 1H), 8.25 (m, br, 2H), 8.09 (m, br, 3H), 7.87 (m, 2H), 7.01 (m, 2H), 4.02 (s, 3H);  $^{13}\text{C-NMR}$  (100 MHz,  $\text{DMSO-d}_6$ )  $\delta$  157.19, 150.61, 149.44, 149.22, 132.06, 128.27, 127.03, 125.09, 122.34, 119.63, 119.21, 118.01, 114.03, 113.72, 56.37 ppm; MS (MALDI-TOF) Calcd  $\text{C}_{24}\text{H}_{16}\text{N}_2\text{O}_2$  [ $\text{M}^+$ ]: 364.121; found: 364.024.

#### 2.3.3.5 10-(pyridin-2-yl)-9*H*-pyreno[4,5-*d*]imidazole (**P5**)



To a mixture of dione 1 (0.23 g, 1 mmol) and picolinaldehyde (0.16 g, 1.5 mmol) in  $\text{CH}_3\text{COOH}$  (10 mL) was added ammonium acetate (0.54 g, 7.5 mmol). The reaction was refluxed overnight to form a precipitate. The reaction was followed by TLC. A green solution was obtained. After that, the mixture was cooled and poured into ice- $\text{H}_2\text{O}$  mixture (10 mL) to remove soluble salt and facilitate a complete precipitate. The solid crude product was filtrated, washed with water, and dried by suction. The yellow solid was purified by column chromatography using 1-10% v/v of  $\text{CH}_2\text{Cl}_2$  – MeOH. 10-(pyridin-2-yl)-9*H*-pyreno[4,5-*d*]imidazole was obtained as yellowed solid in only 0.0460 g, 15% yield.  $^1\text{H NMR}$  (400 MHz,  $\text{CDCl}_3$ )  $\delta$  13.04 (br, NH), 8.92 (d,  $J = 3.1$  Hz, 2H), 8.68 (d,  $J = 7.2$  Hz, 1H), 8.52 (d,  $J = 7.5$  Hz, 1H), 8.21 (m, 2H), 8.14 – 8.05 (m, 4H), 8.00 – 7.95 (m, 1H) 7.52 – 7.46 (m, 1H);  $^{13}\text{C-NMR}$  (100 MHz,  $\text{DMSO-d}_6$ )  $\delta$  161.57, 150.81, 146.38, 145.82, 138.35, 135.99, 132.07, 129.22, 128.73, 128.21, 127.61, 126.73, 126.48, 126.36, 124.94, 123.80, 123.20, 122.98, 120.39, 119.92, 118.70 ppm; MS (MALDI-TOF) Calcd  $\text{C}_{22}\text{H}_{13}\text{N}_3$  [ $\text{M}^+$ ]: 319.111; found: 319.445.

## 2.4 Studies of photophysical properties

### 2.4.1 UV-visible spectroscopy

The UV-Visible absorption spectra of the solutions of fluorophores were recorded at ambient temperature from 200-500 nm. The solution of each compound was prepared in EtOH. The concentration of them was diluted to 10  $\mu\text{M}$ .

### 2.4.2 Molar extinction coefficient ( $\epsilon$ )

The molar extinction coefficient ( $\epsilon$ ) of each fluorophore were calculated from the UV absorption spectra in EtOH at various concentrations. The absorption intensity of maximum wavelengths of each sample was plotted on Y-axis against the molar concentrations at the respective excitation wavelength on X-axis. Each graph should be a straight line and through origin-point. Then, the slope of graph was obtained to be the molar extinction coefficient of each fluorophore into the following equation:

$$A = \epsilon bC$$

Where A is the absorption intensity of sample.

$\epsilon$  is the molar extinction coefficient.

b is the pathlength in centimeter.

C is the molar concentration.

### 2.4.3 Fluorescence spectroscopy

The fluorescence emission spectra of the solution of fluorophores were determined ambient temperature from 350-650 nm. The solution of each compound was prepared in EtOH. The concentration of them was diluted to 10  $\mu\text{M}$ .

### 2.4.4 Relative quantum yield

Fluorescence quantum yield ( $\Phi_F$ ) of **P1**, **P2** and **P3** were performed by using anthracene in EtOH ( $\Phi_F = 0.27$ ) as the standard reference. The UV-visible absorption spectra of reference samples and analytical samples were recorded under the condition that the maximum absorbance of all samples should never be above 0.1 at varied concentrations. The fluorescence emission spectra of the same samples at

varied concentrations using appropriate excitation wavelengths selected were recorded based on the absorption maximum wavelength ( $\lambda_{\text{max}}$ ) of each compound. The integrated fluorescence intensity on Y-axis were plotted against the absorbance at the respective excitation wavelengths on X-axis. Each plot should be straight line with 1 interception. Additionally, the fluorescence quantum yield ( $\Phi_F$ ) could be calculated into the following equation.

$$\Phi_X = \Phi_{\text{ST}} \left( \frac{\text{Grad}_X}{\text{Grad}_{\text{ST}}} \right) \left( \frac{\eta_X^2}{\eta_{\text{ST}}^2} \right)$$

Where  $\Phi_{\text{ST}}$  is the fluorescence quantum yield of standard reference.

$\Phi_X$  is the fluorescence quantum yield of sample.

$\text{Grad}_{\text{ST}}$  is the gradient from the plot of integrated fluorescence intensity vs absorbance of standard reference.

$\text{Grad}_X$  is the gradient from the plot of integrated fluorescence intensity vs absorbance of sample.

$\eta_{\text{ST}}$  is the refractive index of standard reference.

$\eta_X$  is the refractive index of the solvent.

## 2.5 Studies of metal ions sensing properties

The stock solutions of **P1**, **P2** and **P3** were prepared in  $\text{CH}_3\text{CN}$  and the stock solution of metal ions were prepared in Milli-Q water. They were pipetted and diluted to a desired concentration before spectrophotometric analysis

### 2.5.1 Effect of solvents

The stock solutions are diluted into 10  $\mu\text{M}$  by varied solvents such as  $\text{CH}_3\text{CN}$ , THF, EtOH, DMSO and water. The fluorescence intensities of fluorophore without and with analyte were recorded using an excitation wavelength at room temperature.



### 2.5.2 Metal ion selectivity

The stock solutions of metal ions were prepared at 10 mM in Milli-Q water by dissolving commercial salts, LiNO<sub>3</sub>, NaNO<sub>3</sub>, KNO<sub>3</sub>, AgNO<sub>3</sub>, Ca(NO<sub>3</sub>)<sub>2</sub>, Mg(NO<sub>3</sub>)<sub>2</sub>, Ba(NO<sub>3</sub>)<sub>2</sub>, Co(NO<sub>3</sub>)<sub>2</sub>, Cd(NO<sub>3</sub>)<sub>2</sub>, Zn(NO<sub>3</sub>)<sub>2</sub>, Pb(NO<sub>3</sub>)<sub>2</sub>, Ni(NO<sub>3</sub>)<sub>2</sub>, Cu(NO<sub>3</sub>)<sub>2</sub>, Hg(OAc)<sub>2</sub>, Fe(OAc)<sub>2</sub>, Fe(NO<sub>3</sub>)<sub>3</sub>, Al(NO<sub>3</sub>)<sub>3</sub>, and Cr(NO<sub>3</sub>)<sub>3</sub>, except the solution of Bi(NO<sub>3</sub>)<sub>3</sub> was prepared at 5 mM because it could not soluble to 10 mM.

The concentration of fluorophores and metal ions was diluted with solvent to 10 μM and 100 μM, respectively. The final volumes were adjusted to 1 mL.

### 2.5.3 Metal ions interference

The interfering effect of other metal ions on the detection of Bi<sup>3+</sup> was studied by adding the other various competing metal ions into the solution of fluorophore in the presence of Bi<sup>3+</sup>. The final concentration of fluorophore, Bi<sup>3+</sup> and the other various competing metal ions were 10 μM, 100 μM and 100 μM, respectively.

### 2.5.4 Fluorescence titration and Detection limit

Various concentration of Bi<sup>3+</sup> (0-500 μM) was titrated into the solution of **P2** (10 μM). The final volume was adjusted to 1 mL by adding CH<sub>3</sub>CN/ DMSO (8:2 v/v). The fluorescent intensities were recorded from 300 nm to 700 nm at room temperature using an excitation wavelength. Moreover, the limit of detection (LOD) was obtained by plotting of the fluorescence intensity of fluorophore with concentrations of Bi<sup>3+</sup> between 0-20 μM. The detection limit was calculated by the following equation:

$$\text{Detection limit} = \frac{3\delta}{m}$$

Where  $\delta$  is the standard deviation of the standard deviation (S.D) of ten independent measurements of a blank.

$m$  is the slope between fluorescence intensity vs. concentrations of sample.

## 2.6 Studies of sensing mechanism

### 2.6.1 Time dependent

Fluorescence emission of **P2** was investigated after addition of  $\text{Bi}^{3+}$  in every 5 minutes for 30 minutes. The concentration of fluorophore and  $\text{Bi}^{3+}$  were  $10\ \mu\text{M}$  and  $100\ \mu\text{M}$ , respectively.

### 2.6.2 UV-visible and Fluorescence studies

To investigation of the interaction between **P2** and  $\text{Bi}^{3+}$ , concentration of  $\text{Bi}^{3+}$  from  $1\ \mu\text{M}$  to  $500\ \mu\text{M}$  was added to  $10\ \mu\text{M}$  of **P2**. The absorption wavelength and the fluorescence intensity were recorded. Moreover, the solution of sulfide ion ( $\text{S}^{2-}$ ) was added to the solution of **P2** in the presence of  $\text{Bi}^{3+}$  and adjusted with 20% DMSO/ $\text{CH}_3\text{CN}$ . The final concentration of **P2**,  $\text{Bi}^{3+}$  and  $\text{S}^{2-}$  were  $10\ \mu\text{M}$ ,  $100\ \mu\text{M}$  and  $100\ \mu\text{M}$ , respectively.

### 2.6.3 $^1\text{H}$ NMR experiment

The fluorophore (**P2**) was dissolved in deuterated methanol ( $\text{CD}_3\text{OD}$ ) and the  $\text{Bi}(\text{NO}_3)_3$  was dissolved in deuterated water ( $\text{D}_2\text{O}$ ). The  $^1\text{H}$ -NMR data of **P2** with and without excess concentration of  $\text{Bi}^{3+}$  were investigated.

### 2.6.4 Job's plot

The concentration of the fluorophore (**P2**) and  $\text{Bi}^{3+}$  were prepared at  $10\ \mu\text{M}$ . The mole fraction ( $X$ ) of **P2** from 0.1 to 1.0 was used in this experiment. The stoichiometry of metal-sensor complex was obtained by plotting of the fluorescence intensity of sensor's mole fraction,  $((I-I_0)X_{\text{sensor}})$ , with the mole fraction of  $\text{Bi}^{3+}$  ( $X_{\text{metal}}$ ).

## 2.7 Quantitative analysis for $\text{Bi}^{3+}$

### 2.7.1 Effect of water content

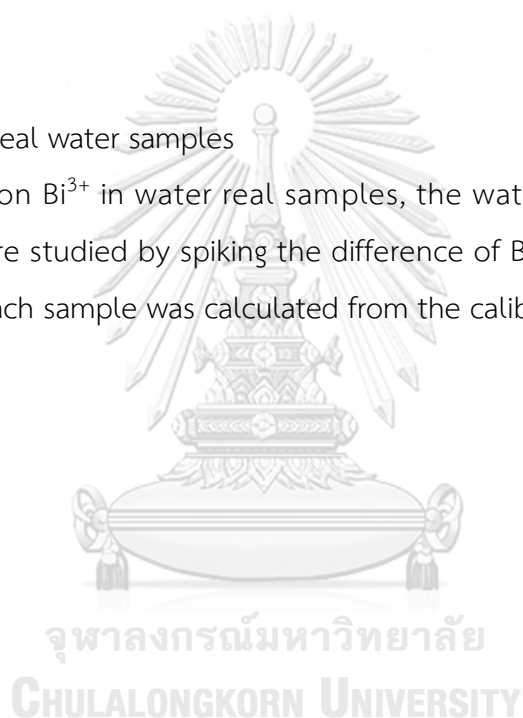
The stock solutions of **P2** are diluted into  $10\ \mu\text{M}$  by varied water content from 10% to 90% water in  $\text{CH}_3\text{CN}$ . The fluorescence intensities of fluorophore were recorded using an excitation wavelength at room temperature.

### 2.7.2 Effect of pH

The pH effect on fluorophores with and without analyte was investigated by data of fluorescence emission spectra in the series of buffer between pH 3.0 – 9.0, using acetate buffer for pH 3.0 and 5.0, HEPES buffer for pH 7.0, glycine-NaOH buffer for pH 9.0. The final concentrations of fluorophore, analyte and buffer solution were 10  $\mu\text{M}$ , 100  $\mu\text{M}$  and 20  $\mu\text{M}$ , respectively. Moreover, the pH effect was studied using 0.1 M HCl and 0.1 M NaOH to adjust the solution to pH 3.0, 5.0, 7.0, 9.0 and 11.0. The final concentrations of fluorophore and analyte were 10  $\mu\text{M}$ , and 100  $\mu\text{M}$ , respectively.

### 2.7.3 $\text{Bi}^{3+}$ in real water samples

To detection  $\text{Bi}^{3+}$  in water real samples, the water samples from tap and drinking water were studied by spiking the difference of  $\text{Bi}^{3+}$  to each water sample. The recovery of each sample was calculated from the calibration curve.

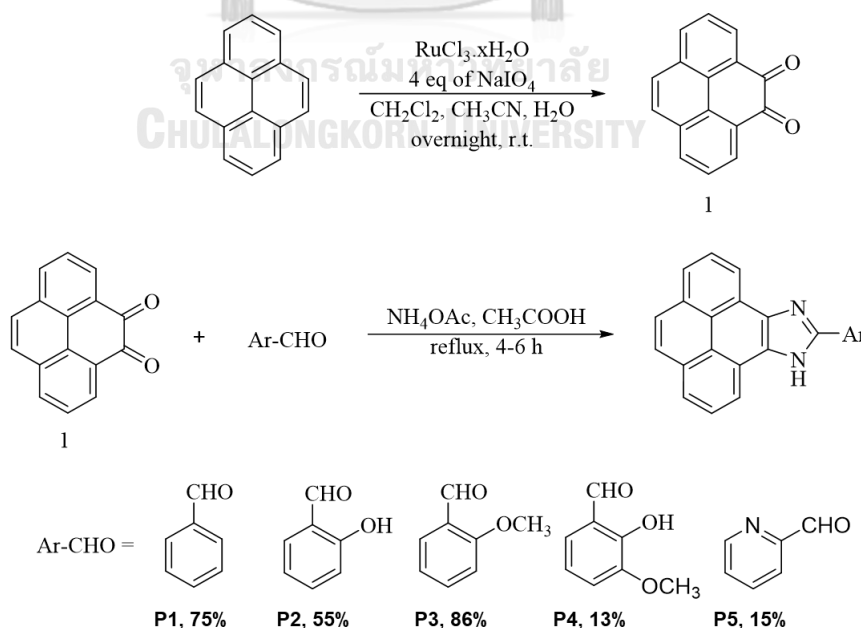


## CHAPTER III

### RESULTS AND DISCUSSION

#### 3.1 Synthesis and characterization of fluorophores (P1-P5)

The synthesis of pyreno[4,5-*d*]imidazole derivatives were started from the oxidation of pyrene using  $\text{NaIO}_4$  and  $\text{RuCl}_3$  as a catalyst to give dione **1** as an orange solid in 47% yield. The spectrum of dione **1** was corresponding with a literature that was reported by Hu et al. in 2015 [51]. Then amination-condensation of dione **1** with aromatic aldehydes and ammonium acetated was performed at reflux temperature in acetic acid for 4-12 h depending on the types of the aromatic aldehydes. The target compound **P1**, **P2**, and **P3** were produced in moderate yield (55-86%) after purification by column chromatography. On the other hand, target compound **P4** was obtained in lower yield (15%) since the product was partially soluble in water even if it was worked-up with ice-water. The yellow aqueous solution was obtained after filtration. For the part of **P5**, many spots of product were shown in TLC so that the compound **P5** was obtained in low yield (15%) and not clean even after recrystallization by chloroform-ethanol. All the target compounds were characterized using  $^1\text{H}$  NMR,  $^{13}\text{C}$  NMR and mass spectrometry.



**Scheme 3.1** Synthesis of pyreno[4,5-*d*]imidazole derivatives (**P1-P5**)

For the NMR characterization, the  $^1\text{H}$  NMR spectrum of dione **1** is shown in Figure 3.1 with 4 signals corresponding to all four aromatic protons of the symmetric molecule. The signal for aromatic proton d appears as a singlet peak at 7.84 ppm., the proton b appears as a triplet peak at 7.74 ppm., and proton a and c appear as doublet peaks at 8.47 and 8.16 ppm., respectively.

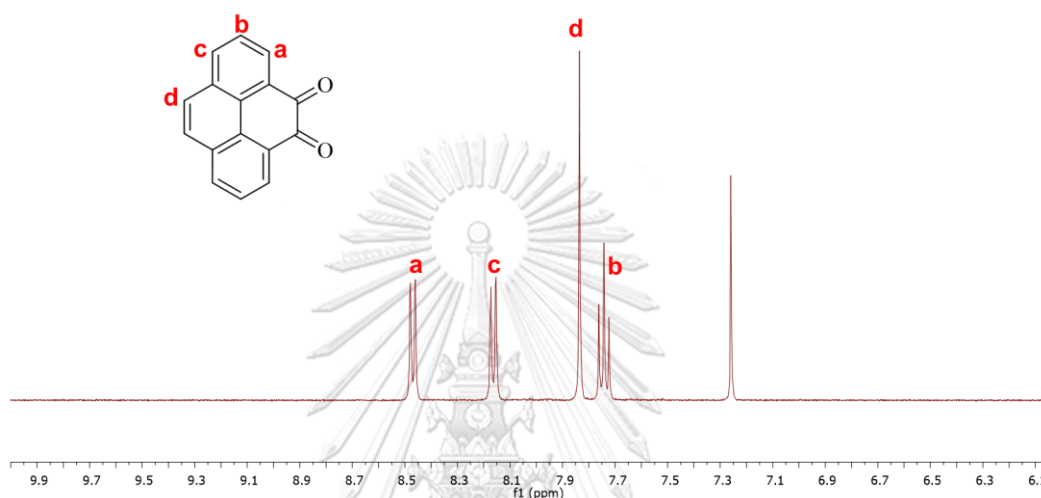


**Figure 3.1**  $^1\text{H}$  NMR spectrum of dione **1** in  $\text{CDCl}_3$

$^1\text{H}$  NMR spectroscopy of the target compounds **P1**, **P2** and **P3** which obtained from condensation of dione **1** with aromatic aldehydes are shown in Figure 3.2. The presence of the imidazole ring was confirmed by the amine proton (NH) which appears at different positions (13.87, 13.21 and 13.07 ppm for **P1**, **P2** and **P3**, respectively). Moreover, the proton signal at 13.99 ppm confirmed the presence of the hydroxyl group (OH) in **P2**. The singlet proton signal at 4.08 ppm of **P3** confirmed the presence of the methoxy group ( $\text{OCH}_3$ ).

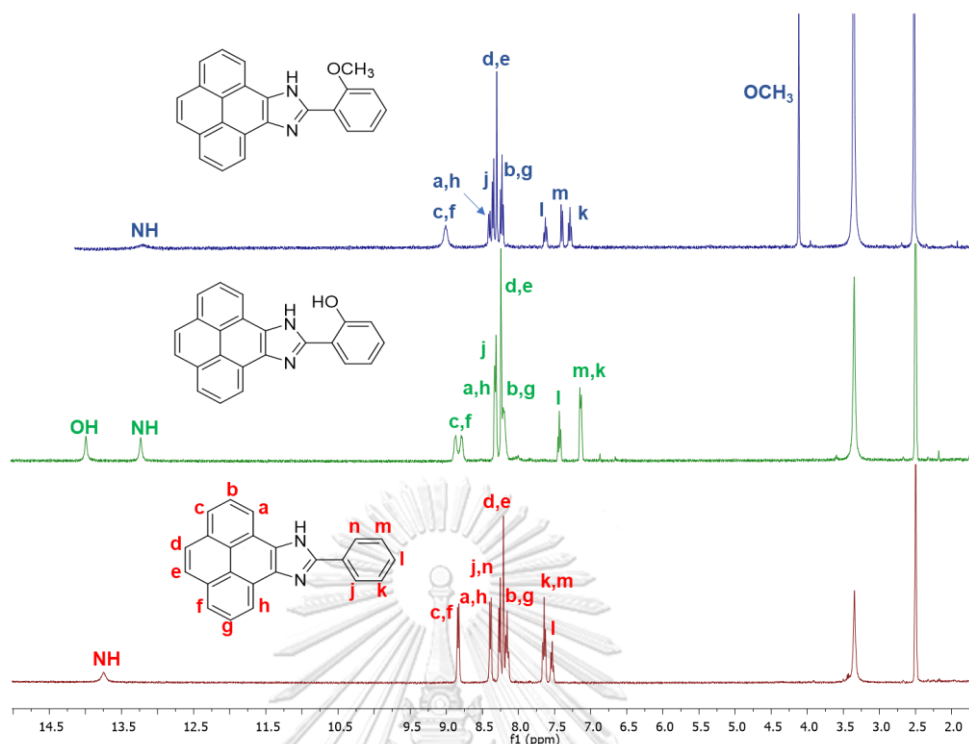


Figure 3.2  $^1\text{H}$  NMR spectra of P1, P2 and P3 in  $\text{DMSO-d}_6$

The  $^1\text{H}$ - $^1\text{H}$  correlation spectroscopy (COSY) was used to identify the coupled proton on phenolic ring as shown in Figure 3.3. The proton k ( $\text{H}_k$ ) has been assigned at 8.40 ppm because the peak of proton at 8.40 ppm is triplet and coupled protons at 8.71 ppm (1H) and 9.49 ppm (1H). While the peak of proton at 8.71 ppm is triplet and coupled the proton at 8.43 ppm that indicated this peak is the proton l ( $\text{H}_l$ ). Therefore, the proton m and j have been assigned at 8.43 and 9.49 ppm, respectively.

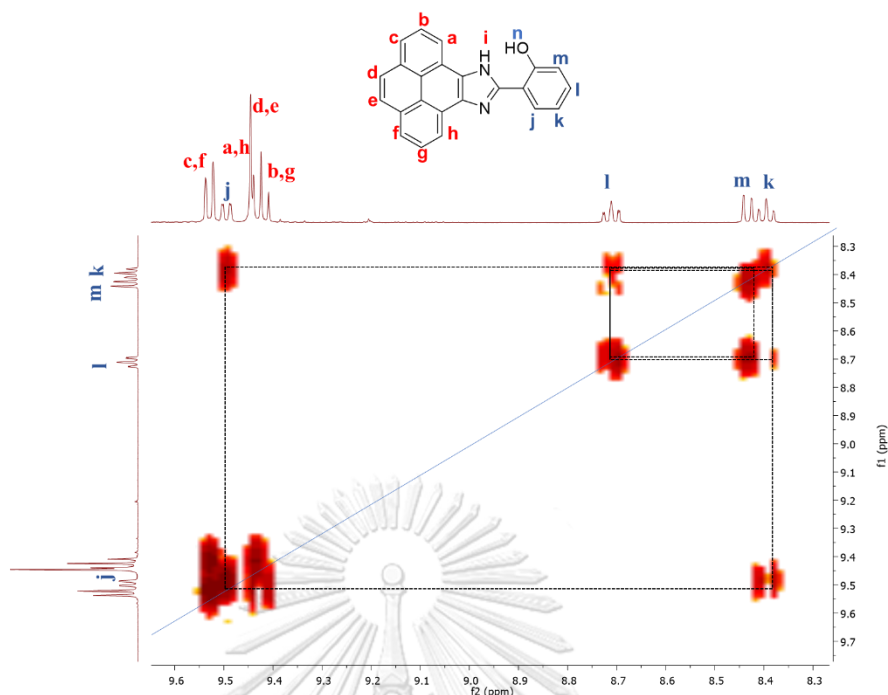


Figure 3.3 The  $^1\text{H}$ - $^1\text{H}$  COSY spectrum of **P2** in  $\text{DMSO-d}_6$ .

Furthermore, FT-IR spectrometer could be confirmed absorption peak of hydroxyl group (-OH) on **P2** at  $3269.68\text{ cm}^{-1}$  that is shown in Figure 3.4. The molecular weights of **P1**, **P2** and **P3** were confirmed by mass spectrometer ( $m/z = 318.027$ ,  $335.02$  and  $348.716$ ) as seen in appendix (Figure A.4, A.8 and A.11).

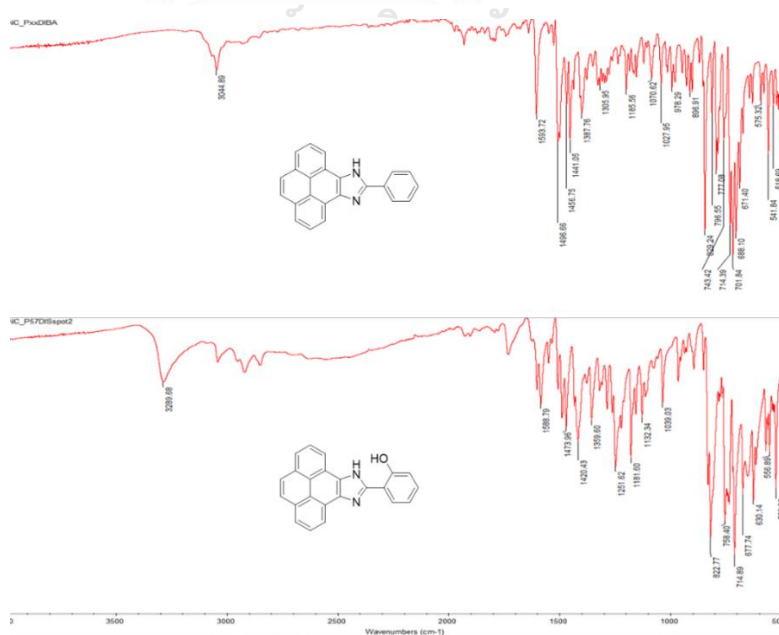


Figure 3.4 FT-IR spectra of **P1** and **P2**

Comparison of  $^1\text{H}$  NMR of compound **P4** with compound **P2** in  $\text{CD}_3\text{OD}$ , proton of the phenyl ring that near the methoxy group ( $\text{H}_i$ ) is shifted to upfield from 7.35 to 7.08 ppm and multiplicity changes from triplet to doublet. Moreover, the presence of the methoxy group was confirmed at 3.95 ppm (Figure 3.5). The molecular weight of **P4** was confirmed by mass spectrometer ( $m/z = 364.027$ ) as seen in appendix (Figure A.14).

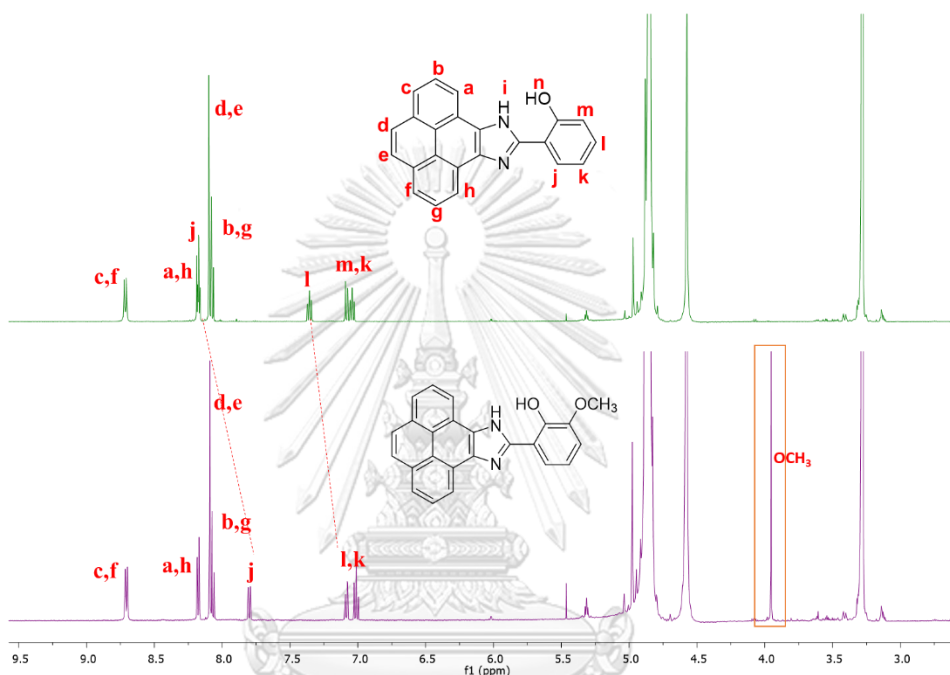
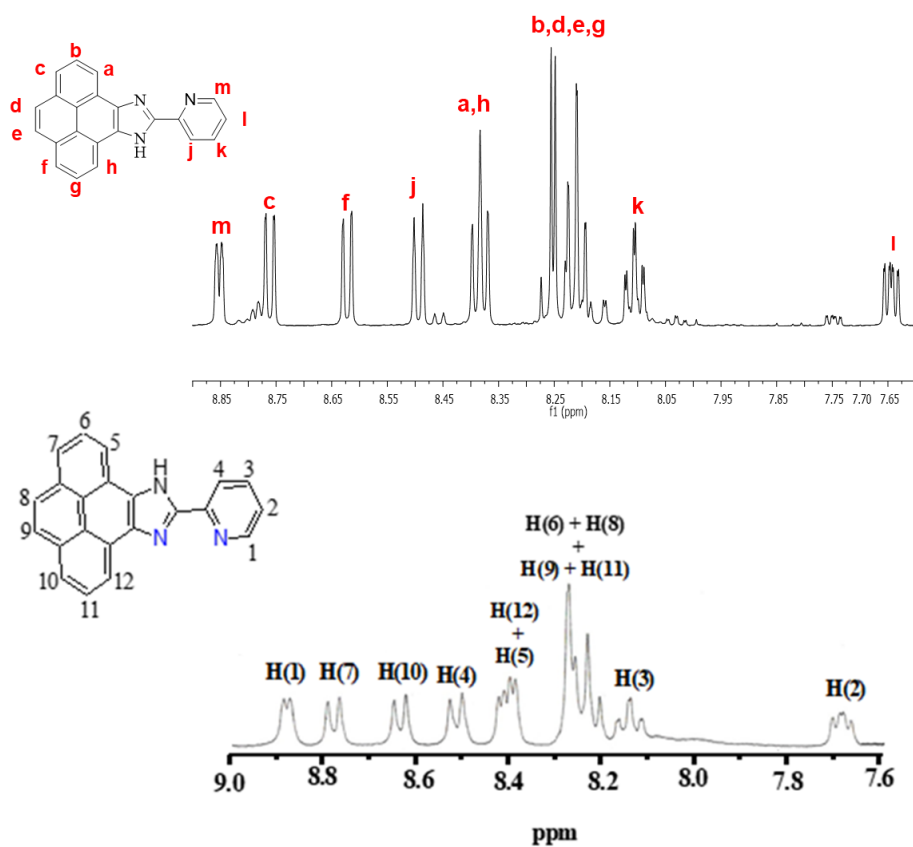


Figure 3.5 Comparison of  $^1\text{H}$  NMR spectra of **P2** and **P4**  $\text{CD}_3\text{OD}$ .

The  $^1\text{H}$  NMR compound **P5** as shown in Figure 3.6 was corresponding with a literature that was reported in 2015 by Mardanya et al. [52].





**Figure 3.6** Comparison of <sup>1</sup>H NMR spectra of each fractions of P5 and picolinaldehyde in CDCl<sub>3</sub>.

After that, mass spectroscopy was confirmed the product P5, the result was obtained at  $m/z = 319$  in Figure 3.7.

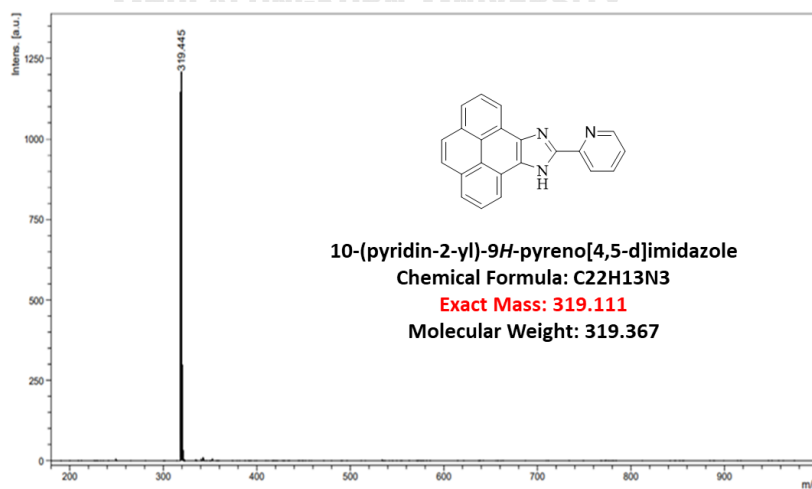


**Figure 3.7** MALDI-TOF-Mass spectrum of P5

### 3.2 Photophysical properties

The absorption and emission of fluorophores (**P1-P5**) were studied in EtOH. The normalized UV-Vis and fluorescence spectra are shown in Figure 3.8. The photophysical properties are summarized in Table 1. All of fluorophores exhibited two maximum absorption peaks which correspond to the characteristic peaks of pyrene derivatives[52]. One peak displayed around 278-290 nm with molar extinction coefficients around 9900-28500 M<sup>-1</sup> cm<sup>-1</sup> and the other showed around 331-335 nm with molar extinction coefficients 8500-21900 M<sup>-1</sup> cm<sup>-1</sup>. The longer maximum absorption wavelengths (331-335 nm) are selected for excitation of each fluorophores to study the emission property. The maximum emission wavelengths for compound **P1-P5** are observed at 407, 448, 389, 388 and 458 nm, respectively. The longest maximum emission in **P2** and **P5** may results from the Excited State Intramolecular Proton Transfer (ESIPT) which was initiated by the intramolecular hydrogen bonding between N atom on imidazole core and hydroxyl group on phenyl ring. Moreover, the ESIPT process has an effected on the fluorescent quantum yields ( $\Phi_F$ ) of **P2** that is lower than two compounds. The relative quantum yields are found at 0.75, 0.41 and 0.78 for **P1**, **P2** and **P3**, respectively.

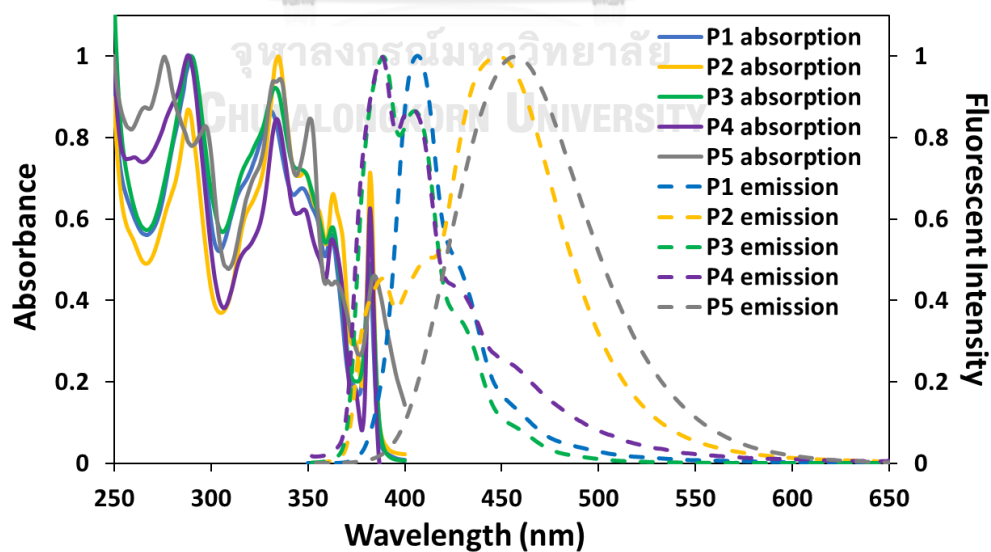


Figure 3.8 Normalized absorption and emission spectra of **P1-P3** in EtOH.

**Table 3.1** Photophysical properties of molecules

compound	Absorption <sup>a</sup>		Emission <sup>a</sup>		
	$\lambda_{\max}$ (nm)	$\epsilon$ (M <sup>-1</sup> cm <sup>-1</sup> )	$\lambda_{\text{ex}}$ (nm)	$\lambda_{\max}$ (nm)	$\Phi^b$
P1	290	9900	331	407	0.75
	331	8500			
P2	289	13000	335	448	0.41
	335	11300			
P3	290	11300	333	389	0.78
	333	10400			
P4	287	28500	334	388	-
	334	21900			
P5	278	27900	335	458	0.24[52]
	335	21100			

<sup>a</sup>solutions in absolute ethanol

<sup>b</sup>Anthracene in ethanol (quantum yield 0.27) was used as the reference compound.

### 3.3 Metal ions sensing properties

#### 3.1.1 Solvent effect

The absorption spectra of **P1-P5** in various solvents such as CH<sub>3</sub>CN, THF, EtOH, DMSO and milli-q water are shown in Figure 3.9. All of target molecule are insoluble in water because of the hydrophobic structure of compounds and could be slightly soluble in DMSO. Therefore, these compounds are dissolved in CH<sub>3</sub>CN, THF and EtOH to study fluorescent properties.

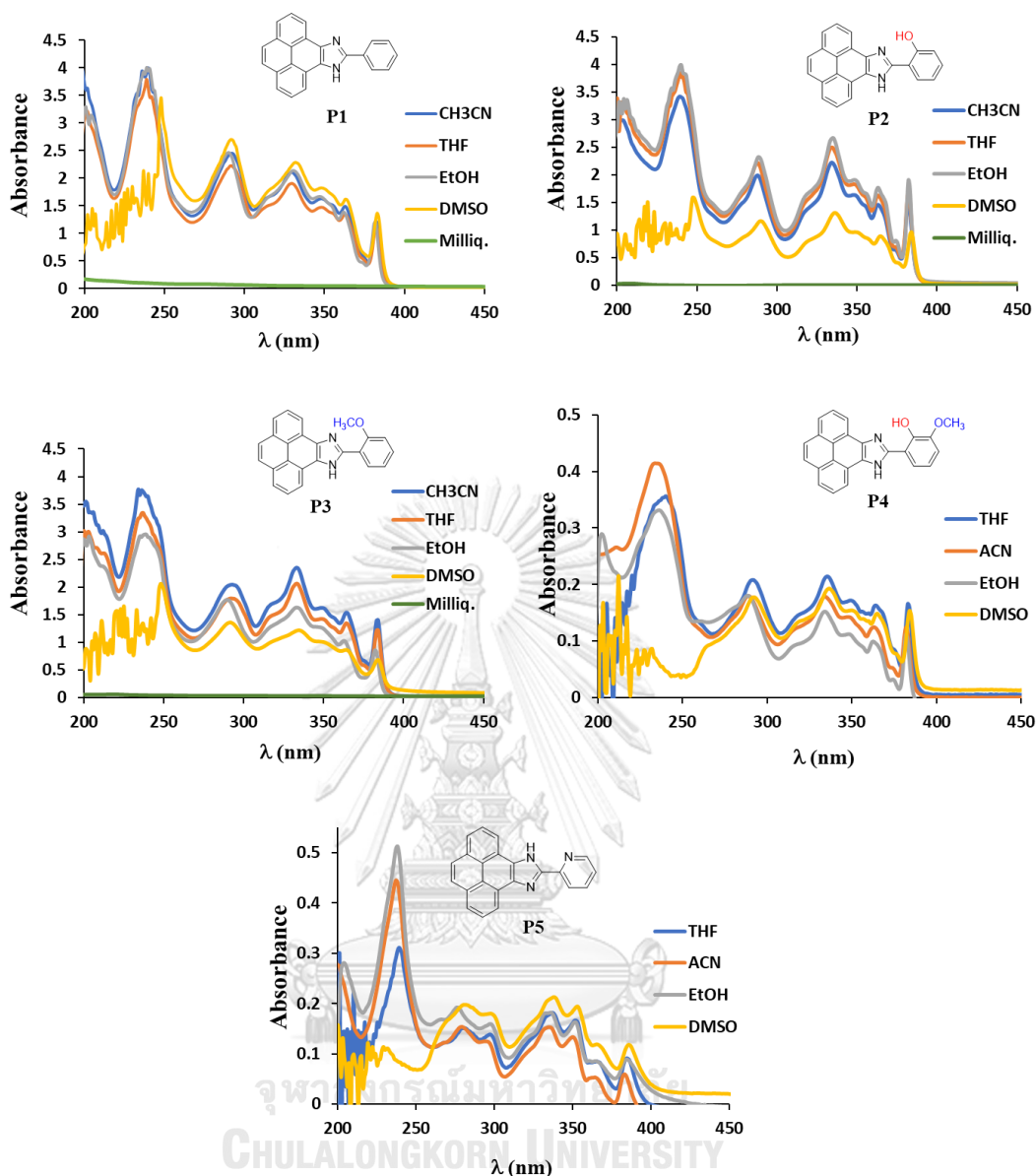


Figure 3.9 Absorption spectra of P1-P5 in various solvents.

The fluorescence spectra of P1-P5 in CH<sub>3</sub>CN, THF, and EtOH are shown in Figure 3.10. The same fluorescence spectra of P1 and P3 in each solvent could be indicated the types of solvent; polar solvent, non-polar solvent, and protic solvent, had no effect on P1 and P3. The fluorescence intensities of P4 are decreased in polar solvent. It may result from the stabilization of polar solvent. On the contrary, the fluorescence spectra of P2 are different in each solvent and the intensity around 450 – 500 nm were expressed that might be the effect of hydroxyl group in

compound. In addition, the fluorescence intensity of **P2** in CH<sub>3</sub>CN is lower than THF and EtOH that might be the ground-state stabilization effect of the polar compound (**P2**) by the high polar solvent. While the fluorescence spectra of **P5** show the different maximum emission wavelength around 400-470 nm in each solvent. As the results, CH<sub>3</sub>CN is interesting to use as solvent for the selectivity screening as the turn-on fluorescence sensor.

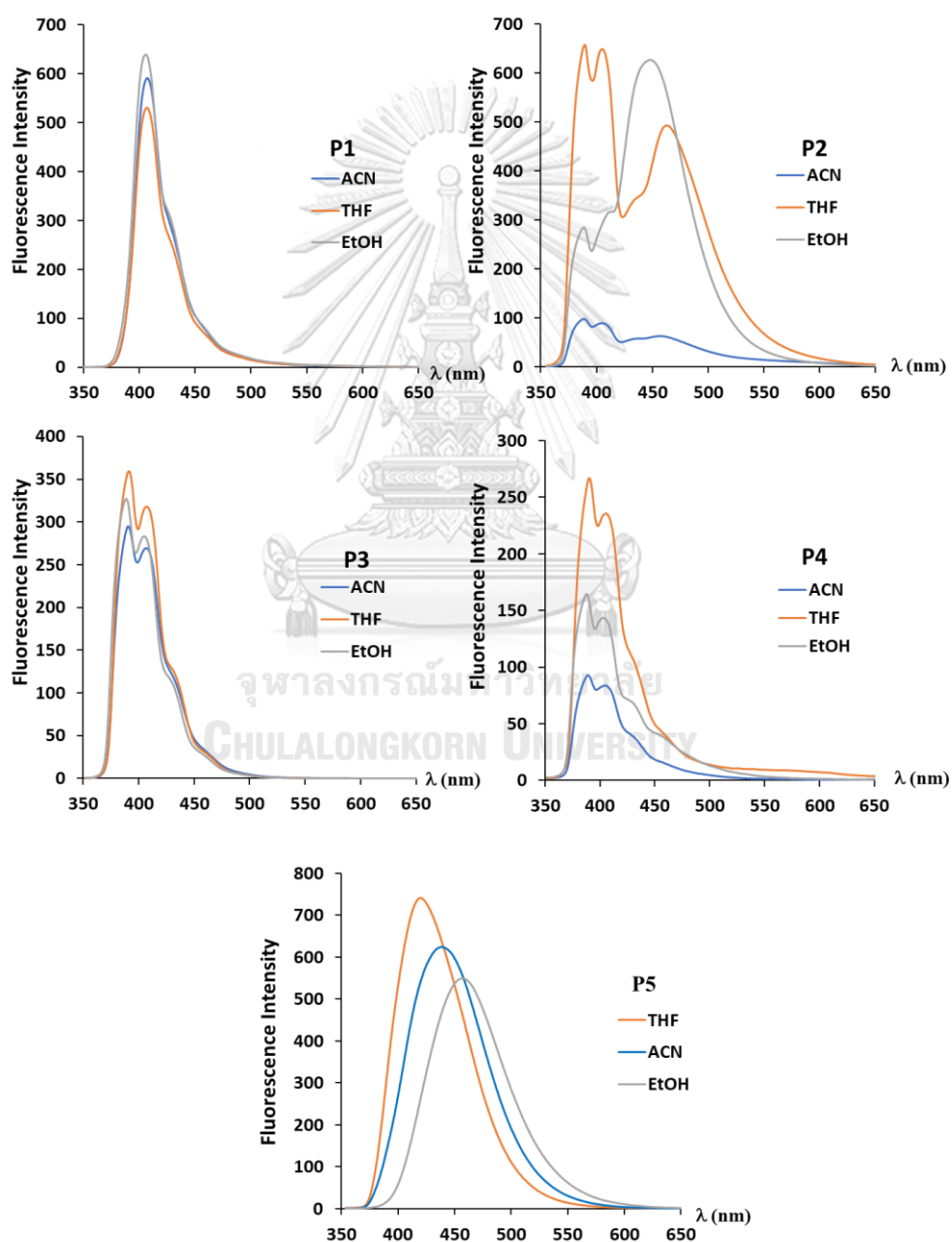


Figure 3.10 Fluorescence spectra of **P1-P5** in CH<sub>3</sub>CN, THF and EtOH

### 3.3.2 Preliminary screening on metal ion selectivity

The selectivity of fluorophore **P1-P5** with various metal ions such as  $\text{Li}^+$ ,  $\text{Na}^+$ ,  $\text{K}^+$ ,  $\text{Ag}^+$ ,  $\text{Mg}^{2+}$ ,  $\text{Ca}^{2+}$ ,  $\text{Ba}^{2+}$ ,  $\text{Co}^{2+}$ ,  $\text{Cd}^{2+}$ ,  $\text{Zn}^{2+}$ ,  $\text{Pb}^{2+}$ ,  $\text{Ni}^{2+}$ ,  $\text{Cu}^{2+}$ ,  $\text{Hg}^{2+}$ ,  $\text{Fe}^{2+}$ ,  $\text{Fe}^{3+}$ ,  $\text{Al}^{3+}$ ,  $\text{Bi}^{3+}$ , and  $\text{Cr}^{3+}$  were determined. After addition of 10 equiv. of metal ions to the solution of **P1-P3** in  $\text{CH}_3\text{CN}$ , the results show no selectivity of all sensor but the maximum emission wavelengths of some metal ions such as  $\text{Fe}^{3+}$ ,  $\text{Al}^{3+}$ ,  $\text{Bi}^{3+}$ , and  $\text{Cr}^{3+}$  were red-shifted to around 450-460 nm. as shown in Figure 3.11. The result of **P1** is like **P3**, the fluorescence spectra show wavelengths shift from 380 -410 nm. to 460 nm. while fluorescence spectra of **P2** show fluorescence enhancement in the presence of trivalent metal ions. The result of **P4** is similar to **P2** but it was slightly enhanced by  $\text{Zn}^{2+}$ ,  $\text{Pb}^{2+}$  and  $\text{Ni}^{2+}$ . The different fluorescence mode of compounds may result from the difference of the complexation between fluorophores and metal ions. However, the fluorescence spectra of **P5** that contains hetero aromatic ring show fluorescence quenching by  $\text{Cu}^{2+}$ ,  $\text{Ni}^{2+}$  and  $\text{Fe}^{3+}$  due to an intra-ligand charge transfer transition (ILCT) from the pyrenyl-imidazole group to the pyridine group [52].

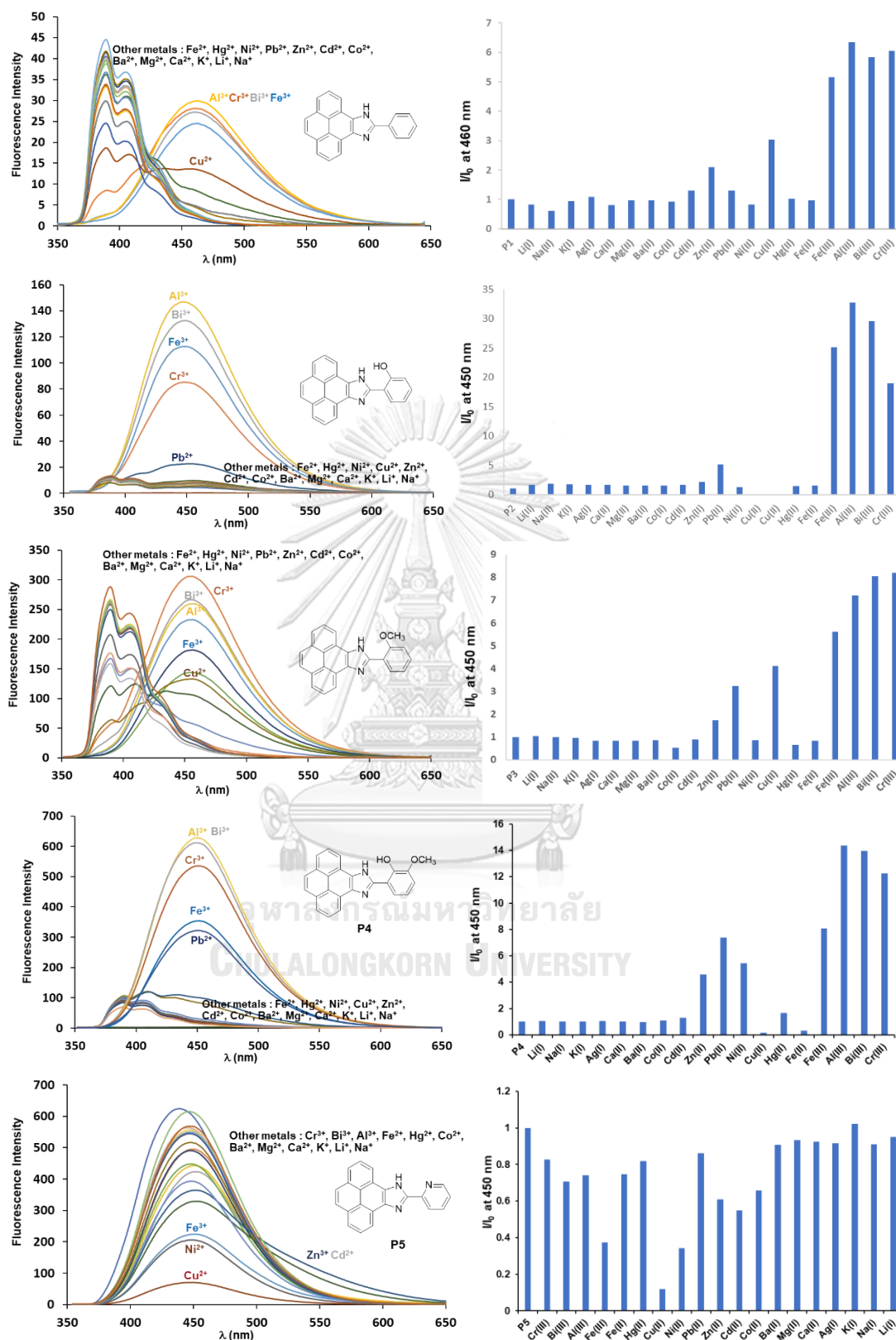
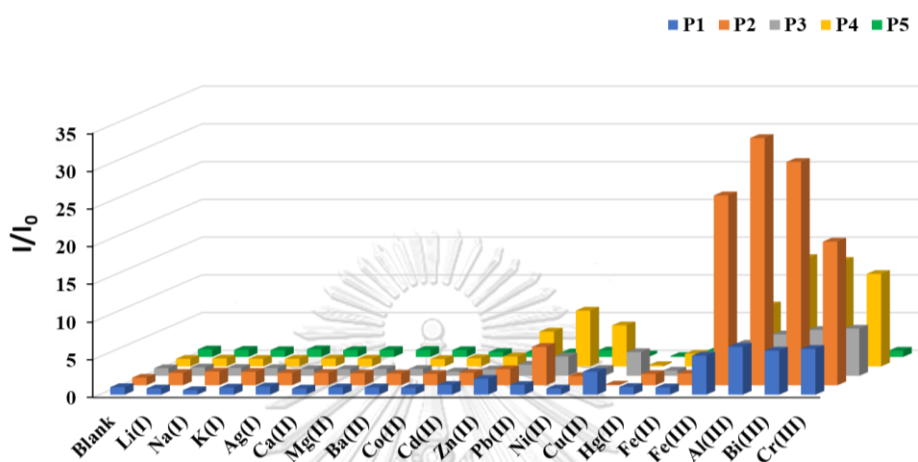


Figure 3.11 Fluorescence spectra and fluorescence enhancement ratio of P1-P5 (10  $\mu$ M) in  $\text{CH}_3\text{CN}$  upon addition of 10 equiv. of various metal ions

Interestingly, the fluorescence enhancement ratio ( $I/I_0$ ) of **P2** is around 30-40 folds for four metal ions that is higher than 3-4 folds of **P4** and 8-10 folds of **P1** and **P3** (Figure 3.12). From this result, **P2** is focused on as the sensor to detection of metal ions.



**Figure 3.12** Comparison of fluorescence enhancement ratio of **P1-P5** (10  $\mu$ M) in  $\text{CH}_3\text{CN}$  upon addition of 10 equiv. of various metal ions

To improve in the selectivity of **P2** under the identical condition, anion effect was studied such as  $\text{F}^-$ ,  $\text{Cl}^-$ ,  $\text{Br}^-$ ,  $\text{I}^-$ ,  $\text{SCN}^-$ ,  $\text{NO}_3^-$ ,  $\text{CH}_3\text{COO}^-$ ,  $\text{S}_2\text{O}_3^{2-}$ ,  $\text{SO}_3^{2-}$ ,  $\text{SO}_4^{2-}$ ,  $\text{CO}_3^{2-}$ , and  $\text{PO}_4^{3-}$ . Upon addition of 10 equiv. of anions, the fluorescence intensity was reduced by phosphate anion ( $\text{PO}_4^{3-}$ ), is shown in Figure 3.13. It might be strong basicity of phosphate ion inhibited ESIPT process of **P2**.

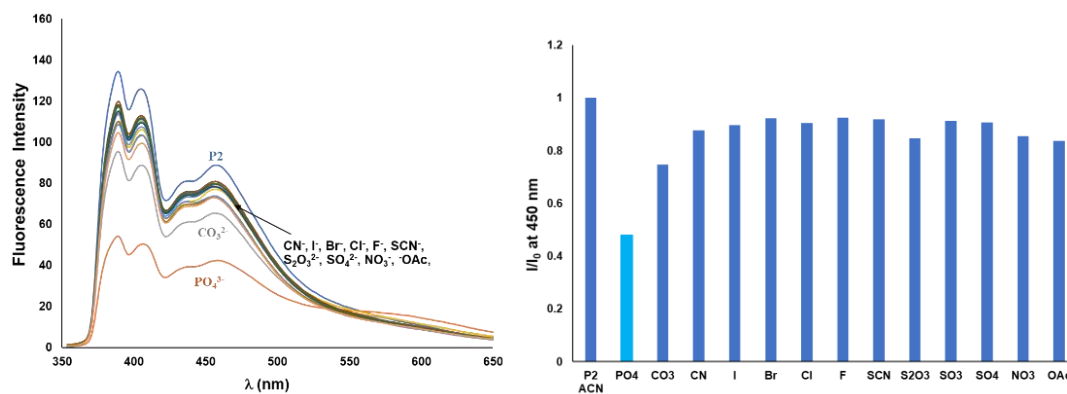


**Figure 3.13** Fluorescence spectra of **P2** (10  $\mu$ M) in  $\text{CH}_3\text{CN}$  upon addition of 10 equiv. of various anions.



Besides, the titration of phosphate anions seem that more than 4 equiv. of phosphate anion did not affect to the fluorescence intensity of **P2** (Figure 3.14). After that, the new condition was observed using 10 equiv. of  $\text{PO}_4^{3-}$  in  $\text{CH}_3\text{CN}$  for screening of selectivity.

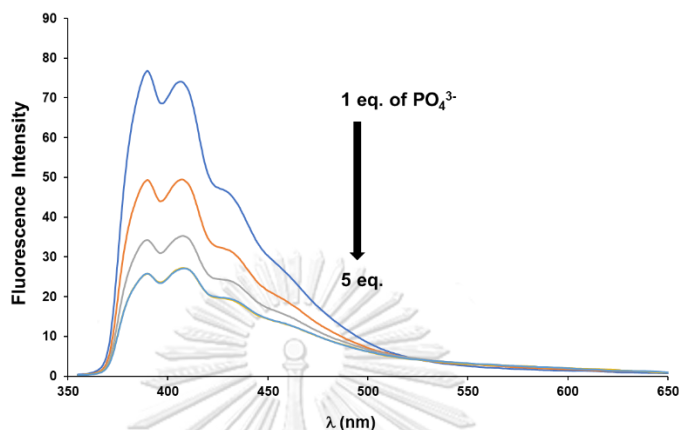


**Figure 3.14** Fluorescence spectra of **P2** (10  $\mu\text{M}$ ) upon addition 1 to 5 equiv. of  $\text{PO}_4^{3-}$  in  $\text{CH}_3\text{CN}$ .

When the selectivity of **P2** towards 10 equiv. of various metal ions were determined, only  $\text{Fe}^{3+}$  could enhanced fluorescent intensity (Figure 3.15) but the enhancement fluorescence ratio is decreased from 25 folds to 5 folds. The selectivity of **P2** with  $\text{Fe}^{3+}$  was attributed to the solubility of phosphate salts that are shown in Table 3.2.

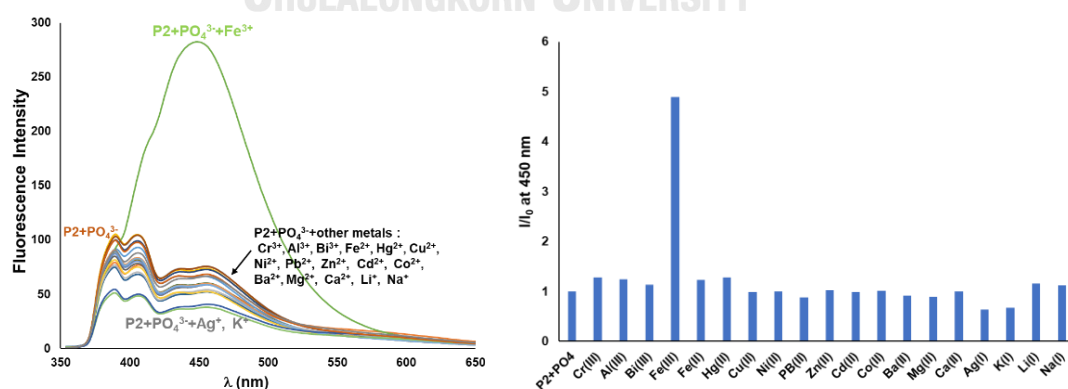


**Figure 3.15** Fluorescence spectra of **P2** (10  $\mu\text{M}$ ) in presence of  $\text{PO}_4^{3-}$  (10 equiv.) upon addition 10 equiv. of various metal ions in  $\text{CH}_3\text{CN}$ .

**Table 3.2** Solubility product constants ( $K_{sp}$ ) [53]

Compound	Formula	$K_{sp}$ at 25 °C
Chromium phosphate	$\text{CrPO}_4$	$2.4 \times 10^{-23}$
Aluminium phosphate	$\text{AlPO}_4$	$9.84 \times 10^{-21}$
Iron(III) phosphate	$\text{FePO}_4$	$9.91 \times 10^{-16}$
Bismuth phosphate	$\text{BiPO}_4$	$1.3 \times 10^{-23}$

The interaction between **P2** and  $\text{Fe}^{3+}$  was studied by UV-Vis titration spectra. After addition of  $\text{Fe}^{3+}$  from 0 to 18 equiv., the absorption band was slightly blue shift from 289 nm to 276 nm (Figure 3.16). The new absorption band might be ascribed to the complexation of **P2** and  $\text{Fe}^{3+}$ .

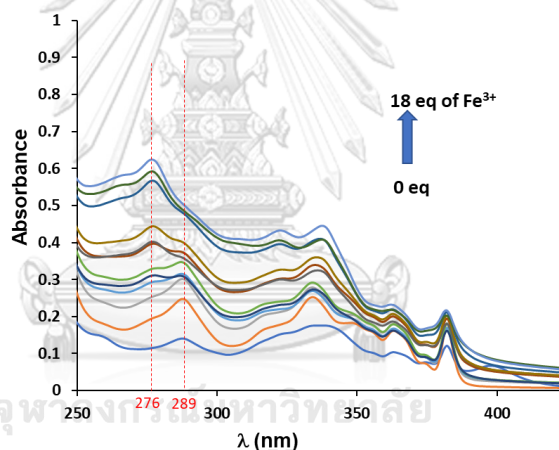


**Figure 3.16** UV-Vis titration spectra of **P2** (10  $\mu\text{M}$ ) in the presence of 10 equiv. of  $\text{PO}_4^{3-}$  upon addition of various concentrations of  $\text{Fe}^{3+}$  in  $\text{CH}_3\text{CN}$ .

However, the quantitative study of  $\text{Fe}^{3+}$  using fluorescence titration experiment showed the limitation of sensing as shown in Figure 3.17. The fluorescence signal of **P2** could not be observed when the concentration of  $\text{Fe}^{3+}$  was less than 6  $\mu\text{M}$  because of the competitive binding between **P2**,  $\text{Fe}^{3+}$  and  $\text{PO}_4^{3-}$  at low concentration.

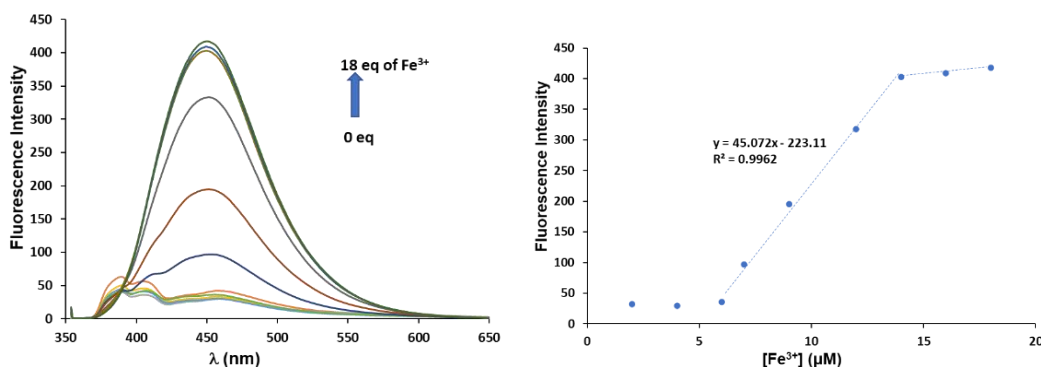


**Figure 3.17** Fluorescence titration spectra of **P2** (10  $\mu\text{M}$ ) in the presence of 10 equiv. of  $\text{PO}_4^{3-}$  upon addition of various concentrations of  $\text{Fe}^{3+}$  in  $\text{CH}_3\text{CN}$ .

According to Zhang et al [54], the mixed organic solvent,  $\text{EtOH-CH}_3\text{CN}$  (1:4, v/v), was used for detection  $\text{Bi}^{3+}$ . In order to improve selectivity of **P2**, another organic solvent was mixed with  $\text{CH}_3\text{CN}$  to alter the solubility of sensor. From the previous screening (Figure 3.7), the emission wavelength of **P2** with trivalent metal ions is approximate around 450 nm so that another organic solvent should not displayed the fluorescence intensity at 450 nm. The fluorescence spectra in Figure 3.18 showed that the mixed solvent between  $\text{CH}_3\text{CN}$  and  $\text{DMSO}$  could not increase the fluorescence intensity at 450 nm while the fluorescence intensities of the mixture of  $\text{CH}_3\text{CN-EtOH}$  appeared around 450 nm.

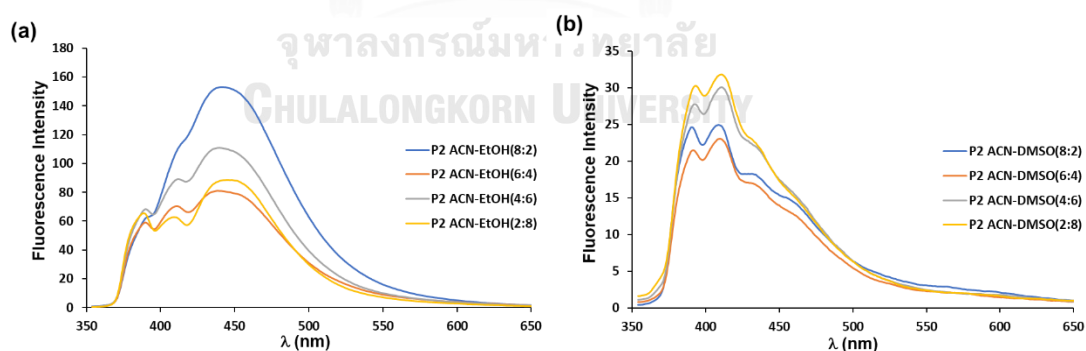


**Figure 3.18** Fluorescence spectra of **P2** (10  $\mu\text{M}$ ) (a) in various ratio of  $\text{CH}_3\text{CN-EtOH}$  (b). in various ratio of  $\text{CH}_3\text{CN-DMSO}$ .

Then, addition 10 equiv. of four trivalent metal ions ( $\text{Fe}^{3+}$ ,  $\text{Al}^{3+}$ ,  $\text{Bi}^{3+}$  and  $\text{Cr}^{3+}$ ) to **P2** in the mixed solvents, the results showed the enhancement ratio at 80%  $\text{CH}_3\text{CN-}$

DMSO in the presence of  $\text{Bi}^{3+}$  is higher than the others. Therefore, 80%  $\text{CH}_3\text{CN}$ -DMSO was optimized as the condition for study the selectivity of **P2** (Figure 3.19).

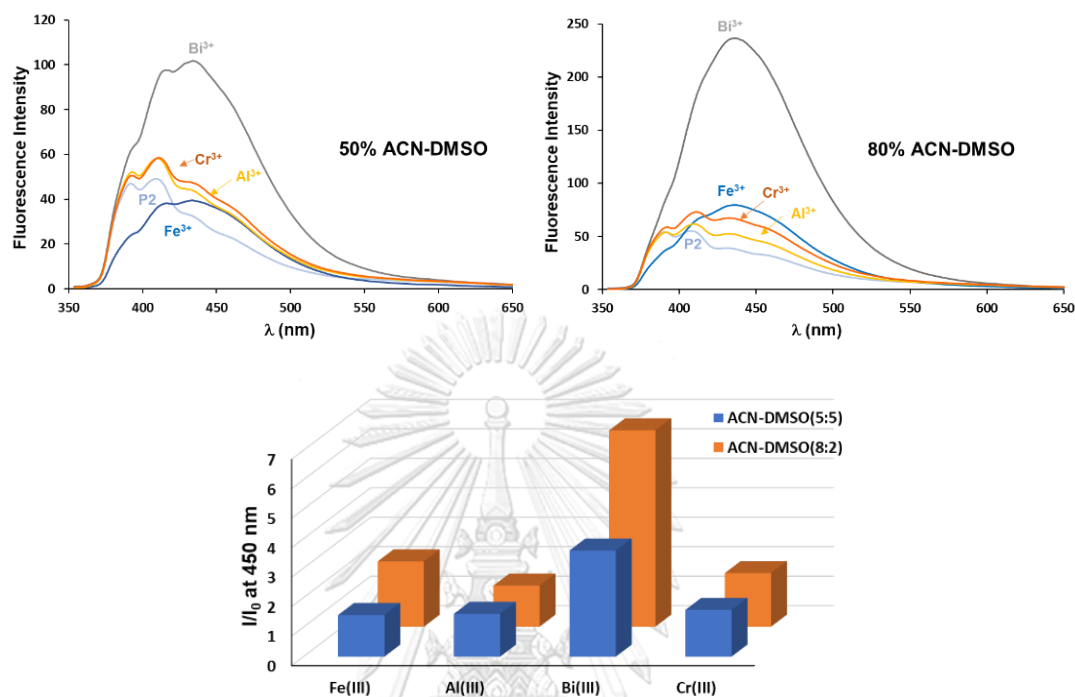


**Figure 3.19** Fluorescence spectra and of fluorescence enhancement ratio of **P2** (10  $\mu\text{M}$ ) in  $\text{CH}_3\text{CN}$ -DMSO 1:1 and 8:2, v/v upon addition of 10 equiv. of trivalent metal ions ( $\text{Fe}^{3+}$ ,  $\text{Al}^{3+}$ ,  $\text{Bi}^{3+}$  and  $\text{Cr}^{3+}$ )

The selectivity of **P2** toward various metal ions under the optimized condition were also studied. The fluorescence intensity at 450 nm was significant increased by addition 10 equiv. of  $\text{Bi}^{3+}$ . The fluorescence enhancement ratio is shown about 7 folds although  $\text{Fe}^{3+}$  was slightly increased about 2 folds. On the other hand, the selectivity of **P1** and **P3** under this solvent system could not be improved that was shown in Figure 3.20.

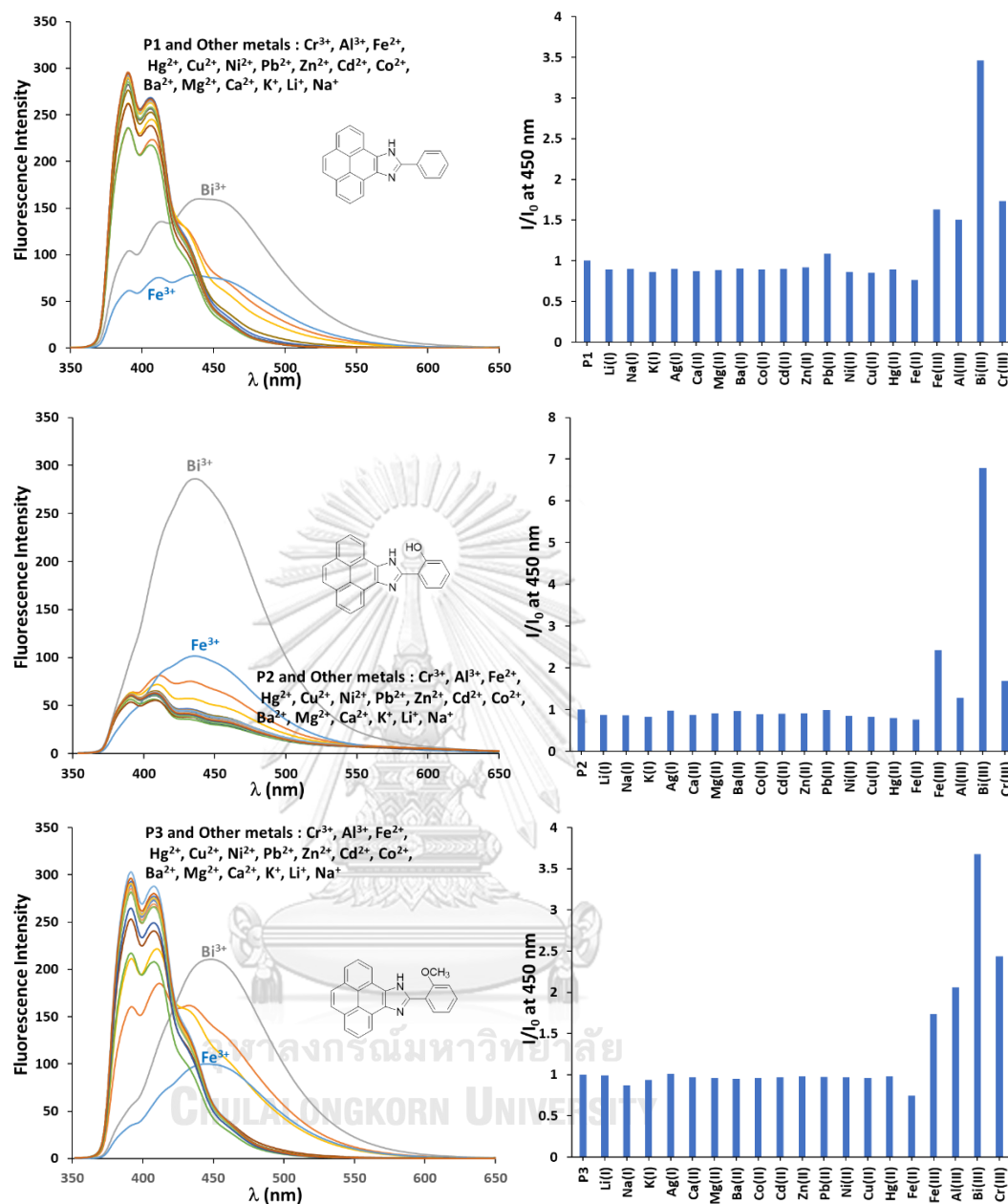


**Figure 3.20** Fluorescence spectra and fluorescence enhancement ratio of **P1-P3** (10  $\mu$ M) in CH<sub>3</sub>CN-DMSO (8:2, v/v) before and after addition 10 equiv. of metal ions.

### 3.3.3 Interference studies

The possible interference of **P2** to Bi<sup>3+</sup> was carried out in the presence of 10 equiv. of other metal ions under CH<sub>3</sub>CN-DMSO (8:2, v/v). From Figure 3.21, it is observed that most metal ions cannot interfere to the detection of Bi<sup>3+</sup>. However, only Fe<sup>3+</sup> can be interfered for Bi<sup>3+</sup> sensing that had small effect to increase the

fluorescence signal. The increasing fluorescence intensity may come from the competition between coordination of **P2** with  $\text{Bi}^{3+}$  and  $\text{Fe}^{3+}$ .

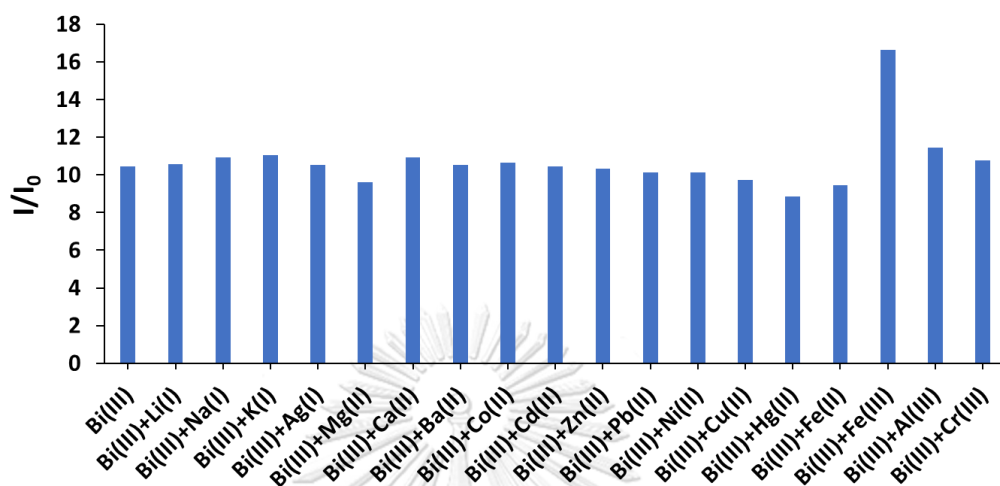


Figure 3.21 Interference of other metal ions (10 eq) on **P2** (10 μM) in the presence of  $\text{Bi}^{3+}$  (10 eq).

### 3.3.4 Fluorescence titration and detection limit

The quantitative analysis of **P2** with  $\text{Bi}^{3+}$  was examined by fluorescence titration experiment as shown in Figure 3.22. The emission intensity at 450 nm was gradually increased with  $\text{Bi}^{3+}$  concentration from 0 to 500 μM.

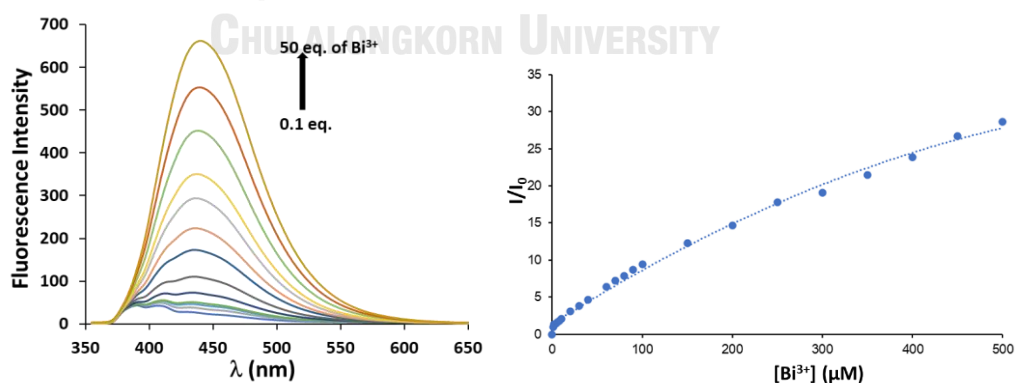
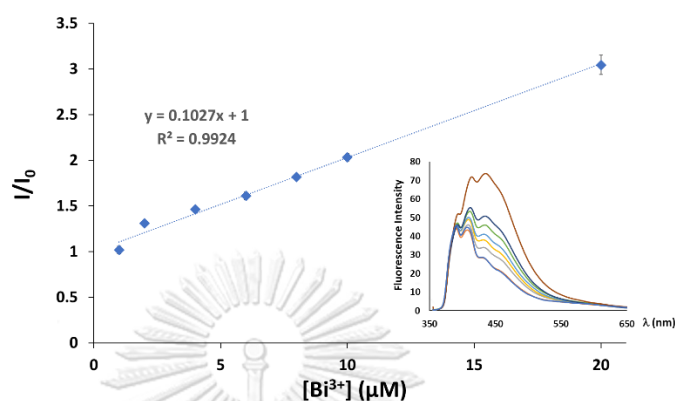


Figure 3.22 Fluorescence spectra of **P2** (10 μM) in the different concentration of  $\text{Bi}^{3+}$ . and relationship between concentration of  $\text{Bi}^{3+}$  and fluorescence enhancement ratio of complex.

A linear relationship between the fluorescence enhancement ratio and the concentration of  $\text{Bi}^{3+}$  was exhibited in the range from 0 to 20  $\mu\text{M}$  with the correlation coefficient of 0.9924 (Figure 3.23). The detection limit of **P2** with  $\text{Bi}^{3+}$  was calculated to be 1.20  $\mu\text{M}$  in  $\text{CH}_3\text{CN}$ -DMSO (8:2, v/v).at three-time noises.



**Figure 3.23** Linear Plot between concentration of  $\text{Bi}^{3+}$  and fluorescence enhancement ratio of complex with **P2** (10  $\mu\text{M}$ ).

### 3.4 Sensing mechanism studies

#### 3.4.1 Time dependence

The binding phenomenon of **P2** in presence of  $\text{Bi}^{3+}$  was determined to prove the complexation of **P2** and  $\text{Bi}^{3+}$  is stable by time effect studied at the period of 0-30 min. The result was showed in Figure 3.24. The fluorescence intensity ratio of **P2** upon addition of 10 equiv. of  $\text{Bi}^{3+}$  remained constantly ratio. It could be indicated that the process of complexation between **P2** and  $\text{Bi}^{3+}$  is stable.

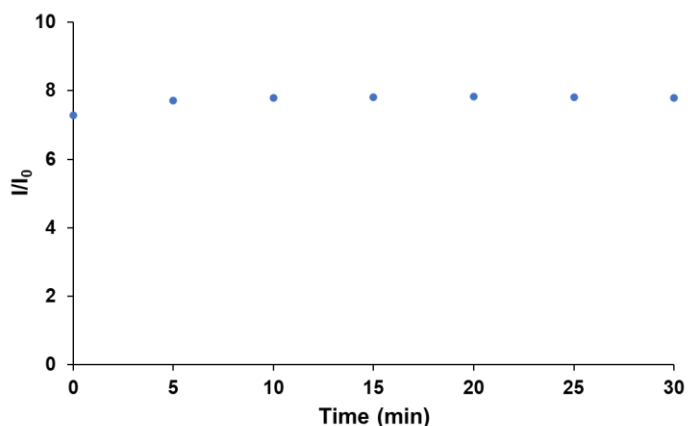


**Figure 3.24** Fluorescence intensity of **P2** (10  $\mu\text{M}$ ) upon addition 10 equiv. of  $\text{Bi}^{3+}$  in  $\text{CH}_3\text{CN}$ -DMSO (8:2, v/v) for 30 min.

### 3.4.2 UV-visible studies and decomplexation

The binding property of **P2** and  $\text{Bi}^{3+}$  was investigated by UV-Vis titration in  $\text{CH}_3\text{CN}$ -DMSO (8:2, v/v) at room temperature. Upon addition of  $\text{Bi}^{3+}$  from 0.1 equiv. to 50 equiv., the absorption band was observed at 278 nm (Figure 3.25). The new band might be attributed to the complexation between **P2** and  $\text{Bi}^{3+}$ .

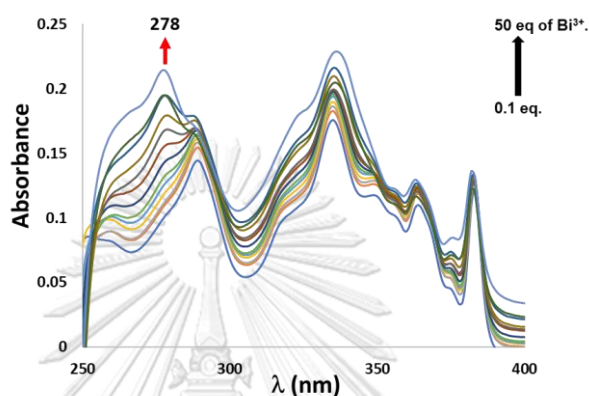


**Figure 3.25** UV-Vis titration of **P2** (10  $\mu\text{M}$ ) upon addition of various concentrations of  $\text{Bi}^{3+}$ .

Moreover, to confirm the complexation, sodium sulfide ( $\text{Na}_2\text{S}$ ) was added to the solution of **P2** in the presence of  $\text{Bi}^{3+}$  in order to decomplexation. However, it is unsuccessful. After addition of  $\text{Na}_2\text{S}$ , although the UV-Vis spectrum shows the absorption band at 278 nm was disappeared, but the upper baseline shift was observed (Figure 3.22, left). It might be result from the formation of insoluble  $\text{Bi}_2\text{S}_3$ . Nonetheless, the fluorescence enhancement intensity at 450 nm was caused by the complexation of **P2** and  $\text{Bi}^{3+}$  which was reduced as same as the emission of **P2** without  $\text{Bi}^{3+}$  upon addition of  $\text{Na}_2\text{S}$  (Figure 3.22, right). The  $\text{Na}_2\text{S}$  could lead to the releasing  $\text{Bi}^{3+}$  and it was one of information for study the mechanism sensing.



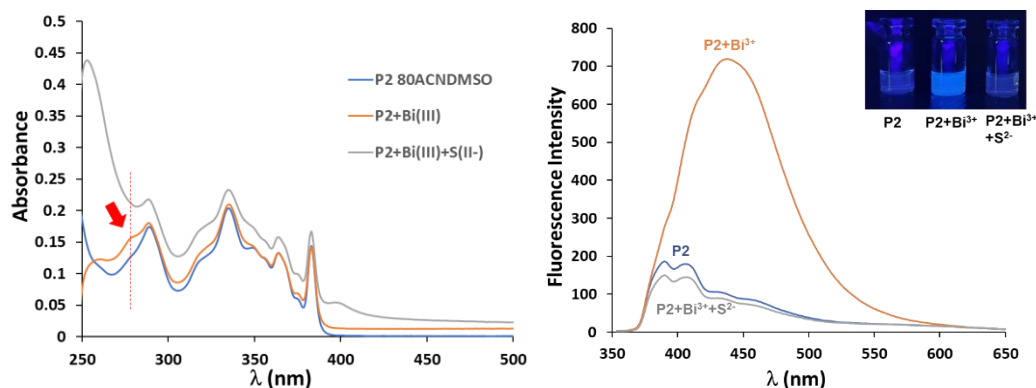


**Figure 3.26** UV-Vis and Fluorescence spectra of the restoration **P2** in the presence of  $\text{Bi}^{3+}$  by  $\text{Na}_2\text{S}$ .

#### 3.4.3 $^1\text{H}$ NMR experiment

The mechanistic experiment was also performed by  $^1\text{H}$  NMR on **P2** in deuterated methanol ( $\text{CD}_3\text{OD}$ ) before and after addition of  $\text{Bi}^{3+}$  that dissolved in deuterated water ( $\text{D}_2\text{O}$ ) as exhibited in Figure 3.23. In the spectrum of **P2**, the peaks at 7.04, 7.08, 7.36 and 8.17 ppm were assigned to the proton signals of phenolic ring ( $\text{H}_k$ ,  $\text{H}_m$ ,  $\text{H}_l$  and  $\text{H}_j$ , respectively) and the others were the proton signals of pyrene. The downfield shift of most of the proton signals were observed except  $\text{H}_j$  which shifted slightly upfield. This result could be not only proved a coordination complex between **P2** and  $\text{Bi}^{3+}$  but also led to the deprotonation of phenolic proton. Consequently, the increasing fluorescence intensity might imply the inhibition of the excited-state intramolecular proton transfer (ESIPT) process.

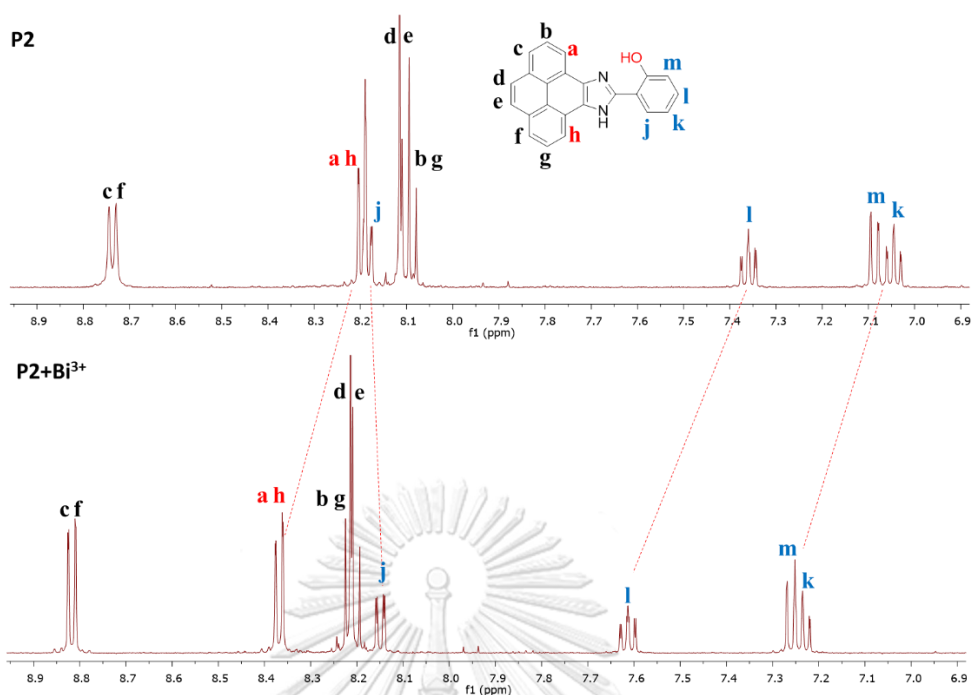


Figure 3.27  $^1\text{H}$  NMR spectra of **P2** in  $\text{CD}_3\text{OD}$  in the absence and the presence of  $\text{Bi}^{3+}$ .

#### 3.4.4 Job's plot

As can be seen in Figure 3.28, the Job's plot analysis was examined on the stoichiometry of the complex between **P2** and  $\text{Bi}^{3+}$ . A plot of mole fraction of  $\text{Bi}^{3+}$  with fluorescence intensity of mole fraction of **P2** showed that the maximum point was obtained at 0.5 of mole fraction of  $\text{Bi}^{3+}$ . The Job's plot confirmed the formation of 1:1 complex of **P2** with  $\text{Bi}^{3+}$ .

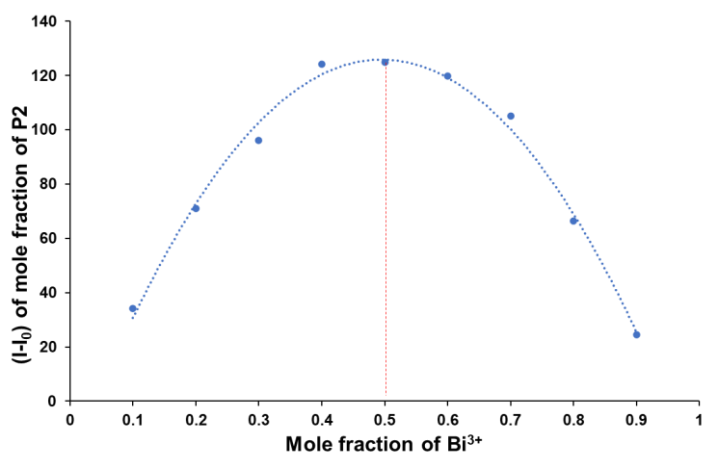


Figure 3.28 Job's plot for determination of binding stoichiometry between **P2** and  $\text{Bi}^{3+}$ .

### 3.5 Quantitative analysis for $\text{Bi}^{3+}$

The application of this sensor was further studied for detection of  $\text{Bi}^{3+}$  in water samples so that the optimization of condition was determined.

#### 3.5.1 Effect of water content

Due to the insolubility of **P2** in water, the content of water was controlled to avoid the precipitate. The UV-Vis spectra of 70-90% of water in  $\text{CH}_3\text{CN}$  disappeared original absorption bands and were broad peaks while 10 -60% of water were not remarkable changes (Figure 3.29). Although emission fluorescence intensity at 440-450 nm is not significant changes, however, 10% of water may be a mild condition to apply.

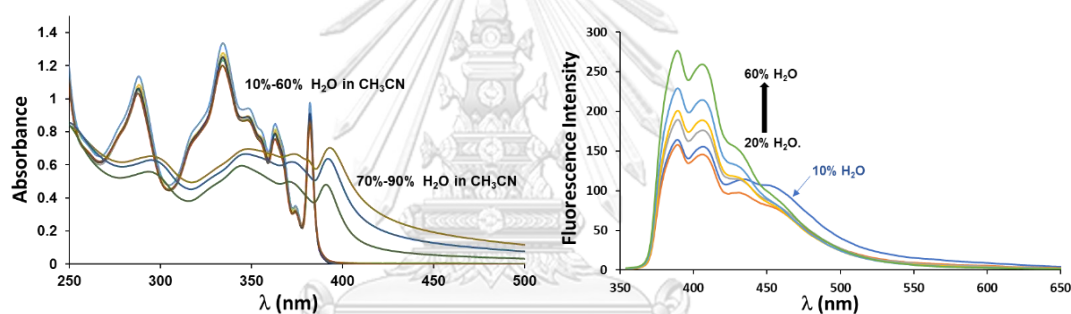


**Figure 3.29** UV-Vis spectra and Fluorescence spectra of **P2** in the presence of water fraction in  $\text{CH}_3\text{CN}$ .

#### 3.5.2 Effect of pH

Then, the pH dependency of **P2** was investigated by fluorescence emission spectra with and without  $\text{Bi}^{3+}$ . The first study, when 20  $\mu\text{M}$  of pH buffers were used to control pH in 10 % water in the mixed organic solution ( $\text{CH}_3\text{CN}$ -DMSO; 8:2, v/v) of **P2** as shown in Figure 3.30, fluorescent intensities were increased in the range between pH 3 and 5 for **P2** in the presence of  $\text{Bi}^{3+}$  but no fluorescent intensity changes in the range between pH 7 and 9. It might be the binding between **P2** and  $\text{Bi}^{3+}$  was disturbed by the solvation of buffer ions that were also observed by error value.

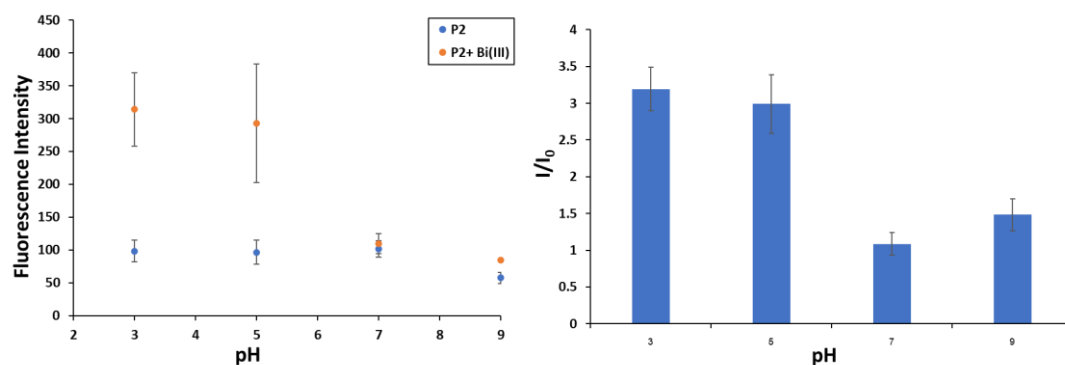


**Figure 3.30** The variation of fluorescent intensity of **P2** (10  $\mu\text{M}$ ) in the absence and presence of 10 equiv. of  $\text{Bi}^{3+}$  with difference pH levels (3-9) and fluorescence enhancement ratio in 10% pH-buffers (20  $\mu\text{M}$ ) in mixed organic solvent  $\text{CH}_3\text{CN}$ -DMSO (8:2, v/v).

To prove this problem, the pH levels were adjusted by 1 mM HCl as acid and 1 mM NaOH as base. In Figure 3.31, the enhancement fluorescent intensity of **P2** with  $\text{Bi}^{3+}$  was observed. However, the fluorescent intensity of **P2** in the presence and absence of  $\text{Bi}^{3+}$  at pH 3 is higher than the others due to the protonation of imidazole nitrogen atom while the hydroxide ion ( $\text{OH}^-$ ) at the pH = 11 might compete for  $\text{Bi}^{3+}$  with **P2** that decreased fluorescent intensity. As the result, pH of real samples was adjusted by HCl and NaOH to 5 for quantitative application.

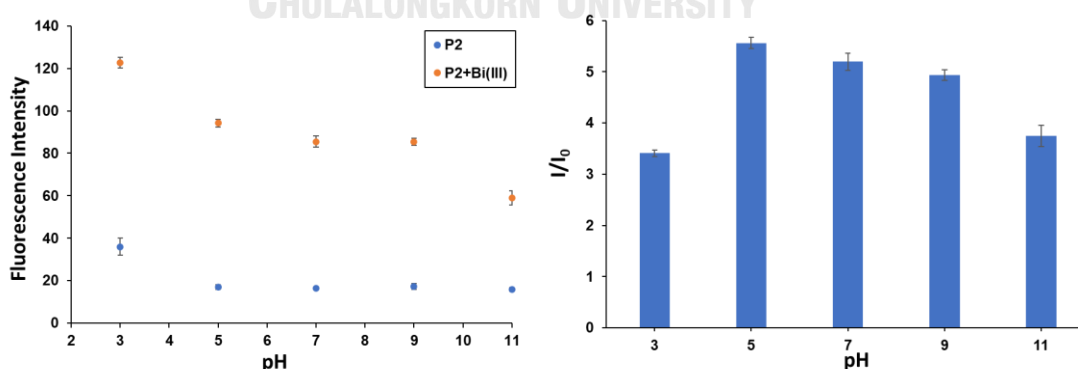


**Figure 3.31** The variation of fluorescent intensity of **P2** (10  $\mu\text{M}$ ) in the absence and presence of 10 equiv. of  $\text{Bi}^{3+}$  and fluorescence enhancement ratio in 10% aqueous solution at various pH (HCl-NaOH) in mixed organic solvent  $\text{CH}_3\text{CN}$ -DMSO (8:2, v/v)

### 3.5.3 Bi<sup>3+</sup> in real water samples

To demonstrate using **P2** as sensor for detection of Bi<sup>3+</sup> in real water samples. A calibration curve was investigated in 10% (v/v) of pH5 aqueous solution in mixed organic solvents, CH<sub>3</sub>CN-DMSO (8:2, v/v) by fluorescence titration as shown in Figure 3.32. The detection limit in this system was calculated to be 3.40 μM with three times noises.

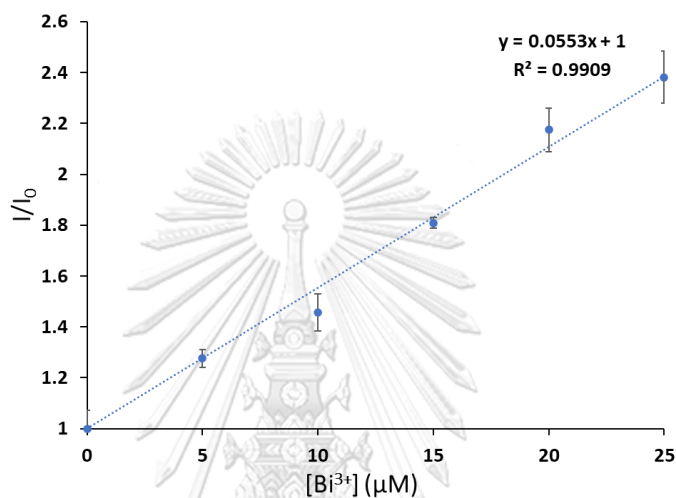


**Figure 3.32** Linear Plot between the concentration of Bi<sup>3+</sup> and fluorescence enhancement ratio of **P2** in 10% (v/v) of pH 5 aqueous solution in mixed organic solvents (CH<sub>3</sub>CN-DMSO (8:2, v/v)).

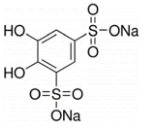
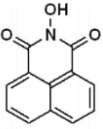
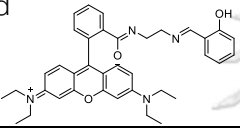
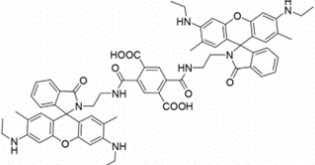
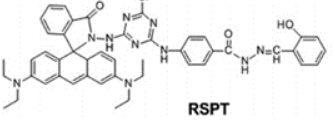
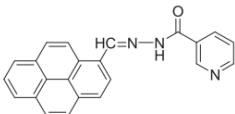
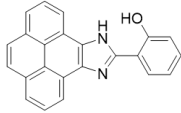
The analysis of real water samples from tap water and drinking water were adjusted to pH at 5 using HCl-NaOH. And then were spiked the known amount of Bi<sup>3+</sup> at 10 and 15 μM. The results were illustrated in Table 3.3, showed that the recovery of Bi<sup>3+</sup> in the spiked water samples at 91-97% was almost completed. The incomplete recover of Bi<sup>3+</sup> might be caused by the anions such as phosphate, sulfate carbonate or sulfide in these water samples that formed or interacted to bismuth compounds so that it might decrease the Bi<sup>3+</sup> ions.

**Table 3.3** Quantitative analysis for Bi(III) in real water samples (n=3)

Samples	Spike ( $\mu\text{M}$ )	found ( $\mu\text{M}$ )	Recovery
Tab water	10.00	$9.72 \pm 0.096$	$97.20\% \pm 0.96$
	15.00	$13.77 \pm 0.09$	$91.80\% \pm 0.60$
Drinking water	10.00	$9.61 \pm 0.08$	$96.10\% \pm 0.80$
	15.00	$14.10 \pm 0.01$	$94.00\% \pm 0.07$

In Table 3.4, the outcome of sensor (P2) is compared to others Bi<sup>3+</sup> fluorescent sensors in terms of structure and detection limited. Even if the detection limited is not the lowest but it could be acceptable.

**Table 3.4** Comparison of the Bi(III) fluorescent sensors

Sensors	Solvent(s)	Sensing mode	LOD $\mu\text{M}$	Ref.
Tiron 	DI water	On-off	0.24	Taher et al., 2014 [55]
N-hydroxy 1,8-Naphthalimide 	$\beta$ -cyclodextrin, aqueous solution	Off-on	2.78	Kavitha and Slatin, 2017 [56]
Rhodamine derivative on Zr-based MOFs 	pH = 6, aqueous solution	Off-on	0.008	El-Sewify et al., 2018 [57]
Rhodamine derivative 	pH 5.0–7.0, Ethanol-CH <sub>3</sub> CN (1:4, v/v)	Off-on	2.69	Zhang et al., 2018 [54]
Rhodamine B derivative 	CH <sub>3</sub> CN-H <sub>2</sub> O (99:1, v/v)	Off-on	0.0086	Guang et al., 2018 [58]
Pyren-1-ylmethylenehydrazide 	HEPES buffer pH 7.4, DMSO-H <sub>2</sub> O (1:1, v/v)	Off-on	0.12	Saravanan et al. 2019 [59]
Pyreno[4,5-d]imidazole-based sensor 	CH <sub>3</sub> CN-DMSO (8:2, v/v)	Off-on	1.20	This work
	pH =5, H <sub>2</sub> O-mixed of CH <sub>3</sub> CN/DMSO (1:9, v/v)	Off-on	3.40	This work

## CHAPTER IV

### CONCLUSION

In summary, five derivatives of pyreno[4,5-*d*]imidazole (**P1-P5**) were successfully synthesized from pyrene-4,5-dione and aromatic aldehydes in moderated to good yields. All of compounds except compound **P5** could exhibit a fluorescent enhancement at 450 nm with trivalent cations such as  $\text{Bi}^{3+}$ ,  $\text{Fe}^{3+}$ ,  $\text{Cr}^{3+}$  and  $\text{Al}^{3+}$  in  $\text{CH}_3\text{CN}$ . However, the compound **P2** that consists of phenolic group could be used as a sensor for selectively turn-on detection of  $\text{Bi}^{3+}$  in  $\text{CH}_3\text{CN}$ -DMSO (8:2 v/v). The detection limit of sensor (**P2**) was calculated at 1.20  $\mu\text{M}$ . The sensing mechanism was investigated by UV-Vis titration,  $^1\text{H-NMR}$ , Job's plot and using  $\text{Na}_2\text{S}$  to the decomplexation study, which suggests a 1 :1 binding to form a complex between the sensor (**P2**) and  $\text{Bi}^{3+}$ . In the system that contains 10% aqueous in mixed organic solvents ( $\text{CH}_3\text{CN}$ -DMSO, (8:2 v/v)), the highest ratio of fluorescent enhancement was obtained by addition of  $\text{Bi}^{3+}$  at pH 5. The detection limit was estimated at 3.40  $\mu\text{M}$ . For application, the quantitative detection of  $\text{Bi}^{3+}$  with **P2** in two real water samples could be recovered in acceptable percentages.



## REFERENCES

- [1] Lakowicz, J. R. Principles of Fluorescence Spectroscopy; 3rd ed.; Springer, Boston, MA, 2006.
- [2] Kaur, N.; Kumar, S. Colorimetric metal ion sensors. Tetrahedron 67(48) (2011): 9233-9264.
- [3] Sun, H.; Li, H.; Sadler, P. J. The Biological and Medicinal Chemistry of Bismuth. Chemische Berichte 130(6) (1997): 669-681.
- [4] Gunnlaugsson, T.; Davis, A. P.; Glynn, M. Fluorescent photoinduced electron transfer (PET) sensing of anions using charge neutral chemosensors. Chemical Communications 24) (2001): 2556-2557.
- [5] Callan, J. F.; de Silva, A. P.; Magri, D. C. Luminescent sensors and switches in the early 21st century. Tetrahedron 61(36) (2005): 8551-8588.
- [6] Wang, H.-F.; Wu, S.-P. A pyrene-based highly selective turn-on fluorescent sensor for copper(II) ions and its application in living cell imaging. Sensors and Actuators B: Chemical 181((2013): 743-748.
- [7] Carter, K. P.; Young, A. M.; Palmer, A. E. Fluorescent Sensors for Measuring Metal Ions in Living Systems. Chemical reviews 114(8) (2014): 4564-4601.
- [8] Martínez-Máñez, R.; Sancenón, F. Fluorogenic and Chromogenic Chemosensors and Reagents for Anions. Chemical reviews 103(11) (2003): 4419-4476.
- [9] Sapsford, K. E.; Berti, L.; Medintz, I. L. Materials for Fluorescence Resonance Energy Transfer Analysis: Beyond Traditional Donor–Acceptor Combinations. Angewandte Chemie International Edition 45(28) (2006): 4562-4589.
- [10] Carlson, H. J.; Campbell, R. E. Genetically encoded FRET-based biosensors for multiparameter fluorescence imaging. Current Opinion in Biotechnology 20(1) (2009): 19-27.
- [11] Höfig, H.; Otten, J.; Steffen, V.; Pohl, M.; Boersma, A. J.; Fitter, J. Genetically Encoded Förster Resonance Energy Transfer-Based Biosensors Studied on the Single-Molecule Level. ACS Sensors 3(8) (2018): 1462-1470.
- [12] Li, S.; Zhao, B.; Kan, W.; Wang, L.; Song, B.; Chen, S. A off–on pH fluorescence

- probe derived from phenanthro[9,10-d]imidazol-fluorescein based on ESIPT and ICT. Research on Chemical Intermediates 44(1) (2018): 491-502.
- [13] Zhou, Y.; He, X.; Chen, H.; Wang, Y.; Xiao, S.; Zhang, N.; Li, D.; Zheng, K. An ESIPT/ICT modulation based ratiometric fluorescent probe for sensitive and selective sensing Hg<sup>2+</sup>. Sensors and Actuators B: Chemical 247((2017): 626-631.
- [14] Cheng, D.; Liu, X.; Yang, H.; Zhang, T.; Han, A.; Zang, L. A Cu(2+)-Selective Probe Based on Phenanthro-Imidazole Derivative. Sensors (Basel, Switzerland) 17(1) (2016): 35.
- [15] de Silva, A. P.; Gunaratne, H. Q. N.; Gunnlaugsson, T.; Huxley, A. J. M.; McCoy, C. P.; Rademacher, J. T.; Rice, T. E. Signaling Recognition Events with Fluorescent Sensors and Switches. Chemical reviews 97(5) (1997): 1515-1566.
- [16] Henary, M. M.; Fahrni, C. J. Excited State Intramolecular Proton Transfer and Metal Ion Complexation of 2-(2'-Hydroxyphenyl)benzazoles in Aqueous Solution. The Journal of Physical Chemistry A 106(21) (2002): 5210-5220.
- [17] Ouyang, J.; Ouyang, C.; Fujii, Y.; Nakano, Y.; Shoda, T.; Nagano, T. Synthesis and fluorescent properties of 2-(1H-benzimidazol-2-yl)-phenol derivatives. Journal of Heterocyclic Chemistry 41(3) (2004): 359-365.
- [18] Nayak, M. K. Synthesis, characterization and optical properties of aryl and diaryl substituted phenanthroimidazoles. Journal of Photochemistry and Photobiology A: Chemistry 241((2012): 26-37.
- [19] Zhang, Y.; Wang, J.-H.; Zheng, W.; Chen, T.; Tong, Q.-X.; Li, D. An ESIPT fluorescent dye based on HBI with high quantum yield and large Stokes shift for selective detection of Cys. Journal of Materials Chemistry B 2(26) (2014): 4159-4166.
- [20] Zhao, J.; Ji, S.; Chen, Y.; Guo, H.; Yang, P. Excited state intramolecular proton transfer (ESIPT): from principal photophysics to the development of new chromophores and applications in fluorescent molecular probes and luminescent materials. Physical Chemistry Chemical Physics 14(25) (2012): 8803-8817.
- [21] Wu, Y.; Wen, X.; Fan, Z. An AIE active pyrene based fluorescent probe for selective sensing Hg<sup>2+</sup> and imaging in live cells. Spectrochimica Acta Part A:

- Molecular and Biomolecular Spectroscopy 223((2019): 117315.
- [22] Islam, M. M.; Hu, Z.; Wang, Q.; Redshaw, C.; Feng, X. Pyrene-based aggregation-induced emission luminogens and their applications. Materials Chemistry Frontiers 3(5) (2019): 762-781.
- [23] Feng, X.; Xu, Z.; Hu, Z.; Qi, C.; Luo, D.; Zhao, X.; Mu, Z.; Redshaw, C.; Lam, J. W. Y.; Ma, D. et al. Pyrene-based blue emitters with aggregation-induced emission features for high-performance organic light-emitting diodes. Journal of Materials Chemistry C 7(8) (2019): 2283-2290.
- [24] Hong, Y.; Lam, J. W. Y.; Tang, B. Z. Aggregation-induced emission: phenomenon, mechanism and applications. Chemical Communications 29) (2009): 4332-4353.
- [25] Zhang, Y.; He, B.; Liu, J.; Hu, S.; Pan, L.; Zhao, Z.; Tang, B. Z. Aggregation-induced emission and the working mechanism of 1-benzoyl and 1-benzyl pyrene derivatives. Physical Chemistry Chemical Physics 20(15) (2018): 9922-9929.
- [26] Jenekhe, S. A.; Osaheni, J. A. Excimers and Exciplexes of Conjugated Polymers. Science 265(5173) (1994): 765.
- [27] Piñeiro, L.; Novo, M.; Al-Soufi, W. Fluorescence emission of pyrene in surfactant solutions. Advances in Colloid and Interface Science 215((2015): 1-12.
- [28] Das, K.; Sarkar, N.; Ghosh, A. K.; Majumdar, D.; Nath, D. N.; Bhattacharyya, K. Excited-State Intramolecular Proton Transfer in 2-(2-Hydroxyphenyl)benzimidazole and -benzoxazole: Effect of Rotamerism and Hydrogen Bonding. The Journal of Physical Chemistry 98(37) (1994): 9126-9132.
- [29] Diring, S.; Camerel, F.; Donnio, B.; Dintzer, T.; Toffanin, S.; Capelli, R.; Muccini, M.; Ziesel, R. Luminescent Ethynyl-Pyrene Liquid Crystals and Gels for Optoelectronic Devices. Journal of the American Chemical Society 131(50) (2009): 18177-18185.
- [30] Shan, T.; Liu, Y.; Tang, X.; Bai, Q.; Gao, Y.; Gao, Z.; Li, J.; Deng, J.; Yang, B.; Lu, P. et al. Highly Efficient Deep Blue Organic Light-Emitting Diodes Based on Imidazole: Significantly Enhanced Performance by Effective Energy Transfer with Negligible Efficiency Roll-off. ACS Applied Materials & Interfaces 8(42) (2016): 28771-28779.
- [31] Zöphel, L.; Beckmann, D.; Enkelmann, V.; Chercka, D.; Rieger, R.; Müllen, K. Asymmetric pyrene derivatives for organic field-effect transistors. Chemical

- Communications 47(24) (2011): 6960-6962.
- [32] Zang, L.; Liang, C.; Wang, Y.; Bu, W.; Sun, H.; Jiang, S. A highly specific pyrene-based fluorescent probe for hypochlorite and its application in cell imaging. Sensors and Actuators B: Chemical 211((2015): 164-169.
- [33] Kumar, A.; Pandith, A.; Kim, H.-S. Pyrene-appended imidazolium probe for 2,4,6-trinitrophenol in water. Sensors and Actuators B: Chemical 231((2016): 293-301.
- [34] Parker, C. A.; Hatchard, C. G. Delayed fluorescence of pyrene in ethanol. Transactions of the Faraday Society 59(0) (1963): 284-295.
- [35] Winnik, F. M. Photophysics of preassociated pyrenes in aqueous polymer solutions and in other organized media. Chemical reviews 93(2) (1993): 587-614.
- [36] Ogino, K.; Iwashima, S.; Inokuchi, H.; Harada, Y. Photoelectric Emission and Electrical Conductivity of the Cesium Complex with Pyrene Derivatives. Bulletin of the Chemical Society of Japan 38(3) (1965): 473-477.
- [37] Tashiro, M.; Yamato, T. Metacyclophanes and related compounds. 4. Halogenations of 8,16-dialkyl-anti-5,13-di-tert-butyl[2.2]metacyclophan-1-enes and 2,7-di-tert-butyl-trans-10b,10c-dialkyl-10b,10c-dihydropyrenes. Journal of the American Chemical Society 104(13) (1982): 3701-3707.
- [38] Dewar, M. J. S.; Dennington, R. D. DEWAR-PI study of electrophilic substitution in selected polycyclic fluoranthene hydrocarbons. Journal of the American Chemical Society 111(11) (1989): 3804-3808.
- [39] Casas-Solvas, J. M.; Howgego, J. D.; Davis, A. P. Synthesis of substituted pyrenes by indirect methods. Organic & Biomolecular Chemistry 12(2) (2014): 212-232.
- [40] Mateo-Alonso, A. Pyrene-fused pyrazaacenes: from small molecules to nanoribbons. Chemical Society Reviews 43(17) (2014): 6311-6324.
- [41] Eseola, A. O.; Adepitan, O.; Görls, H.; Plass, W. Electronic/substituents influence on imidazole ring donor-acceptor capacities using 1H-imidazo[4,5-f][1,10]phenanthroline frameworks. New Journal of Chemistry 36(4) (2012): 891-902.
- [42] Ju, C.-C.; Yin, H.-J.; Yuan, C.-L.; Wang, K.-Z. A fluorescent probe for both pH and Zn<sup>2+</sup> based on 2-(1-phenyl-1H-benzo[d]imidazol-2-yl)phenol. Spectrochimica Acta Part A: Molecular and Biomolecular Spectroscopy 79(5) (2011): 1876-1880.

- [43] Hu, J.; Li, J.; Qi, J.; Chen, J. Highly selective and effective mercury(ii) fluorescent sensors. *New Journal of Chemistry* 39(2) (2015): 843-848.
- [44] Sinha, S.; Chowdhury, B.; Ghosh, P. A Highly Sensitive ESIPT-Based Ratiometric Fluorescence Sensor for Selective Detection of Al<sup>3+</sup>. *Inorganic Chemistry* 55(18) (2016): 9212-9220.
- [45] Chen, Y.; Shi, X.; Lu, Z.; Wang, X.; Wang, Z. A Fluorescent Probe for Hydrogen Peroxide in Vivo Based on the Modulation of Intramolecular Charge Transfer. *Analytical Chemistry* 89(10) (2017): 5278-5284.
- [46] Liu, Y.; Gao, Z.; Wang, Z.; Feng, C.; Shen, F.; Lu, P.; Ma, Y. Synthesis and Characterization of an Imidazole-Containing Pyrene  $\pi$ -System. *European Journal of Organic Chemistry* 2013(32) (2013): 7267-7271.
- [47] Mardanya, S.; Karmakar, S.; Mondal, D.; Baitalik, S. An imidazolyl-pyrene-imidazole conjugate as a cyanide sensor and a set–reset memorized sequential logic device. *Dalton Transactions* 44(36) (2015): 15994-16012.
- [48] Mardanya, S.; Karmakar, S.; Bar, M.; Baitalik, S. Pyrene-biimidazole based Ru(ii) and Os(ii) complexes as highly efficient probes for the visible and near-infrared detection of cyanide in aqueous media. *Dalton Transactions* 44(48) (2015): 21053-21072.
- [49] Mardanya, S.; Karmakar, S.; Maity, D.; Baitalik, S. Ruthenium(II) and Osmium(II) Mixed Chelates Based on Pyrenyl–Pyridylimidazole and 2,2'-Bipyridine Ligands as Efficient DNA Intercalators and Anion Sensors. *Inorganic Chemistry* 54(2) (2015): 513-526.
- [50] Tabasi, Z. A.; Younes, E. A.; Walsh, J. C.; Thompson, D. W.; Bodwell, G. J.; Zhao, Y. Pyrenoimidazolyl-Benzaldehyde Fluorophores: Synthesis, Properties, and Sensing Function for Fluoride Anions. *ACS Omega* 3(11) (2018): 16387-16397.
- [51] Hu, J.; Zhang, D.; Harris, F. W. Ruthenium(III) Chloride Catalyzed Oxidation of Pyrene and 2,7-Disubstitued Pyrenes: An Efficient, One-Step Synthesis of Pyrene-4,5-diones and Pyrene-4,5,9,10-tetraones. *The Journal of Organic Chemistry* 70(2) (2005): 707-708.
- [52] Mardanya, S.; Karmakar, S.; Das, S.; Baitalik, S. Anion and cation triggered

- modulation of optical properties of a pyridyl-imidazole receptor rigidly linked to pyrene and construction of INHIBIT, OR and XOR molecular logic gates: A combined experimental and DFT/TD-DFT investigation. Sensors and Actuators B: Chemical 206((2015): 701-713.
- [53] James Speight, P. D. Lange's Handbook of Chemistry, Sixteenth Edition; 16th ed. / ed.; McGraw-Hill Education: New York, 2005.
- [54] Zhang, E.; Ju, P.; Li, Q.; Hou, X.; Yang, H.; Yang, X.; Zou, Y.; Zhang, Y. A novel rhodamine 6G-based fluorescent and colorimetric probe for Bi<sup>3+</sup>: Synthesis, selectivity, sensitivity and potential applications. Sensors and Actuators B: Chemical 260((2018): 204-212.
- [55] Taher, M. A.; Rahimi, M.; Fazlirad, H. A sensitive fluorescence quenching method for determination of bismuth with tiron. Journal of Luminescence 145((2014): 976-980.
- [56] Ramasamy, K.; Thambusamy, S. Dual emission and pH based naphthalimide derivative fluorescent sensor for the detection of Bi<sup>3+</sup>. Sensors and Actuators B: Chemical 247((2017): 632-640.
- [57] El-Sewify, Islam M.; Shenashen, M. A.; Shahat, A.; Yamaguchi, H.; Selim, M. M.; Khalil, M. M. H.; El-Safty, S. A. Dual colorimetric and fluorometric monitoring of Bi<sup>3+</sup> ions in water using supermicroporous Zr-MOFs chemosensors. Journal of Luminescence 198((2018): 438-448.
- [58] Guang, S.; Wei, G.; Yan, Z.; Zhang, Y.; Zhao, G.; Wu, R.; Xu, H. A novel turn-on fluorescent probe for the multi-channel detection of Zn<sup>2+</sup> and Bi<sup>3+</sup> with different action mechanisms. Analyst 143(2) (2018): 449-457.
- [59] Saravanan, A.; Shyamsivappan, S.; Suresh, T.; Subashini, G.; Kadirvelu, K.; Bhuvanesh, N.; Nandhakumar, R.; Mohan, P. S. An efficient new dual fluorescent pyrene based chemosensor for the detection of bismuth (III) and aluminium (III) ions and its applications in bio-imaging. Talanta 198((2019): 249-256.



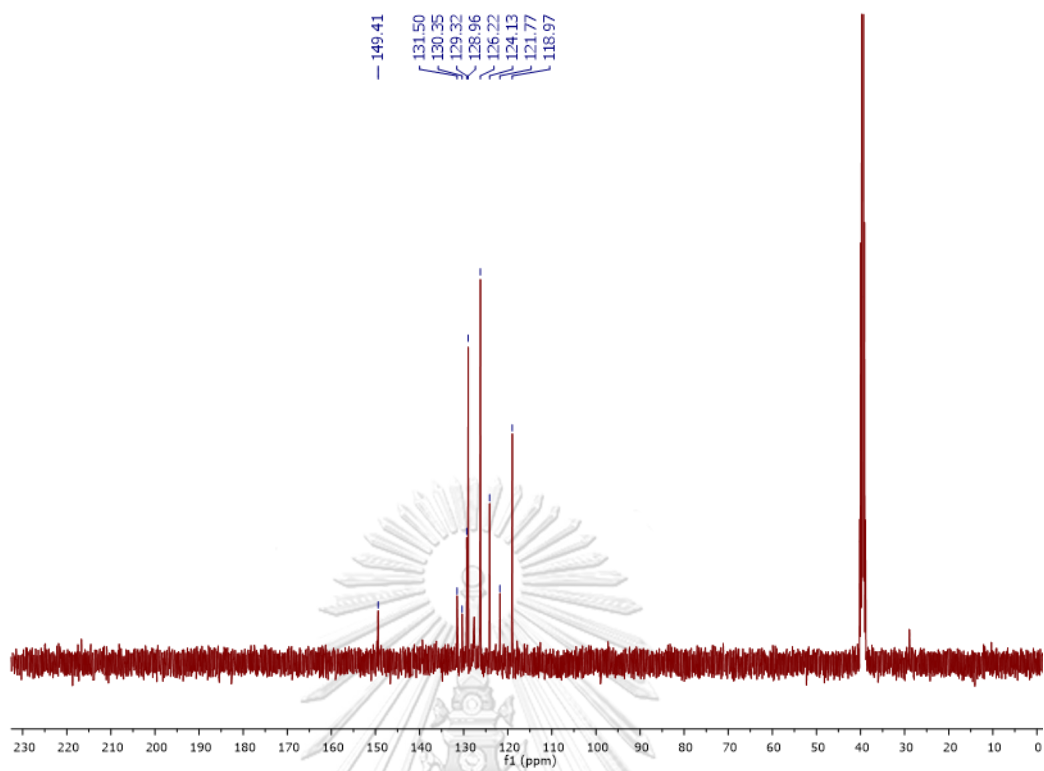


Figure A.3  $^{13}\text{C}$  NMR spectrum of P1 in  $\text{DMSO-d}_6$

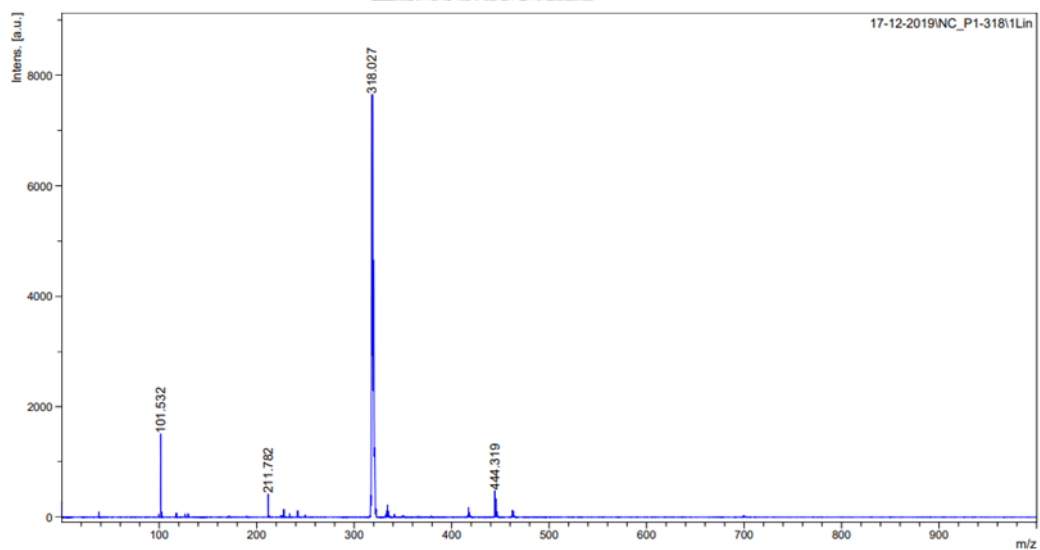


Figure A.4 MALDI-TOF-Mass spectrum of P1



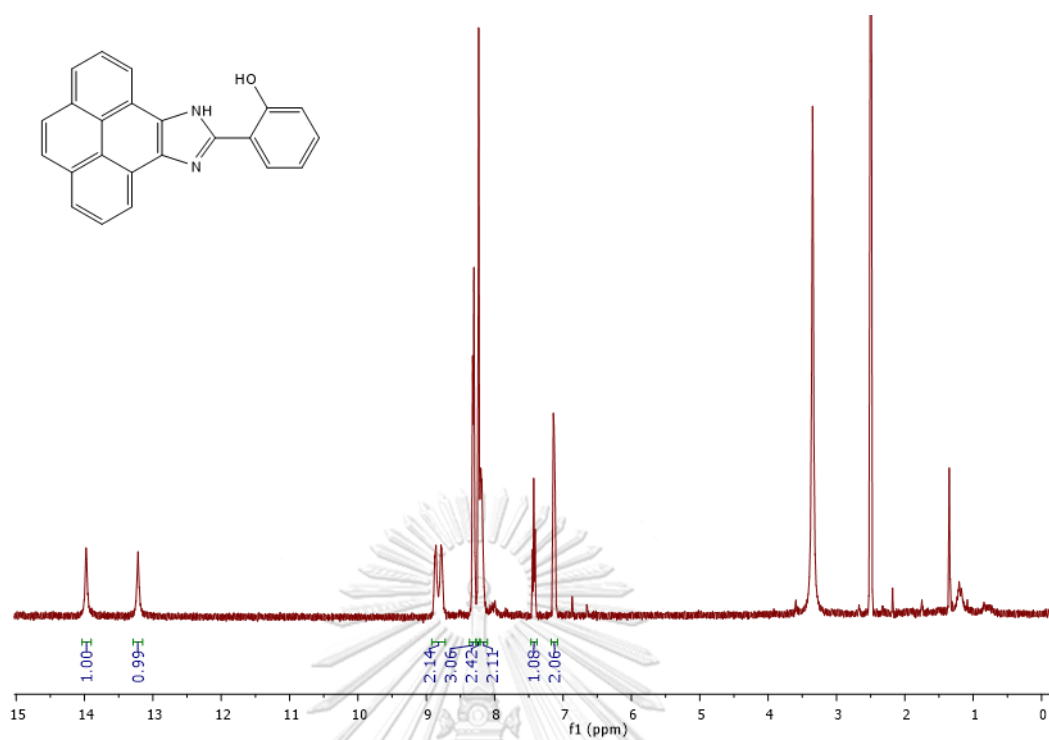


Figure A.5  $^1\text{H}$  NMR spectrum of P2 in  $\text{DMSO-d}_6$

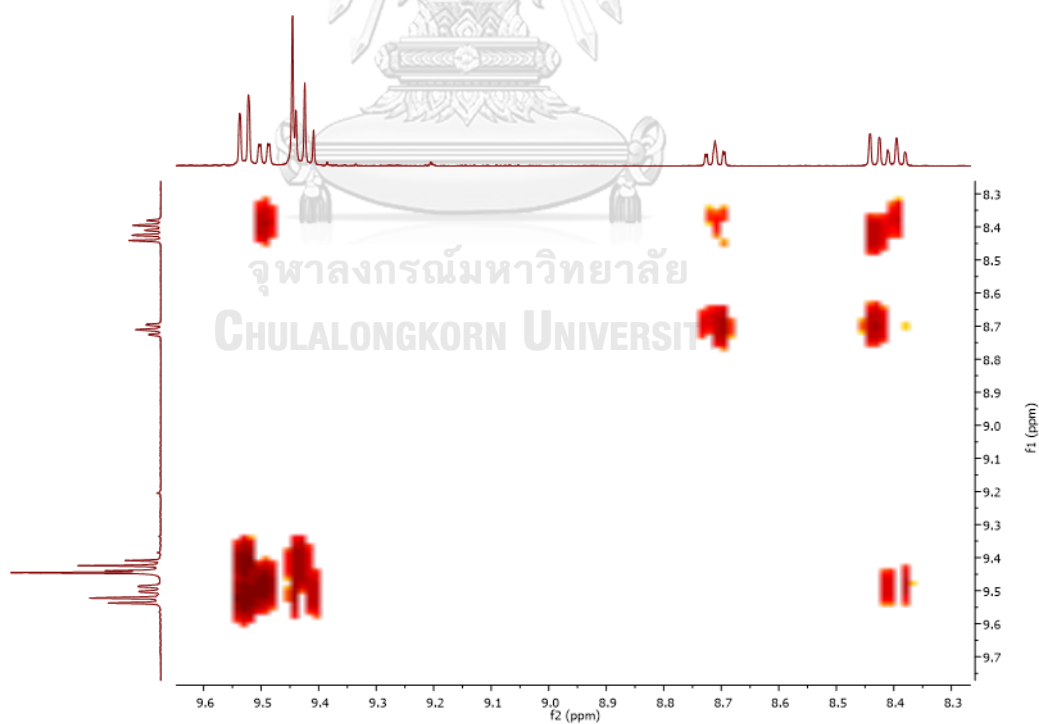


Figure A.6  $^1\text{H}$ - $^1\text{H}$  COSY NMR spectrum of P2 in  $\text{DMSO-d}_6$

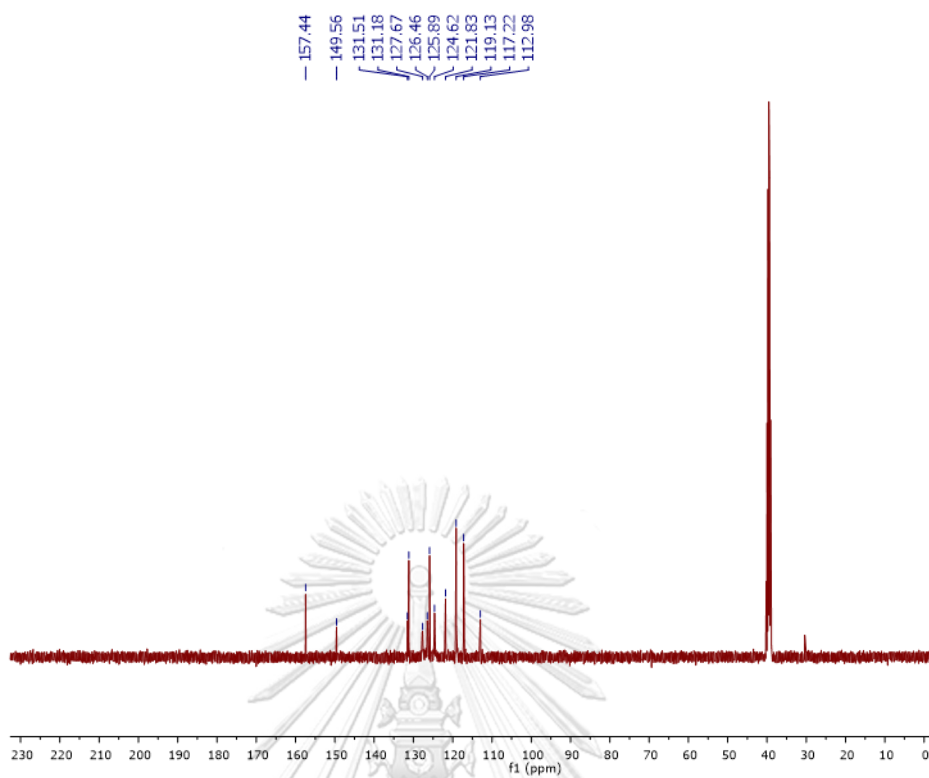


Figure A.7  $^{13}\text{C}$  NMR spectrum of P2 in DMSO- $d_6$

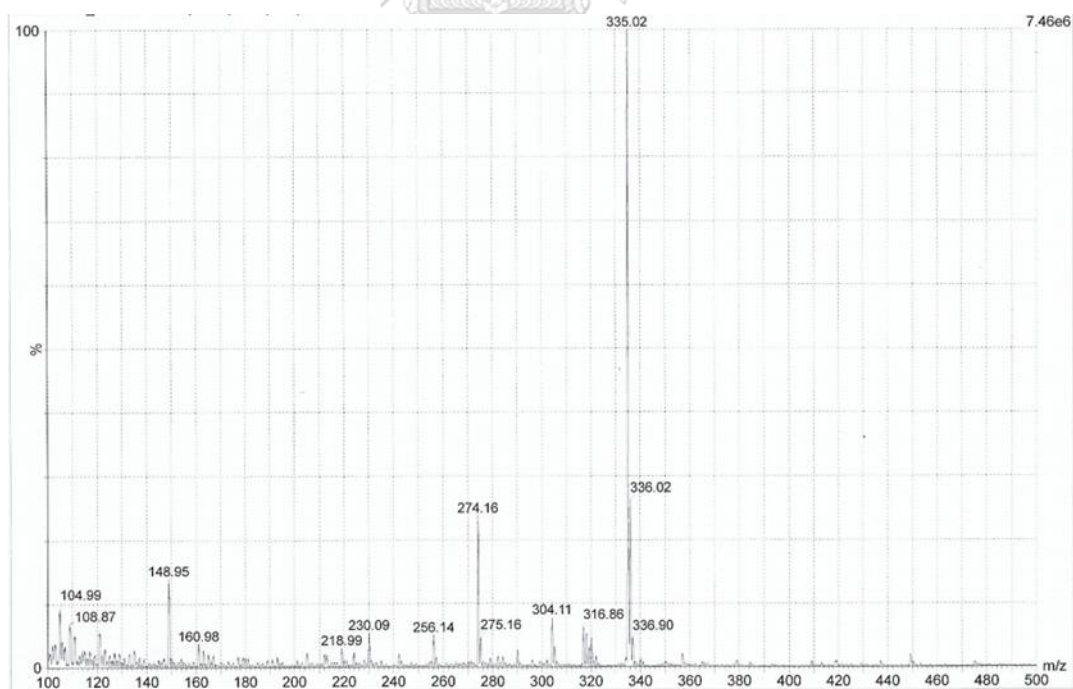


Figure A.8 ESI Mass spectrum of P2

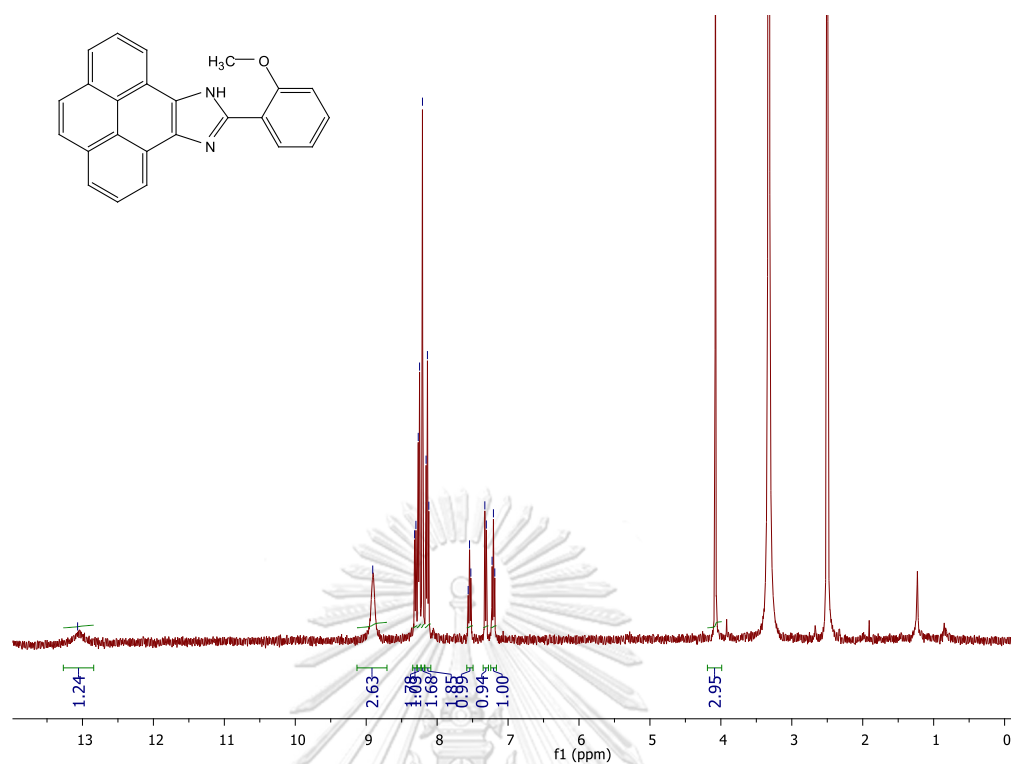


Figure A.9  $^1\text{H}$  NMR spectrum of P3 in DMSO- $d_6$

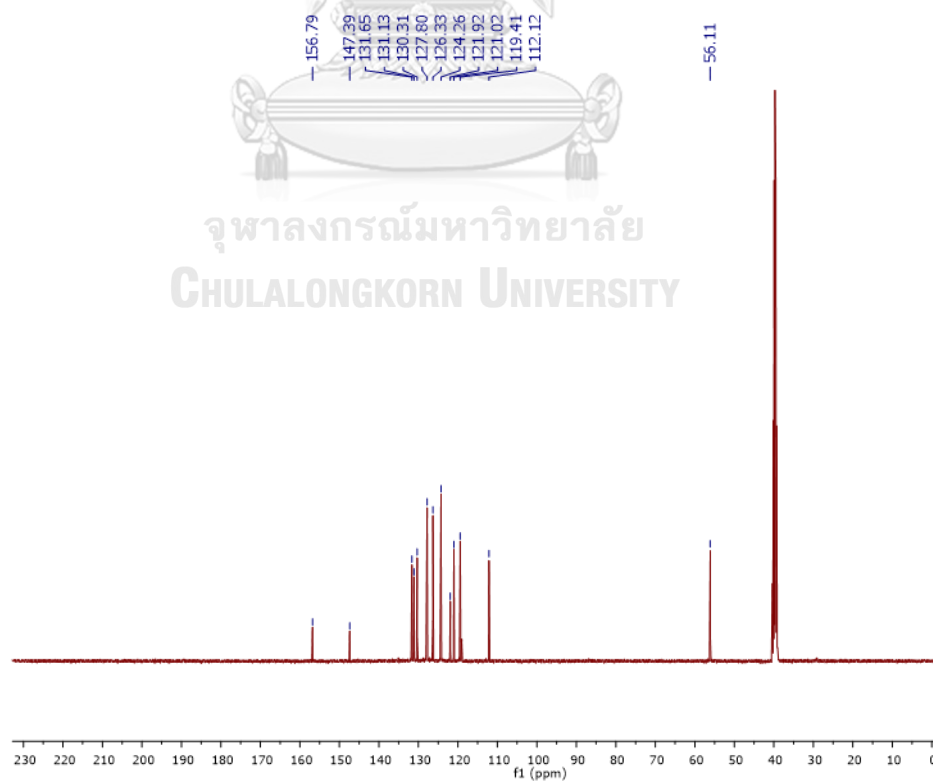


Figure A.10  $^{13}\text{C}$  NMR spectrum of P3 in DMSO- $d_6$

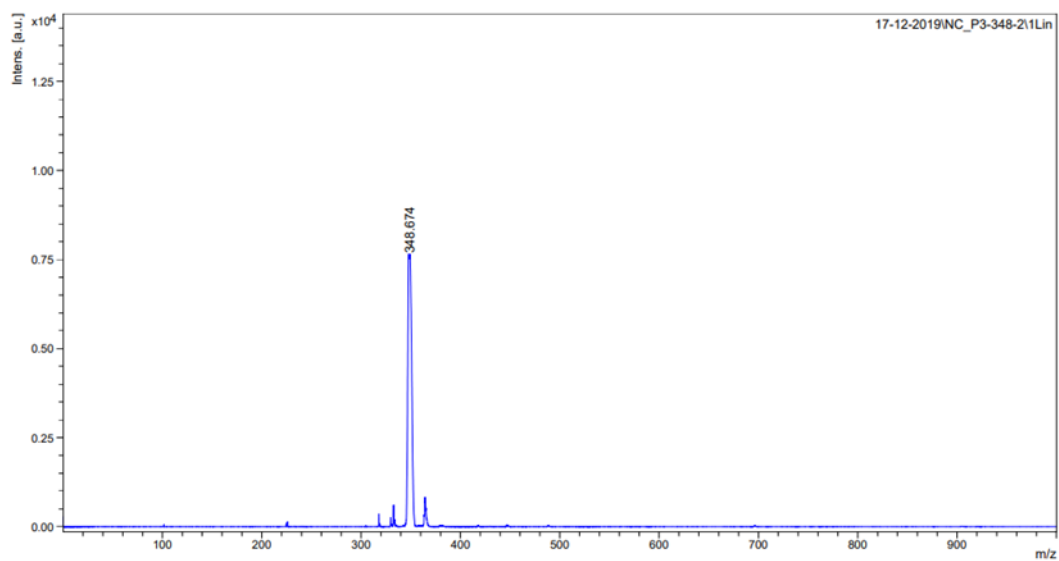


Figure A.11 MALDI-TOF-Mass spectrum of P3

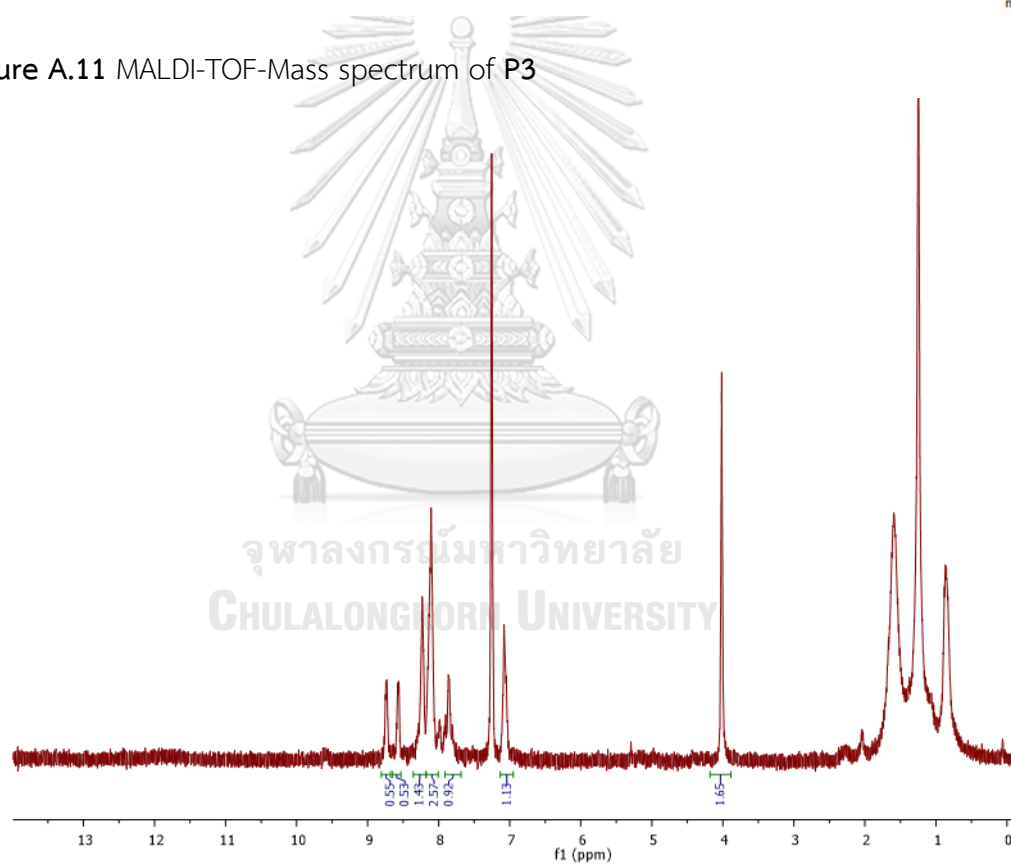


Figure A.12 <sup>1</sup>H NMR spectrum of P4 in CDCl<sub>3</sub>

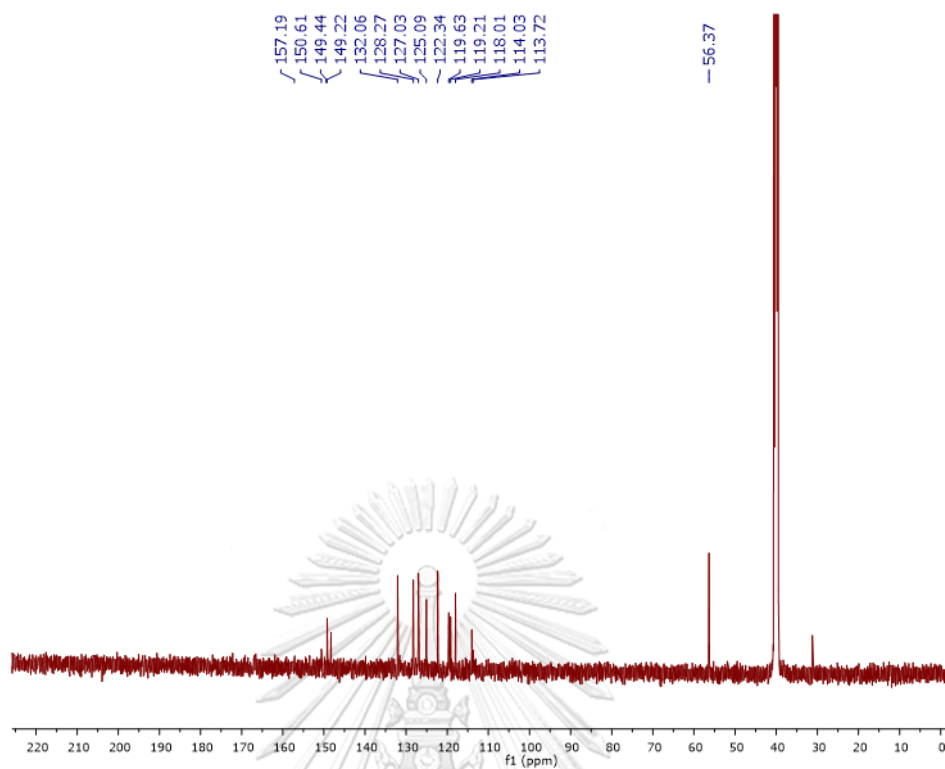


Figure A.13  $^{13}\text{C}$  NMR spectrum of P4 in  $\text{DMSO-d}_6$

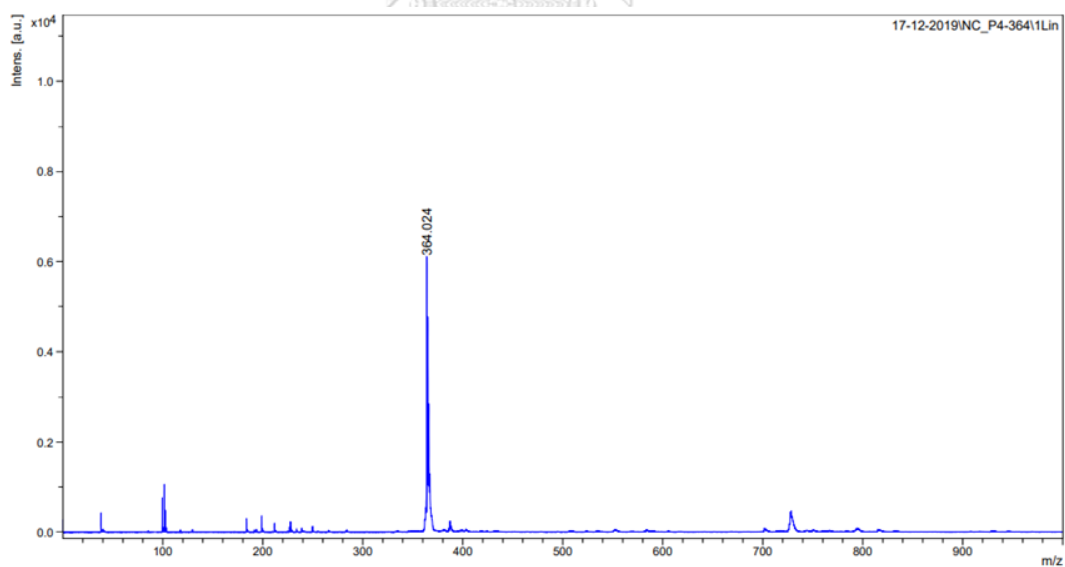


Figure A.14 MALDI-TOF-Mass spectrum of P4

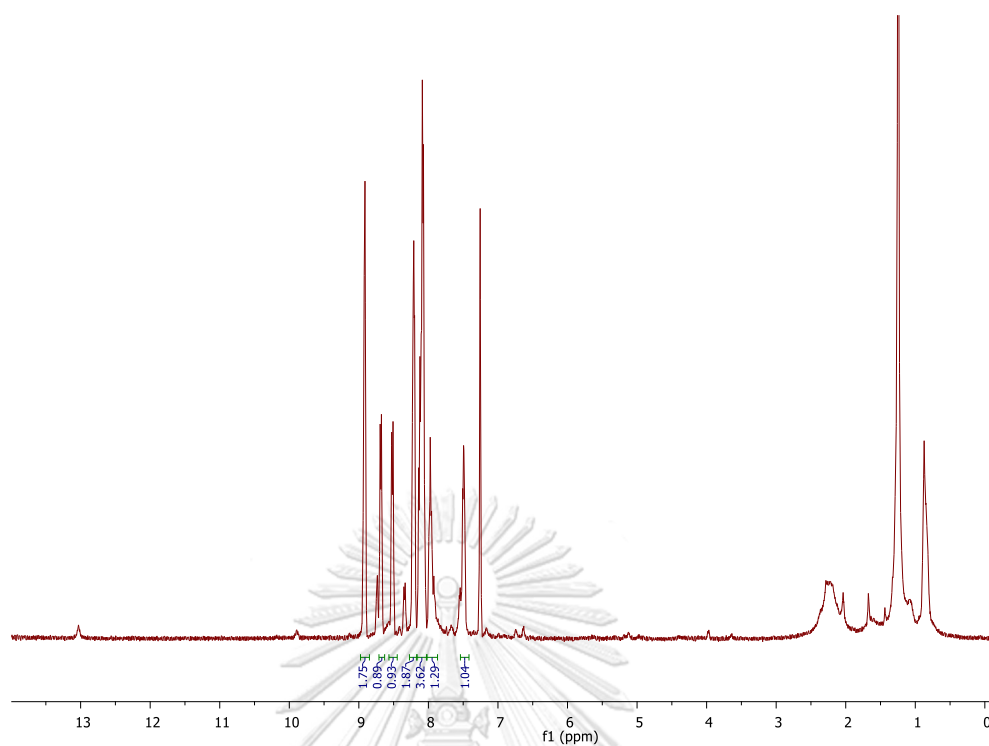


Figure A.15  $^1\text{H}$  NMR spectrum of P5 in  $\text{CDCl}_3$

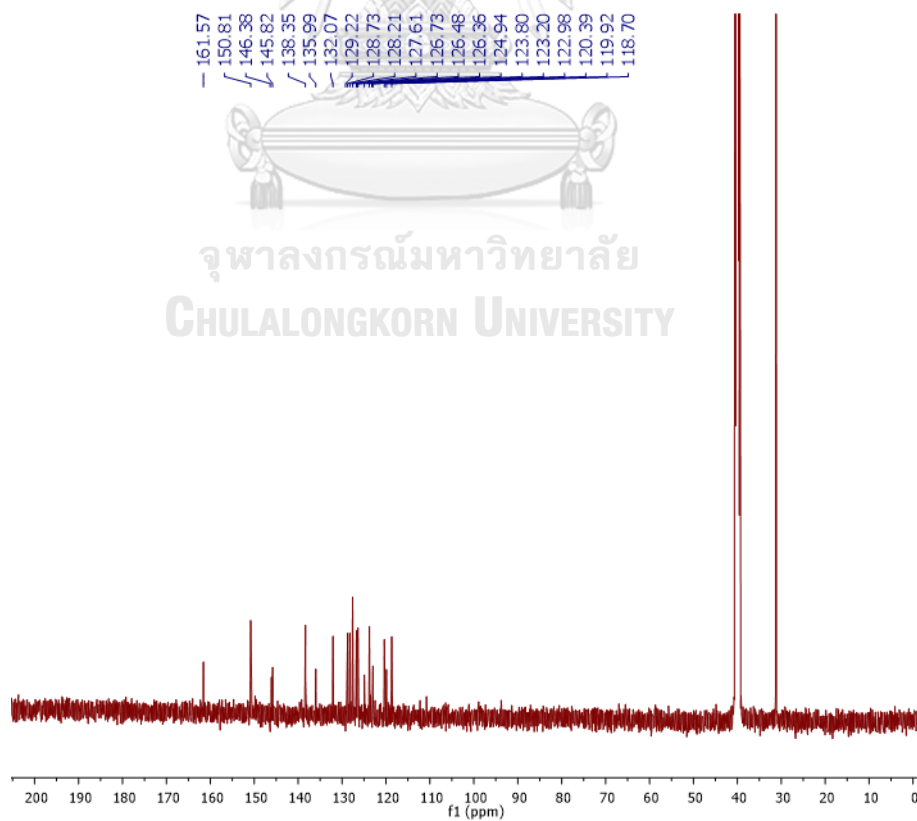


Figure A.16  $^{13}\text{C}$  NMR spectrum of P5 in  $\text{DMSO-d}_6$

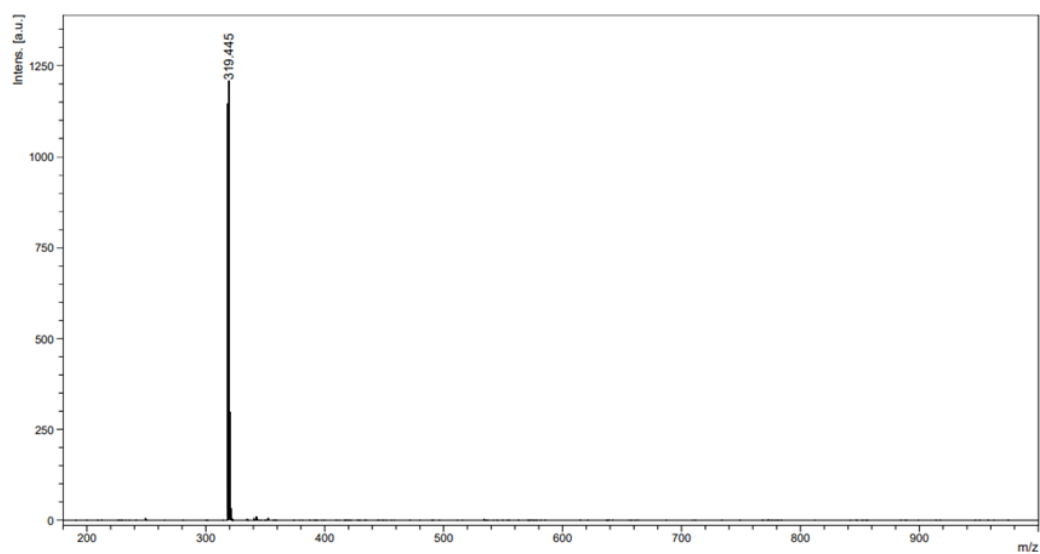


Figure A.17 MALDI-TOF-Mass spectrum of P5



## VITA

**NAME** Nichapa Chanawungmuang

**DATE OF BIRTH** 17 April 1986

**PLACE OF BIRTH** Phuket

**INSTITUTIONS ATTENDED** Bachelor's Degree of Science, majoring in Chemistry, Faculty of Science, Kasetsart University in 2008.  
Master Degree of Science, majoring in Chemistry (organic chemistry), Faculty of Science, Kasetsart University in 2012.  
Since 2014, She has been a graduate student in chemistry and become a member of Material Advancement and Proficient Synthesis (MAPS) group under supervision of Professor Dr. Paitoon Rashatasakhon. She graduated with a Ph.D. Degree in Chemistry in academic year 2020. She received the scholarship from Development and Promotion of Science and Technology Talents Project (DPST).

**HOME ADDRESS** 12/20 Moo.3 Kwang Road, Vichit, Meuang, Phuket, Thailand, 83000

**PUBLICATION** Chanawungmuang, N., Sukwattanasinitt, M., and Rashatasakhon, P. Fluorescence Sensors for Bismuth (III) Ion from Pyreno[4,5-d]imidazole Derivatives. Photochemistry and Photobiology, Accepted, <http://doi.org/10.1111/php.13331>